

**Amplification of Nucleic Acids using Lesion-Induced DNA Amplification
at Room-Temperature**

By

Bibi Safeenaz Alladin-Mustan

**A thesis submitted in partial fulfillment of the requirements for the degree of
Doctor of Philosophy**

Department of Chemistry

University of Alberta

© Bibi Safeenaz Alladin-Mustan, 2020

Abstract

The ability to amplify nucleic acid biomarkers at room temperature has remained elusive despite the great need of diagnostics suitable for the point of care. This thesis explores the probability of making lesion-induced DNA amplification (LIDA) an equipment-free platform that can work at room temperature. In LIDA, previous work in our group had shown a destabilizing lesion, specifically a model abasic group, could be used to achieve turnover and isothermal amplification. Therefore, to exponentially amplify DNA within a wide range of ambient temperatures (18-26 °C), we explored the addition of a second destabilizing group (a mismatch or another abasic group) in our isothermal lesion-induced DNA amplification system. We showed that we could tune the optimum temperature (T_o) at which the ligation reaction works best below 30 °C by the addition of a second destabilizing group to the system as this change results in further destabilization in LIDA. The magnitude of the destabilization is dependent on the type or mismatch or second abasic lesion present. Since this temperature range covers a wide range of room temperatures, we next demonstrate rapid DNA amplification at the bench without a heat source using a set of LIDA probes containing an A:C mismatch and an abasic site. These results show that the presence of a second lesion in the system makes the LIDA reaction faster at lower temperatures. However, when performed in one pot, that is in the presence of both the mismatched probe and the perfect probes, the more complementary system dominates the amplification process compared to the less complementary system.

RNA is another important biomarker for disease diagnosis. One challenge in point-of-care diagnostics is the lack of room-temperature methods for RNA detection based on enzymatic amplification and visualization steps. Therefore, our next goal was to show the versatility of LIDA towards RNA as a target. We performed a reverse transcription ligase chain reaction using our

isothermal lesion-induced DNA amplification technique that can be tuned to operate at any desired temperature. Using RNA-triggered LIDA, we can detect as little as ~100 attomoles of target RNA and can distinguish RNA target from total cellular RNA. Lastly, we demonstrate that the resulting DNA amplicons can be detected colorimetrically, also at room temperature, by rapid, target-triggered disassembly of DNA-modified gold nanoparticles. This integrated amplification/detection platform requires no heating or visualization instrumentation, which is an important step towards realizing instrument-free POC testing.

Finally, I will discuss our efforts to decrease the background-triggered ligation reaction observed in LIDA. This background-triggered reaction occurs in the absence of a template and stems from the four probes used in LIDA. The four probes form a pseudo-blunt end, which is slowly ligated by T4 DNA ligase to generate the target template, triggering LIDA. T4 DNA ligase uses ATP as cofactor and is involved in all the three steps involved in the mechanism of ligation by the enzyme. The Hili group showed that modified ATP influences the specificity of the ligation reaction of nicked DNA duplexes. Therefore, we hypothesized that using ATP derivatives bearing different modifications, the pseudo-blunt end ligation might be perturbed to a much bigger extent compared to the DNA-templated reaction. We screened three ATP derivatives and one of them, 2-amino-ATP, gave better separation between the kinetic traces of LIDA initiated by template and no template at 1 mM 2-amino-ATP concentration. We found that ligation occurs only in the cycle that has the 5'-phosphate abasic and 3'-hydroxy adenosine, and that this pseudo blunt end ligation reaction is significantly decreased when the 2-amino-ATP and 6-methylamine-ATP were used.

In conclusion, this thesis explores the amplification of DNA and RNA at room temperature using lesion-induced DNA amplification as well as the effect of various ATP derivatives to reduce the background-triggered reaction observed in LIDA.

Preface

Chapter 2 was originally conceived and initiated by an undergraduate student, Catherine Mitran during a summer placement under the supervision of Professor Julianne M. Gibbs. Preliminary experiments were performed by Catherine Mitran and when she left, I took over this project. I continued and expanded the project. Professor J. M. Gibbs mentored and guided me throughout this project as well as contributed in the writing and editing of the manuscript. The latter resulted in a paper ‘Achieving Room Temperature DNA Amplification by Dialling in Destabilization’ published in *Chemical Communication*.

In Chapter 3, the idea of adapting LIDA to RNA targets was originated from Professor J. M. Gibbs and a former Master student Yimeng Li. Upon her graduation, Professor J. M. Gibbs and I mentored several undergraduates on this project namely Camilla Mendes, Jesse Yuzik and Daria Raquel Queiroz de Almeida. Finally, I took over this project and led it to a completely new direction. The RNA LIDA was coupled with a gold nanoparticle assay to allow colorimetric read-out. The aggregated gold-nanoparticles used in this project were synthesized and characterized by Yuning Liu. He also took some of the pictures of the gold nanoparticles for the colorimetric assay. The whole project benefited from the valuable input of Professor J. M. Gibbs from the very beginning to end. This project has evolved into a manuscript entitled ‘Reverse Transcription Lesion-Induced DNA Amplification: An Instrument-Free Isothermal Method to Detect RNA’ and is currently under review at *Analytica Chimica Acta*.

The idea of assessing the 15 different ATP derivatives in LIDA was originated from a conversation between Professor J. M. Gibbs and R. Hili during a conference. After that, I followed up with the Hili group and received the 15 modified ATP from them. The dissolving, aliquoting and characterization by HPLC of the ATP cofactors were performed by me. All the experiments

were conceived by me under the supervision of Professor J. M. Gibbs. The blunt end ligation experiment was done by Sarah Hales during her Chem 403 in our lab. Some of the preliminary experiments using modified ATP-1 and ATP-2 were done by Jisu An, an undergraduate student, during her Chem 401 time in our lab and under my supervision. All the amplification experiments using ATP-1 and ATP-2 that she did were repeated by me and new experiments were conducted too. Moreover, experiments involving ATP-3 were performed by me.

لِيُجْزَىٰ كُلُّ نَفْسٍ بِمَا تَسْعَىٰ

“Everyone is rewarded for the efforts they make”

(The Quran, Surah Taha, 20:15)

To my parents

Acknowledgements

I would like to express my deep gratitude to my supervisor, Professor Julianne M. Gibbs, for her guidance and mentorship throughout my time as a graduate student. She was always helpful and never failed to give good guidance, sound advice and suggestions. Under her supervision, I adapted well to university life in Edmonton. Professor J. M. Gibbs gave me confidence. Her compassion and understanding put me on the right track and molded me to become a scientist. It was not easy combining motherhood, family life and research work. Thanks to Professor J. M. Gibbs, I managed. I will always be grateful to her.

I am equally thankful to my thesis committee members, namely, Professor Dennis Hall and Professor Robert Campbell, who reviewed my progress continuously and gave me unfailing support and advice. I am also thankful to Professor Sheref Mansy and Professor Matthew Macauley for being part of my supervisory committee at such short notice. My thanks also to Gareth Lambkin in Biological Sciences for giving me access to use various molecular biology equipment and always willing to help whenever I encountered any difficulty. I appreciate the support received from my organic TA coordinator, Dr. Hayley Wan. The experience as an organic laboratory TA and session TA was very useful. It broadened my perspective and increased my confidence in both research and teaching. I am grateful to Alberta Innovates Technology Futures for the two-year graduate fellowship, which took me off from my TA commitment and allowed me to focus on my research only.

I also want to acknowledge former group member, Abu Kausar who introduced me to the world of DNA. I would like to thank all the former and current Gibbs lab students. In one way or another, they have all impacted on my academic life. A very special appreciation to Dr. Eiman Osman, for all the time we spent together in the Gibbs lab and outside. We started our doctoral

program together, and over time our relationship developed into a long-lasting friendship. Her support and humor were very important in keeping me focused when things got difficult. Special thanks to Eiman and Nahida for proof-reading my thesis.

I would like to thank my husband, Ridwan, for standing by me and supporting me during my time at the University of Alberta. He took care of the kids during my long hours of work in the laboratory as well as when I was writing my thesis. My two children, Maeyra and Zeyaan, took me away from my studies for two years. Although it delayed my research, the time spent with them was well deserving. They are wonderful children and taught me how to become more organized so that I could combine professional life with family life.

My parents are amazing people. Despite being far away, we are always close. Their love and encouragement are invaluable. My brother Saleem and his wife Tabassoom, my sister Sabeba and her husband Gilles and my younger sister Sameena have all been very supportive. I cannot forget the little guys in my life, namely, nephews Farhaan, Noam and Ashfaaq.

I would like to mention my late grandparents for making me the person I am today; their blessings gave me strength. I must express my gratitude to a special person, my uncle Dr. Ibrahim Alladin, a former graduate and professor at the University of Alberta. He introduced the university to me and guided me to get to Alberta. Since I was in high school, he mentored me and pushed me to pursue my studies. I was amazed by his willingness to proofread the countless pages of a chemistry dissertation. Special thanks to my Aunty Naseem and my late Uncle Assen as well as my mother-in-law and my late father-in-law, and to everyone that played a part to help me complete my studies.

I am a spiritual person and therefore, acknowledge the presence of the Almighty, for giving me the energy, inspiration and guidance to reach where I am today.

Table of Contents

Title	i
Abstract	ii
Preface	iiiv
Acknowledgements	viii
Table of Contents	x
List of Tables	xvi
List of Figures and Schemes	xvii
List of Symbols/Abbreviations	xxiv
Chapter 1	1
General Introduction	1
1.1 Global Threat	2
1.2 Ideal Point-of-Care Test.....	6
1.3 Overview of ASSURED Criteria	7
1.3.1 Affordable.....	7
1.3.2 Sensitivity	9
1.3.3 Specificity.....	9
1.3.4 User-Friendly.....	9
1.3.5 Rapid and Robust.....	10
1.3.6 Equipment-Free	10
1.3.7 Deliverable to End-Users.....	11
1.3.8 Application of ASSURED.....	11

1.4	Nucleic Acid Testing	11
1.4.1	Defining Room Temperature.....	15
1.4.2	Enzymatic NAAT Suitable for 30 °C or Below	17
1.4.2.1	Rolling Circle Amplification (RCA).....	17
1.4.2.2	Recombinase Polymerase Amplification (RPA).....	21
1.4.2.3	Multiple Displacement Amplification.....	24
1.4.2.4	Catalytic Hairpin Assembly Coupled with Nicking Endonuclease.....	26
1.4.3	Non-Enzymatic Room Temperature NAAT.....	28
1.5	Objectives	35
Chapter 2	39
Achieving Room Temperature DNA Amplification by Dialling in Destabilization.....		39
2.1	Introduction.....	40
2.2	Cross-Catalytic Amplification using Two Destabilizing Elements	41
2.2.1	One Destabilizing Lesion: Abasic Group.....	43
2.2.2	Two Destabilizing Lesion: Abasic and A:G Mismatch.....	43
2.2.2.1	Single Turn-Over Reaction.....	43
2.2.2.2	Cross-Catalytic Reaction	44
2.2.3	Influence of Abasic + Different Mismatches on T_0	47
2.2.4	Correlation Between Stability of Mismatch Versus T_0	50
2.3	LIDA using Abasic + A:C Mismatch at Room Temperature	51
2.4	Competing Ligation Reaction	53
2.5	Conclusion	55

2.6	Experimental.....	56
2.6.1	General.....	56
2.6.2	Preparation of Oligonucleotides.....	57
2.6.3	StainsAll Preparation for Strand's Purity.....	58
2.6.4	MALDI Characterization.....	60
2.6.5	Thermal Dissociation Experiment.....	61
2.6.6	15% Denaturing Polyacrylamide Gel Electrophoresis.....	61
2.6.6.1	Sample Preparation for PAGE.....	62
2.6.6.2	Preparation of 15% PAGE.....	62
2.6.6.3	Running PAGE Gel.....	63
2.6.6.4	Quantifying Ligation Yields and Turnover Numbers (TON).....	63
2.6.7	DNA Ligation Experiments.....	64
2.6.7.1	Single Turn-Over Reaction.....	64
2.6.7.2	Cross Catalysis.....	64
2.6.8	Gel Images.....	65
Chapter 3	73
Reverse Transcription Lesion-Induced DNA Amplification: An Instrument-Free Isothermal Method to Detect RNA	73
3.1	Introduction.....	74
3.2	Design of Isothermal RNA Transcription Lesion-Induced DNA Amplification.....	76
3.3	Optimization of RNA Transcription-Lesion Induced DNA Amplification.....	78
3.3.1	Influence of ATP Concentration in the RNA-Templated Synthesis of cDNA.....	78

3.3.2	Tuning the Temperature of the cDNA-Initiated LIDA	80
3.3.3	Combining RNA Transcription and LIDA.....	81
3.4	Sensitivity of the Assay	83
3.5	Selectivity of the Assay	85
3.6	Detection of RNA Target Spiked in Total RNA Samples	86
3.7	Colorimetric Detection.....	89
3.7.1	RT-LIDA Followed by Colorimetric Detection at Room Temperature	89
3.7.2	RT-LIDA in the Presence a Mismatched and Random RNA.....	92
3.7.3	RNA Spiked in HLTR Samples.....	94
3.8	Conclusion	95
3.9	Experimental.....	96
3.9.1	General.....	96
3.9.2	Synthesis and Characterization of DNA.....	97
3.9.3	Preparation of DNA-Modified AuNPs.....	100
3.9.4	RNA-Transcription LIDA Protocol.....	100
3.9.5	Preparation and Running of Denaturing Polyacrylamide Gel Electrophoresis	101
3.9.6	Quantifying Ligation Yields and Δ POI	101
3.9.7	Gel Images.....	102
Chapter 4	108
Influence of the ATP Derivatives on Lesion-Induced DNA Amplification	108
4.1	Introduction.....	109
4.2	Source of Background-Triggered LIDA.....	110

4.3	ATP-Dependent T4 DNA Ligase.....	112
4.4	Reports Investigating Various ATP Derivatives as a Cofactor for T4 DNA Ligase	119
4.5	Our Experimental Approach.....	124
4.5.1	Preparation and Characterization of ATP Cofactor.....	125
4.5.2	LIDA using T4 DNA Ligase in the Presence of ATP Derivatives.....	126
4.5.3	LIDA using T4 DNA Ligase in the Presence of the Modified ATP Cofactors	128
4.5.4	Efficiency of ATP-2 and ATP-3 in LIDA	130
4.5.5	Effect of ATP and Modified ATP on Pseudo-Blunt End Ligation.....	131
4.6	Conclusion	134
4.7	Experimental.....	135
4.7.1	General.....	135
4.7.2	Quantification and Analysis	135
4.7.3	Preparation of Ligation Buffer	136
4.7.4	LIDA: Cross Catalysis.....	136
4.7.4	Pseudo-Blunt End Experiment	137
4.7.5	HPLC Procedure and HPLC Chromatogram.....	137
Chapter 5	141
Conclusions and Future Plans	141
5.1	General Conclusions	142
5.2	Future Plans	144
5.2.1	Reducing the Background-triggered Amplification of LIDA	144
5.2.2	Detection of Real Target with Sample Preparation	146

References..... 148

List of Tables

Table 1.1 Example of the ASSURED criteria. Table reproduced with permission from reference 33. Copyright © 2012 World Health Organization.	8
Table 1.2 Current isothermal NAAT. ^{25, 44-46}	13
Table 1.3 Example of some of the current FDA-approved NAAT. ^{37-38, 75, 78}	15
Table 2.1 DNA sequences used in this project.....	59
Table 2.2 MALDI-TOF of DNA sequences.....	60
Table 3.1 DNA and RNA sequences.....	98
Table 3.2 DNA sequences for colorimetric detection with DNA-modified AuNPs.....	98
Table 3.3 MALDI characterization.	99
Table 4.1 Discrimination factor of ATP and modified ATPs	131
Table 4.2 Probe DNA sequences involved in the pseudo-blunt end ligation. Color coded according to probes in Figure 4.1.	132
Table 4.3 DNA sequences used in this project.....	135
Table 5.1 Room temperature isothermal nucleic acid techniques.....	145

List of Figures and Schemes

Figure 1.1 Process of clinical testing for central laboratory and point-of-care testing. Image regenerated with permission from reference 26.....	6
Figure 1.2 Map of Africa representing the mean indoor and outdoor mean temperatures during the month of January, April, July and October.....	16
Figure 1.3 Schematic representation of rolling circle amplification (RCA).....	18
Figure 1.4 Scheme representing A) double-stranded circular genome of PV using multiply primed rolling circle amplification.....	20
Figure 1.5 Scheme representing the process of recombinase polymerase amplification. A complex is formed between the DNA primers (blue and green).	22
Figure 1.6 Schematic representation of multiple displacement amplification (MDA). The double stranded DNA is denatured into single stranded DNA,.....	25
Figure 1.7 Schematic representation of catalytic hairpin assembly. The target hybridizes with the overhang of the hairpin H1 causing its opening	27
Figure 1.8 Schematic representation of the toehold-mediated strand displacement strategy. This image was redrawn with permission from reference 107	29
Figure 1.9 Schematic representation of the process of hybridization chain reaction (HCR). DNA hairpin 1 (H1) opens in the presence of an initiator.....	29
Figure 1.10 Schematic representation of dual catalytic DNA circuit-induced gold nanoparticle aggregation. Brief description in text.....	31
Figure 1.11 Schematic representation of HCR based assays. A) The presence of target DNA triggers the opening of hairpin DNA-AgNCs, H1.	34

Scheme 2.1 Isothermal lesion-induced DNA amplification (LIDA) using different destabilizing elements for coarse and fine temperature control.	42
Figure 2.1 A) Scheme illustrating the four components in the single-turnover experiment (oval = abasic; Star: fluorescent label; X = base across	44
Figure 2.2 Oval: abasic lesion; Star: fluorescent label. Comparison of LIDA with one destabilizing element (abasic only, where X = T) or two destabilizing elements.....	45
Figure 2.3 Melting profile of the nicked duplex corresponding to DNA-I: DNA-IIa: DNA-IIb(G) . A melting temperature of 11.8 °C was observed.	46
Figure 2.4 The % yield of F-DNA-I formed as a function of time with different concentrations of initial DNA-I template and lower replicator concentrations than standard conditions.	47
Figure 2.5 Temperature-dependent LIDA for two destabilizing element systems containing an abasic group and various mismatches.....	49
Figure 2.6 Linear fit of $\Delta\Delta G$ against the optimum replication temperature for the corresponding matched or mismatched base.	50
Figure 2.7 A) LIDA performed on benchtop at room temperature (21 °C) with two destabilizing elements (abasic (Ab) + mismatch (X = C)).....	52
Figure 2.8 LIDA performed on benchtop at room temperature (24 °C) with two destabilizing elements (abasic (Ab) + mismatch (X = C)) * Reaction was performed only once.	52
Figure 2.9 Comparison of LIDA with one and two destabilizing elements (abasic (Ab) and abasic + mismatch, respectively). A) Cross-catalytic amplification.....	54
Figure 2.10 Chemical structures of the phosphoramidites used in this study. DMT is 4,4'-dimethoxytrityl.....	58

Figure 2.11 Polyacrylamide gel electrophoresis image of a ligation reaction. <i>Lower band</i> : small fluorescent probe and <i>upper band</i> : ligated fluorescent product.....	62
Figure 2.12 Gel images representing the ligation reaction using destabilizing probes (Ab and no mismatch) as a function of time in minutes	65
Figure 2.13 Gel images representing ligation reactions using destabilizing probes containing the abasic and mismatch as a function of time and at different temperatures	66
Figure 2.14 Gel images representing ligation reactions using destabilizing probes containing the abasic and mismatch as a function of time and at different temperatures	67
Figure 2.15 Gel images representing ligation reactions using destabilizing probes containing the abasic and mismatch as a function of time and at different temperatures	68
Figure 2.16 Gel images representing ligation reactions using destabilizing probes containing the abasic and mismatch as a function of time and at different temperatures	69
Figure 2.17 Gel images representing the ligation reaction done on the bench top using destabilizing probes containing the abasic and mismatch	70
Figure 2.18 Gel images representing the single turnover ligation reaction using destabilizing probes (Ab and X=T/G/C mismatch) as a function of time.....	71
Figure 2.19 The concentration of F-DNA-I formed as a function of time with different concentrations of initial DNA-I template and lower replicator	72
Figure 3.1 Schematic of reverse transcription lesion-induced DNA amplification (RT-LIDA). First the RNA target is transcribed into a cDNA strand	78
Figure 3.2 A) Polyacrylamide gel image of the RNA-templated DNA ligation at different ATP concentrations and time points. Lane 1: 10	79

Figure 3.3 A) Kinetics of LIDA using the probe without the A:C mismatch (perfectly matched probe is F-DNA-Ia' which yields F-DNA').....	80
Figure 3.4 Kinetics of cross-catalytic formation of F-DNA at 28 °C initiated by cDNA formed from the templated ligation of 105 fmol (purple, green, red, blue traces).....	82
Figure 3.5 Kinetics of cross-catalytic formation of F-DNA at 28 °C initiated by 14 nM (red and blue trace) or 0 nM (black) RNA.....	83
Figure 3.6 A) Kinetics of cross-catalytic formation of F-DNA at 28 °C initiated by 14 nM (105 fmol), 1.4 nM (10.5 fmol), 140 pM (1.05 fmol), 14 pM (105 amol).....	85
Figure 3.7 Specificity of reverse transcription LIDA. A) Kinetics of F-DNA formation at 28 °C for cross catalysis initiated 14 nM; (105 fmol) of various targets	86
Figure 3.8 Formation of F-DNA initiated by 105 fmol matched RNA (solid trace) and 0 mol matched RNA (faint trace) in the presence of human lungs total RNA	87
Figure 3.9 Kinetics of F-DNA formation at 28 °C for cross catalysis initiated by various concentration of target RNA using lower probe concentration	88
Figure 3.10 Reverse transcription lesion-induced DNA amplification (RT-LIDA) depicting overhangs on probes that lead to an overhang on the cDNA	89
Figure 3.11 Left: Bar graph representing bench-top RNA triggered LIDA performed at room temperature. Red bar represents the concentration of F-DNA formed.....	91
Figure 3.12 Room temperature colorimetric detection of amplicons using toehold mediated DNA-modified gold nanoparticles.....	92
Figure 3.13 Image of DNA-AuNP aggregates after the addition of 3 μ L aliquots of the RT-LIDA reaction initiated by 14 nM (105 fmol) of various targets	93

Figure 3.14 Left: Kinetics of cross-catalytic formation of F-DNA at 28 °C initiated by 105 fmol and 0 mol target RNA in the presence and absence (4 μg) of HLTR.....	94
Figure 3.15 Reduced DNA-AuNP aggregates (33.3%) A) Tubes representing the disaggregation of the DNA-AuNP in the presence of 5 pmol.....	95
Figure 3.16 Structure of thiol-modifier C6 S-S and 3'-thiol-modifier C3 S-S CPG used to synthesize Probe A and Probe B . CPG means controlled pore glass.....	97
Figure 3.17 Gel images representing the ligation reaction using destabilizing probes (Ab and no mismatch) as a function of time in minutes (data shown in Figure 3.3A).....	102
Figure 3.18 Gel images representing the ligation reaction using destabilizing probes (Ab and A:C mismatch) as a function of time in minutes (data shown in Figure 3.3B).....	102
Figure 3.19 Gel images representing the single stoichiometric ligation reaction initiated by 1.4 μM RNA at various ATP concentrations at time points 60 minutes.	103
Figure 3.20 Gel images representing the single stoichiometric ligation reaction initiated by 1.4 μM RNA at 10 μM ATP. These data are exhibited in Figures 3.2B.	103
Figure 3.21 Gel images representing ligation reactions with various wait times for the RNA templated DNA ligation reaction as a function of time.	104
Figure 3.22 Gel images representing control experiment initiated by 14 nM RNA but in the absence of ddDNA as a function of time. These data are exhibited in Figure 3.5, blue trace.....	104
Figure 3.23 Gel images representing ligation reactions with various targets for the RNA templated DNA ligation reaction as a function of time. These data are exhibited.....	105
Figure 3.24 Gel images representing ligation reactions in the presence of human lung total RNA (HLTR) as a function of time. These data are exhibited in Figure 3.8 (red bars).....	105

Figure 3.25 Gel images representing ligation reactions in the presence of <i>E. coli</i> total RNA (EcTR) as a function of time. These data are exhibited in Figure 3.8 (blue bars).....	105
Figure 3.26 Gel images representing ligation reactions with various RNA target concentration. as a function of time in hours.....	106
Figure 3.27 Gel images representing the ligation reaction done on the bench top as a function of time in minutes and at room temperature (shown in Figure 3.11).....	106
Figure 4.1 A) Schematic representation of lesion-induced DNA amplification in the presence of a template. B) The duplex formation of probes in the absence of a template.	111
Figure 4.2 Schematic illustration of a: A) blunt end, B) sticky-end, and C) pseudo-blunt end. D) Chemical representation of the two fragments resulting in a pseudo-blunt end.....	112
Figure 4.3 Mechanism of ligation catalyzed by T4 DNA ligase.	115
Figure 4.4 Structure of T4 DNA ligase-DNA complex: molecular surface(A), cartoon illustration(B), protein surface based on electrostatic potential.....	117
Figure 4.5 AMP interactions with the residues in the NTase domain. Red and green crosses represent water molecules and a magnesium ion present.	119
Figure 4.6 Structure of adenosine triphosphate (ATP), deoxy-adenosine triphosphate (dATP) and 2-aminopurine riboside triphosphate (2AP-TP).....	120
Figure 4.7 ATP analogs used as cofactor for T4 DNA ligase enzyme. (G) Polyacrylamide gel image of the ligation reaction after being stained by Stains-All dye.....	122
Figure 4.8 Schematic representation of LOOPER. In the presence of a template consisting of multiple codon reading frames and a library of pentanucleotides	124
Figure 4.9 A) Modification regions of the ATP cofactor. B) Structure and naming system of modified ATP cofactors.....	125

Figure 4.10 Kinetics F-DNA-I formation at 30 °C for cross catalysis initiated 14 nM (+) and 0 M (-) target DNA-I using NEB buffer or prepared buffer + ATP.....	127
Figure 4.11 Kinetics F-DNA-I formation at 30 °C for cross catalysis initiated 14 nM (+) and 0 M (-) target DNA-I using prepared buffer	129
Figure 4.12 Kinetics of F-DNA-II formation at 16 °C using prepared buffer and 1 mM or 0.025 mM of ATP, ATP-1, ATP-2 and ATP-3	133
Figure 4.13 HPLC chromatogram of ATP.....	138
Figure 4.14 HPLC chromatogram of ADP	138
Figure 4.15 HPLC chromatogram of ATP-1	139
Figure 4.16 HPLC chromatogram of ATP-2	139
Figure 4.17 HPLC chromatogram of ATP-3	140
Figure 5.1 Nucleic acid test scheme. Image reproduced with permission from reference 37. Copyright © 2012, Royal Society of Chemistry.....	146

List of Symbols/Abbreviations

AMP	Adenosine monophosphate
ASSURED	Affordable, sensitive, specific, user-friendly, rapid and robust, equipment-free, deliverable
ATP	Adenosine triphosphate
AuNP	Gold nanoparticle
cDNA	Complementary DNA
CEU	Cohesive end unit
COVID-19	Coronavirus disease 2019
CPG	Controlled pore glass
CT	Computer tomography
CXR	Chest x-ray
DMT	Dimethoxy trityl
DNA	Deoxyribonucleic acid
DSN	Duplex-specific nuclease
DTT	Dithiothreitol
EcTR	<i>E. coli</i> total RNA
EDTA	Ethylenediaminetetraacetic acid
EXPAR	Exponential amplification reaction
FDA	Food and Drug Administration
F-DNA	Fluorescent DNA
HDA	Helicase dependent amplification
HIC	High-income country

HIV	Human immunodeficiency viruses
HLTR	Human lungs total RNA
HPLC	High-performance liquid chromatography
LAMP	Loop mediated isothermal amplification
LIC	Low-income country
LIDA	Lesion-induced DNA amplification
LOOPER	Ligase-catalyzed oligonucleotide polymerization
LRS	Low resource setting
MALDI	Matrix-assisted laser desorption/ionization
MALDI-TOF	Matrix-assisted laser desorption/ionization time-of-flight
MDA	Multiple displacement amplification
miRNA	micro RNA
mRNA	Messenger RNA
NAAT	Nucleic acid amplification tests
NAD ⁺	Nicotinamide adenine dinucleotide
NASBA	Nucleic acid sequence-based amplification
NAT	Nucleic acid tests
NEAR	Nicking enzyme amplification reaction
NEB	New England Biolabs
NFW	Nuclease-free water
PAGE	Polyacrylamide gel electrophoresis
POC	Point-of-care
POI	Point-of-inflection

PPi	Inorganic pyrophosphate
PBS	Phosphate-buffered saline
RAM	Ramification amplification method
RCA	Rolling circle amplification
RDT	Rapid diagnostic test
RNA	Ribonucleic acid
RNaseH	Ribonuclease H
RPA	Recombinase polymerase amplification
RT-PCR	Reverse transcription polymerase chain reaction
SARS-CoV-2	Severe acute respiratory syndrome coronavirus 2
SDA	Strand displacement amplification
TBE	Tris-borate-ethylenediaminetetraacetic acid
TEMED	Tetramethylethylenediamine
T _o	Optimum temperature
TRIS-HCl	Tris(hydroxymethyl)aminomethane hydrochloric acid
WHO	World Health Organization

Chapter 1

General Introduction

1.1 Global Threat

In December 2019, a new virus caused by severe acute respiratory syndrome coronavirus 2 (SARS-CoV-2) and labelled Coronavirus Disease 2019 (COVID-19) by the World Health Organization (WHO) was identified in Wuhan, China.¹⁻³ As the year was coming to an end and everyone was wrapping up 2019, very few had a clue that 2020 would see the beginning of a ‘viruwar’.⁴ Within four months, the entire world was affected by this pandemic with over 7,823,289 confirmed cases and 431,541 deaths (as of June 15, 2020).^{1,5} In Canada, 99,147 cases and 8,175 deaths (as of June 15, 2020) have been reported.⁶ As the death toll mounts, scientists are working hard to develop a vaccine since this will be the most logical way to stop the pandemic.⁷ However, the process of developing and testing a vaccine for global use is lengthy, in terms of time.⁷⁻⁸ Therefore, a complementary approach is to accelerate the diagnosis, which will lead to early treatment, in this case isolation of patients to prevent spreading the virus.

Currently, various methods are being used for the detection of COVID-19, for example chest x-ray (CXR), computer tomography (CT) scanning, serological test and molecular-based method. CXR and CT scanning are performed on the patient chest and the image is evaluated for COVID-19 pneumonia. Despite being used in some situations, this technique is not recommended as first-line testing for patients because it is hard to differentiate whether the infection is due to COVID-19 or seasonal influenza (flu) and the cleaning process after each patient is tedious to remove any COVID-19 virus.⁹⁻¹⁰ On the other hand, rapid lateral flow assays for the detection of antibodies produced during the infection are considered as a useful supplementary tool rather than a diagnostic tool for early infection. The seroconversion of the disease typically occurs around 14 days and peaks around 28 days, which limits early detection using this biomarker.¹¹⁻¹² However,

serological methods would play an important role in studying the epidemiology of the disease and the understanding and determining the threshold of immunity in people who was infected.¹²

The current standard method for the diagnosis of COVID-19 is reverse transcription polymerase chain reaction (RT-PCR) using upper respiratory tract specimens, which include nasopharyngeal swab (NPS) or viral throat swab.¹³ RT-PCR is performed in two steps. The viral RNA is extracted from the collected specimens using RNA extraction kits and then reverse transcribed into a complementary DNA that is then amplified using PCR. Despite being the gold standard, this technique is currently facing several challenges in the detection of COVID-19. Sample collection is invasive and tricky to collect while RT-PCR can be done only in clinical settings using expensive instruments and highly trained technicians.^{2, 9, 13} Another problem with RT-PCR is the risk of false negative and false positive results.¹³ Several cases have been reported where the patient was experiencing symptoms indicating potential contamination with COVID-19 but the test was negative.¹³ For example, in this case report, a 34-year-old male who presented symptoms of COVID-19 (chills and fever, coarse breath sound in the lung) was diagnosed negative by real time RT-PCR four times on four consecutive days. Several CXR and CT scans were performed that revealed various changes in the lungs, which slowly progressed to the entire lung surface within a few days. Finally, on the fifth day, a positive test was obtained by RT-PCR.¹⁴ Therefore, a negative test cannot be used to rule out whether the patient is infected or not. Further and multiple testing using different methods and monitoring are required.¹³⁻¹⁴ Various factors have been attributed to the possible cause of false-negative for COVID-19.¹³⁻¹⁴ Currently, sampling is the major factor contributing for false-negative for COVID-19 and this varies between different hospitals.¹³⁻¹⁴ The health care personnel performing the nasal or throat swab must ensure the proper collection, handling, storing and transportation of the sample. As for the patient, this procedure

can be quite uncomfortable and painful and full cooperation is required.¹³⁻¹⁴ Testing may also be false negative if done too early or too late from the onset of the infection.¹³ If done too early, the viral load might be below detectable level while if done too late, the virus might have already migrated to the lower respiratory tract. Additionally, since this virus is new, the viral load kinetics is still under investigation to determine the timing when it peaks.¹³ Another key factor that decreases the performance of the assay is the genetic diversity and rapid evolution of the virus. Several studies have shown that mutation in the COVID-19 genomic RNA leads to mismatches between target sequence and the primer used in RT-PCR.¹³⁻¹⁴ To circumvent this issue, multiple primers are being used that target the several highly conserved regions of the genomic RNA of the virus.

The above-mentioned challenges are being faced in both high-income countries (HIC) and low-income countries (LIC). In case of inconclusive tests, HIC has the resources and capabilities of redoing the test multiple times and using several other methods to confirm the infection. However, this is not the case for LIC, for example the sub-Saharan countries in Africa, that has a vulnerable health care system with limited financial resources.¹⁵ In case of a rapid widespread of COVID-19, these countries will not be able to afford large scale diagnostics to control the outbreak.¹⁶ Therefore, one strategy to make testing more rapidly and widely available is to develop a point-of-care nucleic acid test.¹⁶ According to WHO, point-of-care test is a medical test that can be performed near, or at, the site of patient care.¹⁷⁻¹⁸ For example, these tests can be conducted in a hospital, emergency department, at the site of an accident, in a physician office or even at home.¹⁸⁻¹⁹ Therefore, such test would be advantageous for low-income countries to deliver timely and quality medical care where health-care infrastructure is weaker.¹⁶⁻¹⁷ The most ideal point-of-care platform for near-patient testing are rapid diagnostic tests (RDT), which by definition are fast

and cost-effective and can be implemented in resource-limited settings. The development of a POC device would also alleviate bottlenecks in testing in case of pandemic outbreak where mass testing is required such as the current situation of COVID-19. Many high-income countries such as the US, Germany, and France are experiencing major delays in delivering test results due to shortage in test kits (reagents and RNA extraction kits) and insufficient test production levels.²⁰⁻²¹ Therefore, the ability to easily mass produce such tests is a key factor.

This problem is not new, though the current pandemic increases the need of POC. Many infectious diseases such as tuberculosis, HIV, Zika, Ebola amongst others have been a threat to many nations especially low-income countries.²² For example, in case of HIV, which is considered the greatest pandemics in human history has caused 32 million deaths since it was first discovered in 1983.²³ In 2018, WHO reported 37.9 million people living with HIV globally with the highest burden in African countries (67% of the total burden).²³ Additionally, a total of 770,000 deaths were recorded due to HIV with 61% in African countries.²³ Although these values are shocking and high, WHO reports that there has been 56% decrease in the number of deaths since 2004 which was its peak and this was attributed to the progress in diagnostics and treatments that was made amenable to high burden regions of the world.²³⁻²⁴ Though there has been major advances with well-established POC tests available for HIV, the high rate of infected individual and death signifies there is still room for improvement. Therefore, much work has been focusing on the development of nucleic-acid based POC that would be applicable to resource-limited settings. The WHO has outlined a series of ideal characteristics that would make the perfect diagnostic tests for low-resource environments.¹⁷ These attributes are referred as the ASSURED criteria, which stand for Affordable, Sensitive, Specific, User-friendly, Rapid and Robust, Equipment-Free, Deliverable.^{17, 25} The overall aim of ASSURED devices is reduce the time it takes from testing to

diagnosis and treatment (Figure 1.1): that is the patient gets tested at the health care facility or in a decentralized POC setting using a point-of-care diagnostic tool and then receives the results the same day, which in turn leads to same day treatment.²⁵

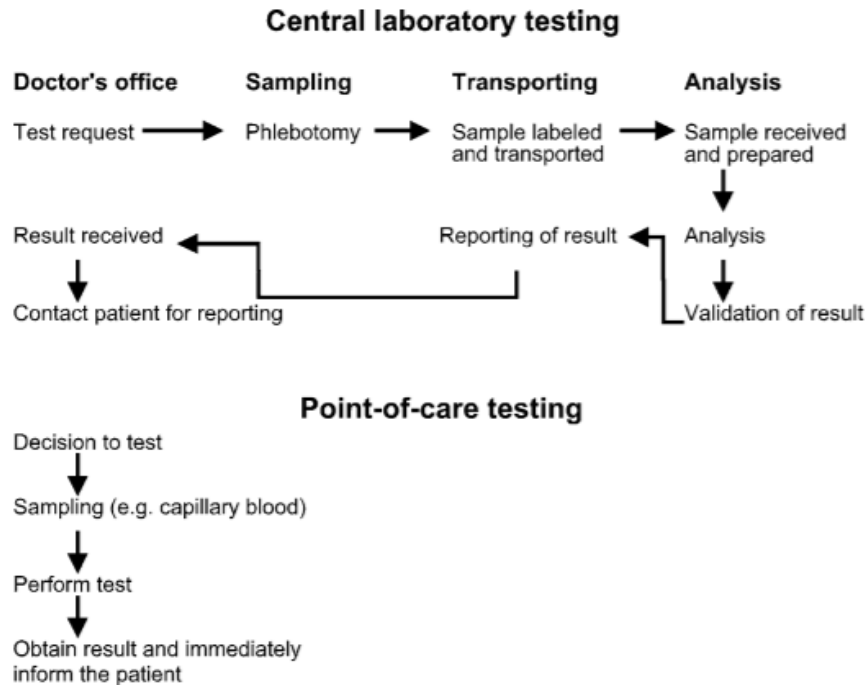


Figure 1.1 Process of clinical testing for central laboratory and point-of-care testing. Image regenerated with permission from reference 26. Copyright © 2005, Elsevier Inc. All rights reserved.

1.2 Ideal Point-of-Care Test

Though the ASSURED criteria are very precise, WHO notes that they are somewhat malleable in certain situations as each diagnostic test needs to be adapted for its specific need. For example, for the diagnosis of human immunodeficiency viruses (HIV) in LRS, low-cost antibody tests are used. However, this is not recommended for infants because it may not accurately reflect the antibodies of the infant. Rather, it will be a combination of the maternal HIV antibodies along

with the infant antibodies or only the maternal one in case the infant is not infected.²⁷ Instead, a viral test is recommended which cannot be performed at the LRS. The only step that can be done remotely in this case is the collection of dried blood sample.¹⁷ Therefore, in these cases, the scope of ASSURED is widened while reviewing the diagnostic test during the selection process.¹⁷

Moreover, it is true that a perfect ASSURED test would be challenging to develop since its direct competition would be the elite laboratory-based assays.¹⁷ Although, the targeted POC test that follows the ASSURED criteria need to be better or equal in performance to “gold standard” tests performed using high-end equipment in a laboratory setting, a less sensitive POC could still be useful if it leads to the most diagnosed cases. For instance, a less sensitive POC test may result in the diagnosis and treatment of more infected individuals as compared to those patients that must wait for several days to get their results as the samples have been sent to a laboratory for testing. In this case, many patients do not come back for the result and treatment.²⁸ For example, in situations where POC is not easily available close to the patient, the latter has to walk to the clinic, which can be far away from their house to get diagnosed.²⁹ If the test requires the patient to come back another day for results, there is high probability the patient never come back which leads to no treatment.²⁹ The same concept applies to all the different attributes of ASSURED. Below is a brief description of the different attributes of the ASSURED criteria.

1.3 Overview of ASSURED Criteria

1.3.1 Affordable

According to the World Bank, low-income countries are defined as countries that have a gross national income (GNI) of less than US \$1,026 per capita.³⁰ A high level of poverty is observed in these countries and therefore accessing proper health care is a challenge especially if it is expensive. This is a challenging situation because typically for low income countries around

50% of the health care finances come from out-of-pocket.³¹ For example, Kenya, which is a sub-Saharan country with a GNI of US \$681 per capita.³² A high level of poverty prevails in this country with 46% of the population living on a budget of US \$1 or less per day.³² In terms of health care, 30% is subsidized by the government, another 19% comes from donations from international and domestic organizations and insurance funds while the remaining 51% are contributed from the population. Having to contribute such a big share for health care makes it difficult for the population to access such services especially if the test is expensive.³² Where the diagnosis and treatments are free, the challenge is raising enough funds to buy supplies to test every patient that comes in. Therefore, while developing point-of-care tests, it is imperative that the cost is kept at its lowest so that to maximize amounts of tests that can be bought and those at risk can afford it.^{17, 25, 28} In a report published in the Bulletin of the WHO, Wu and Zaman reported that the targeted cost of a POC machine for HIV should be less than US \$500 and per test it should cost less than US \$10 (Table 1.1).³³

Table 1.1 Example of the ASSURED criteria. Table reproduced with permission from reference 33. Copyright © 2012 World Health Organization.

Characteristic	Target specification
Affordable	Less than US\$ 500 per machine, less than US\$ 10 per test
Sensitivity, specificity	Lower limit of detection: 500 HIV RNA copies per mL, 350 CD4+ T-cells per μ L
User-friendly	1–2 days of training, easy to use
Rapid and robust	< 30 minutes for diagnosis, < 1.5 hours for HIV load monitoring, minimal consumables (i.e. pipettes), shelf life > 1 year at room temperature, high throughput

Equipment-free	Compact, battery powered, on-site data analysis, easy disposal, easy sample handling, no cold chain
Deliverable	Portable, hand-held

1.3.2 Sensitivity

The sensitivity known as the ‘true positive’ is the number of patients who have the disease that test positive. For instance, a sensitivity of 93% suggests that 93 infected people out of 100 have received a positive result using a particular assay. The remaining 7% is called the false negative (the patient has the disease and should have been tested positive, but the assay tested that person as negative). In general, the higher the sensitivity, the better the assay.^{17, 25, 28}

1.3.3 Specificity

On the other hand, specificity is the ability of a test to generate a true negative. In this case, a high specificity indicates that almost everyone that does not have the disease will test negative and a very low number of false positives are generated. For example, a specificity of 93% means that 93 out of 100 persons that are not infected test negative while the remaining 7% test positive (false positive) even though they do not carry the pathogen.^{17, 25, 28}

1.3.4 User-Friendly

Under the ASSURED criteria, user-friendly signifies that the test should be simple to perform with minimal to no training of the personnel.^{29, 33} Often, health workers who are recruited to work at resource-limited facilities especially those found in rural areas have limited training yet are required to run and maintain equipment. Thus, having an assay that is easy to perform with minimal scientific training would be beneficial.^{17, 25, 28-29} The assay should come with clear visual instructions with minimal steps about how the test is performed.

1.3.5 Rapid and Robust

A rapid test is one that facilitates testing and treatment at the first visit.^{29, 33} This is key for low-income countries because the sick patient can get their result and treatment the same day rather than coming back another day. Very often patients waiting for results that take a long time never come back for a follow-up.²⁷ There are many personal and economic reasons why people do not show up.²⁹ Therefore, having a test that is fast would be advantageous.^{17, 25, 28-29}

A point-of-care diagnostic device that is stable at room temperature and has reagents that can survive temperature fluctuations is a robust one.^{25, 29, 33} The need for refrigeration is a setback as it adds another barrier to its use in resource-limited settings where the number of centralized laboratories are limited.^{29, 33} Most clinics in rural regions have an unstable power supply or no access to electricity.²⁵ Some of these facilities are also found in remote places where it is difficult to transport materials in and out.²⁹ If refrigeration, stable temperature control, and power are the requirements, it will be hard to implement these tests in those areas. Therefore, a test that does not have any storage requirement and a long shelf life is preferred.^{17, 25, 28}

1.3.6 Equipment-Free

As mentioned earlier, POC tests should be operable at resource-constrained environments, which do not have stable power supply and only basic equipment.^{25, 33} Some permanent clinics are lacking in infrastructure, while other clinics might be temporary, i.e. in non-sterile environments like a tent.^{29, 33} In these cases, a test that requires reliable electric supply or extensive instrumentation is unlikely to be implemented.^{17, 19, 25, 28}

1.3.7 Deliverable to End-Users

Physicians, health care workers, nurses and other end-users should be able to access and use the test easily. A portable and hand-held device would be easier than a bigger instrument that comes in multiple pieces and requires several steps to be used.^{17, 25, 28}

1.3.8 Application of ASSURED

Many research groups and diagnostic companies are working on the realization of POC tests that abide by the ASSURED criteria.²⁹ While sensitivity and specificity of assays are widely explored, other criteria from the WHO framework for the perfect diagnostic tool are often neglected.²⁵ One such, is the ‘equipment-free’ parameter, which is often not addressed.²⁹ POC tests that have successfully implemented the ASSURED criteria are typically based on the detection of proteins or small biomolecules such as p24 viral protein for HIV, hCG hormone for pregnancy or glucose for blood sugar level.^{19, 27, 34} The most widely used POC platforms are lateral flow devices that includes glucose meters and pregnancy tests.³⁴ However, although these platforms are simple and easy to use, they still have some drawbacks.³⁴ The main limitations are the high cross reactivity, lack of sensitivity and specificity and quantification.³⁵ Additionally, some of these biomarkers, for example antibodies could take several days to weeks to appear in the bloodstream to allow positive detection.³⁶ Another challenge involved with antibody testing is that the test cannot differentiate whether the antibody detected is due to an active infection, past infection or the result of a vaccination.³⁶ To circumvent these limitations, tests based on nucleic acid was developed.³⁶

1.4 Nucleic Acid Testing

Nucleic acid test (NAT) is a molecular diagnostic technique that detects the nucleic acid (DNA or RNA) of a pathogen from biological samples like urine, blood, saliva, etc.³⁷ Detection of

the genetic material allows accurate and early detection of diseases.³⁶ NAT also facilitates the detection of multidrug resistant strains of a disease as well as allows multiplex detection.³⁸ Using this method, asymptomatic patients for certain diseases like COVID-19 can be diagnosed, resulting in timely course of action or treatment.³⁹ However, during an infection, the amount of pathogens present in a patient is typically low, which results in a low concentration of its genetic material.⁴⁰ Therefore, a key step to identify nucleic acids is to amplify the sequence of interest to detectable levels. In other words, take a tiny amount of the nucleic acid and multiply it using amplification methods to attain a detectable amount. Such NAT methods are called nucleic acid amplification tests, NAAT. The most popular NAAT for genetic material amplification is the polymerase chain reaction (PCR).³⁷ PCR employs repeated heating and cooling to amplify a target nucleic acid exponentially. Consequently, the thermocycler requirement makes the equipment complex, expensive and difficult to implement as a point-of-care test in resource-limited settings.²⁵ To address this issue, less complex isothermal amplification platforms such as loop mediated isothermal amplification (LAMP), strand displacement amplification (SDA), rolling circle amplification (RCA) and nucleic acid sequence-based amplification (NASBA) have been developed.²⁵

The use of a constant temperature has simplified the instrumentation tremendously, which has led to a reduction of costs.²⁵ Also, being isothermal made them more amenable to POC diagnostics compared to PCR.²⁵ Nevertheless, the use of a heat incubator is still required since these strategies operate best at relatively high temperatures (Table 1.2).²⁵ Taking into consideration the ‘equipment-free’ criteria from ASSURED, a number of research groups have come up with various ways to circumvent this problem by incorporating portable temperature controllers that do not rely on external power supplies to operate. For example, LaBarre *et al.* developed an incubator

that uses heat from an exothermic reaction that is linked to an engineered phase change material.⁴¹ In another effort, Snodgrass *et al.* used sunlight and flame to provide heat for a LAMP reaction in a device they called TINY.⁴² Interestingly, Crannell *et al.* proposed body heat as a low cost solution to incubate RPA reaction for the detection of HIV-1 DNA. They tested four spots, the fist, pocket, abdomen and axilla (armpit), for harnessing body heat.⁴³ All of these electricity-free isothermal NAAT platforms have great potential but are still under research and are yet to reach clinical trials. However, many NAAT exist that are Food and Drug Administration (FDA)-approved but they are mostly limited to well-equipped clinical and laboratory facilities or only for research purposes.³⁷⁻
³⁸ Among those, PCR has been most widely implemented, while isothermal methods are now becoming more and more available.

Table 1.2 Current isothermal NAAT.^{25, 44-46}

Method	Full Name	Reaction Temp. (°C)
NASBA	Nucleic Acid Sequence Based Amplification	37-41 ⁴⁷
HDA	Helicase Dependent Amplification	37-65 ⁴⁸⁻⁵⁰
LAMP	Loop Mediated Isothermal Amplification	60-65 ⁵¹⁻⁵⁶
NEAR	Nicking Enzyme Amplification Reaction	55-59
RCA	Rolling Circle Amplification	Room Temp., 30-65 ⁵⁷⁻⁶¹
RPA	Recombinase Polymerase Amplification	30-42 ⁶²⁻⁶⁵
RAM	Ramification Amplification Method	35 ⁶⁶
EXPAR	Exponential Amplification Reaction	60 ⁶⁷
MDA	Multiple Displacement Amplification	30-37 ⁶⁸
SDA	Strand Displacement Amplification	37, 49 ⁶⁹⁻⁷⁰
LIDA	Lesion-Induced DNA Amplification	30 ⁷¹⁻⁷³

Though based on PCR, one recent example of a POC that still requires access to steady power-supply and highly trained staff is the most current test from Cepheid, the Xpert® Xpress SARS-CoV-2, which has been approved by the FDA for point-of-care testing of COVID-19. What makes this equipment so special is that it comes with a cartridge that contains all the reagents (liquid and lyophilized) required for extraction, purification, amplification and detection.⁷⁴ This platform can be used in clinics and hospitals instead of sending samples to laboratories, and as such it is a POC technique. However, it is still not suitable for places that are limited in terms of infrastructure, power supply, and resources. Adding to that, the equipment and the cartridges are quite expensive for low-and middle-income countries especially if testing needs to be scaled up. The GeneXpert IV module/desktop or laptop is currently being marketed at a price of ~ US \$ 17,500 and the cartridges are being sold at a price of US \$20 in 145 low- and middle- income countries including my home country Mauritius (<https://www.finddx.org/pricing/genexpert/>). If the government of Mauritius (population of 1.2 million) has to do 10,000 tests in the coming days, the cost of the cartridges alone will be US \$20,000. This is equivalent to 8,000,000 Mauritian rupees, which is significant for Mauritius. Likewise, there are many approved FDA NAAT that are in the market but limited to centralized laboratories.^{38, 75} Some examples are listed in Table 1.3.

Despite all efforts, these isothermal amplification techniques have been severely restricted for point-of-care applications.⁷⁶ Thereby, an isothermal nucleic acid amplification platform that is fast and operates at room temperature with simple reaction conditions would be ideal.⁷⁶ Such assays, will be energy-saving and cost-effective as no thermocycler and expensive instrumentation would be required.⁷⁷ Therefore, I will next focus on reviewing POC diagnostic assays that are

instrument-free with special attention to those that operate at room temperature for nucleic acids biomarkers.

Table 1.3 Example of some of the current FDA-approved NAAT.^{37-38, 75, 78}

Platform	Manufacturer	Amplification technique
GeneXpert	Cepheid	PCR
Liat Analyzer	IQuum	PCR
MDx	Biocartix	PCR
Twista	TwistDX	RPA
BART	Lumora	LAMP
Genie II & Genie III	Optigene	LAMP
LA-320	Eiken Chemical Company Ltd	LAMP
SAMBA	Diagnostic for the Real World	NASBA
ProbeTec	Becton Dickinson & Co	SDA
APTIMA®	Hologic® Inc.	TMA
AmpliVue	Quidel Corporation	HDA

1.4.1 Defining Room Temperature

Room temperature, also known as ambient temperature, is the parameter that I will be addressing throughout my thesis. Therefore, it is imperative to understand the concept of room temperature. According to Oxford dictionary, room temperature refers to the normal temperature inside a building.⁷⁹ Room temperature varies from country to country as well as from the time of the day.

In terms of room temperature point-of-care, it is more applicable for resource-constraint countries. As of 2020, there are currently 32 low-income countries with the majority located in sub-Saharan Africa.⁸⁰ Glunt *et al.* reported the mean indoor and outdoor temperatures throughout Africa (mostly sub-Saharan countries).⁸¹ As shown in Figure 1.2, the mean outdoor temperature was 13-30 °C and the mean indoor room temperature range from 17-30 °C.⁸¹ Therefore, we conclude that an assay that works at room temperature must operate between 17-30 °C.

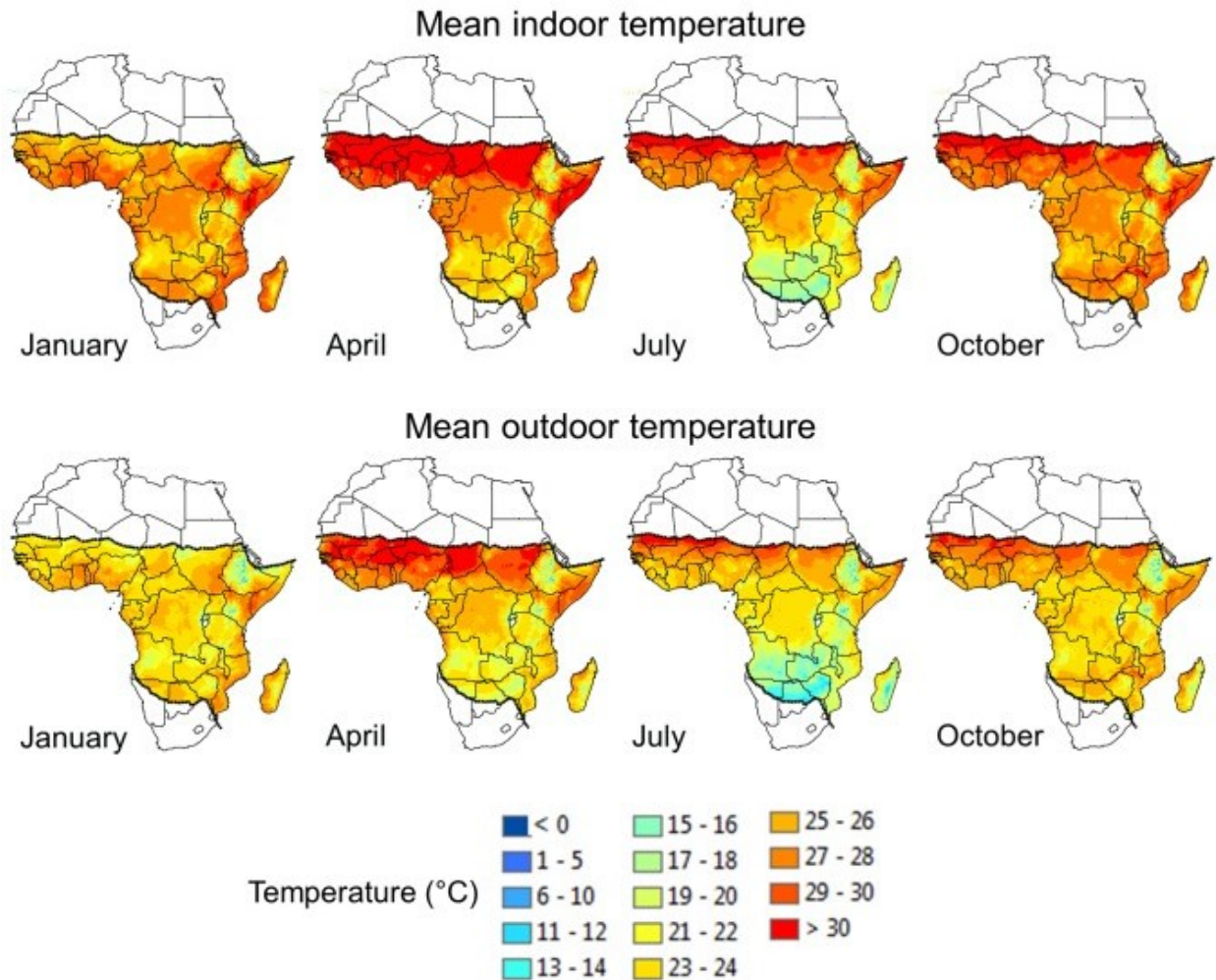


Figure 1.2 Map of Africa representing the mean indoor and outdoor mean temperatures during the month of January, April, July and October. Images were adapted with permission from reference 81. Copyright © 2013, Glunt *et al.*

1.4.2 Enzymatic NAAT Suitable for 30 °C or Below

Enzymatic NAAT are techniques that rely on enzyme(s) for the amplification of the DNA or RNA biomarker sequence. Depending on the method and the target, one or more enzymes are employed.⁷⁸ For example, RCA uses a ligase for ligation of a circular DNA and a polymerase with strand displacement capability for polymerization.^{57-58, 82} On the other hand, HDA uses a helicase enzyme, which mimics the natural DNA replication process by unwinding the duplex DNA followed by replication of the biomarker using a DNA polymerase.⁴⁹ LAMP uses only one enzyme, a polymerase that has the properties of displacing DNA from the template, while RT-LAMP uses a reverse transcriptase and a polymerase.⁸³ Among all the enzymatic amplification methods, only RCA, RPA, and MDA were found to work at or near room temperature albeit not over the identified range of 17-30 °C.

1.4.2.1 Rolling Circle Amplification (RCA)

RCA is an isothermal nucleic acid amplification method that can use linear or circular DNA/RNA as template to generate a long single stranded DNA.^{57-58, 84} A padlock DNA probe hybridizes in a circular fashion to form a nicked duplex in the presence of a target DNA as shown in Figure 1.3. The nicked duplex is then ligated using a DNA ligase to form a product duplex, which consists of a circular DNA and the target DNA. Following that, the target DNA or another short strand of DNA acts as a primer and is extended in the presence of a polymerase while displacing the downstream complementary strand as it copies the circular DNA. Consequently, a tandem-repeat complementary to the circular DNA is generated. Derived from *Bacillus subtilis* bacteriophage, Phi29 or Φ29 DNA polymerase is the most often used enzyme for RCA due to high processivity (this enzyme adds an average of 70 000 nucleotides each time it binds to the primer-target DNA before dissociating⁸⁵) and strand displacement activity.^{60, 85} RCA has

shown excellent amplification over a wide range of temperature, from 25 °C to 60 °C.^{44, 59-61} This ability to work at room temperature (25-30 °C) makes it a possible method to be implemented for instrument-free point-of-care diagnostic analysis in certain climates.

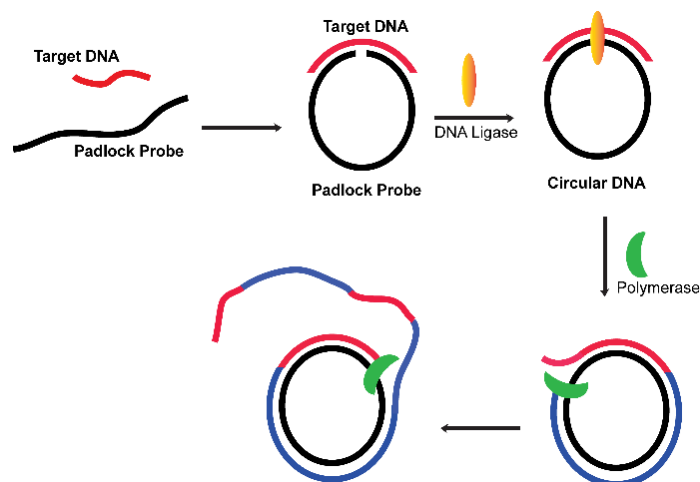


Figure 1.3 Schematic representation of rolling circle amplification (RCA).

As an example of RCA performed at lower temperature for infectious disease detection, Annabel *et al.* reported the amplification of papillomavirus using multiply primed RCA. The genome of this virus is a double-stranded circular DNA, which makes it suitable to be used directly as a template for RCA. After a denaturation step at 95 °C for 3 min to generate single stranded circular DNA, several short hexamers that act as primers hybridize to both circular templates and get extended by Φ 29 polymerase (Figure 1.4A). The amplification was performed at 30 °C for 16 hours and followed by an enzyme deactivation step at 65 °C for 5 min to stop the reaction.⁸⁶

RCA has also been used to amplify non-circular targets such as linear DNA targets at lower temperatures. In a report where RCA was used for *Salmonella* detection, a ligation step was performed prior to RCA (Figure 1.4B). AmpLigase was used to ligate a padlock DNA after hybridization with the *Salmonella* DNA target. The ligation step was performed by thermocycling

(20-40 cycles) between 92 °C (1 min) and 62.5 °C (20 to 120 s). Following that, the RCA was conducted for 30-60 min at 30 °C using an incubator and for 60 min at room temperature (~25 °C).⁵⁷ RCA was also employed near room temperature for the detection of miRNA, which are important biomarkers for medical conditions like various type of cancers and Alzheimer's amongst others.^{58, 87-89} Xu *et al.* used let-7a miRNA target to template the ligation of a padlock DNA using T4 DNA ligase at 16 °C for 2 hours (an annealing step was performed prior to the ligation step: 90 °C for 3 min followed by cooling down to room temperature). As shown in Figure 1.4C, the miRNA was used as primer, which was then extended using Φ 29 polymerase for 2 hours at 30 °C. The reaction was stopped by denaturing the enzyme at 90 °C for 2 min. In this work, the RCA was followed by strand displacement amplification to facilitate detection (37 °C for 2 hours).⁵⁸ In another work using RCA for the detection of miRNA-21, the ligation step was performed at 16 °C overnight followed by RCA at 30 °C for 6 hours.⁸⁷

Though RCA is isothermal and works at a room temperature of 25 °C or 30 °C, the above examples illustrate that most applications of the method employ different temperatures prior and/or after the amplification step, which make the whole process non-isothermal and incompatible for instrument-free point-of-care.⁷⁷ However, it should be noted that the focus of these reports employing RCA for the detection of nucleic acids did not refer to themselves as POC platforms. On the other hand, several other works that were motivated based on POC purposes were found to work at an amplification temperature higher (37 to 60 °C) than our defined criteria for room temperature.⁹⁰⁻⁹² Despite the attempt to be suitable for point-of-care, these reports still suffer from the same limitation of multiple changes in temperature, which would make them difficult to implement as a POC platform for low-resource setting. Adding to that, long-term storage and

mass-production is not suitable for RCA reagents as it is known to cause non-specific cross-linking.⁷⁸

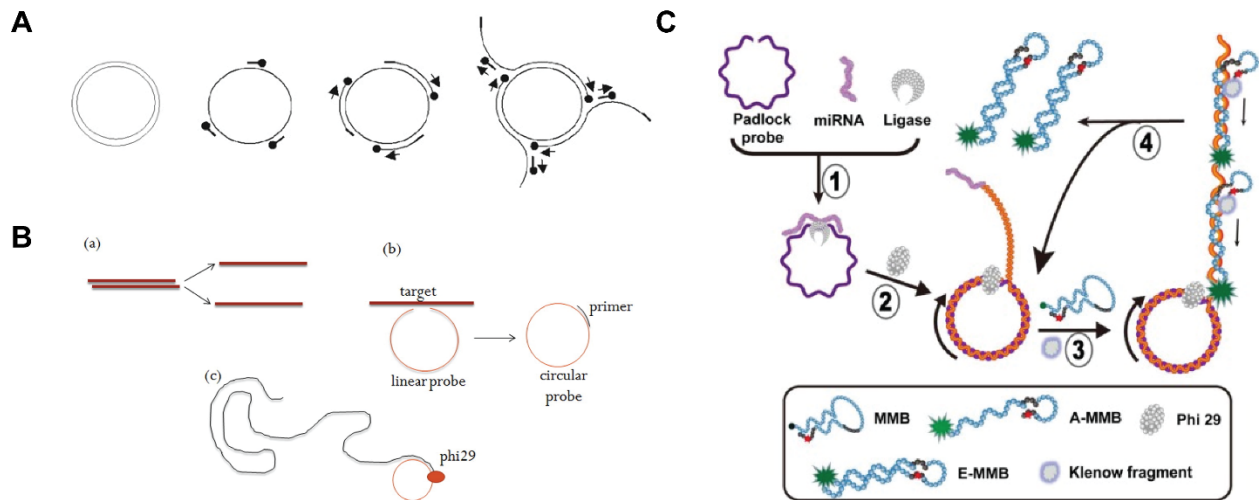


Figure 1.4 Scheme representing A) double-stranded circular genome of PV using multiply primed rolling circle amplification. Multiple primer hybridizes with the circular DNA which is then extended using $\Phi 29$ polymerase. This figure was adapted and modified with permission from reference 86. Copyright © 2004, American Society for Microbiology. B) Salmonella DNA was used as a target for ligation of a padlock probe using T4 DNA ligase. Then upon hybridization of a primer to the cyclized padlock probe, rolling circle amplification was conducted. This image was regenerated with permission from reference 57. Copyright © 2016, Elsevier B.V. C) in the first step, let-7a miRNA template the ligation of a padlock DNA probe which was then followed by rolling circle amplification using the miRNA as primer. The RCA product then triggers the opening of a multifunctional molecular beacon, which leads to a fluorescence response. The last step is to strand displacement amplification that occurs on the MMB to liberate it from the occupied site of the RCA product. Scheme regenerated with permission from reference 58. Copyright © 2018, Elsevier B.V.

1.4.2.2 Recombinase Polymerase Amplification (RPA)

Recombinase polymerase amplification (RPA), currently commercialized by TwistDx (www.twistdx.co.uk) was first reported by Piepenburg *et al.* in 2006.⁹³ This isothermal amplification platform has a simple primer design and operates over a wide range of temperature without precise temperature control, typically 37 to 42 °C.⁹³⁻⁹⁴ However, it was also found to work as low as 30 °C, which falls at the edge of our room temperature range.^{62, 94-95} The RPA reaction illustrated in Figure 1.5 starts by the formation of recombinase nucleoprotein filament, which is the complex formed between the recombinase and the single stranded DNA (ssDNA) primers with the help of loading factor. The filament then scans the double stranded DNA (dsDNA) target in search of the complementary sequence corresponding to the primers. Once the homologous sequence is found, the dsDNA is locally separated to form a D-loop structure. The primer then hybridizes to the complementary side while the other unwound side is stabilized by single-stranded binding proteins. The recombinase is recycled for the next pair of primers. Next, the primers are extended by a DNA polymerase with strand displacement ability to form double-stranded DNA each bearing a parent strand. The whole RPA process is then repeated in an exponential fashion.⁶⁵

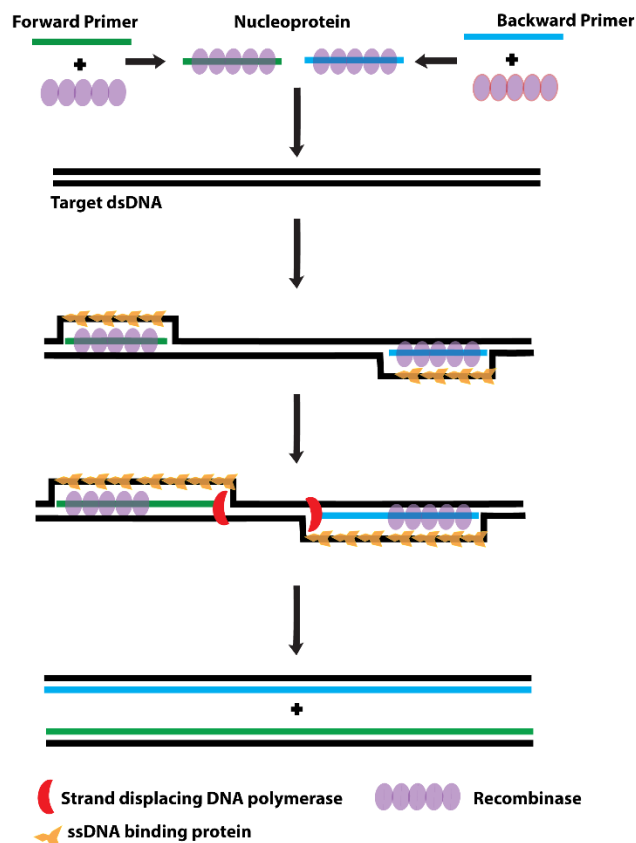


Figure 1.5 Scheme representing the process of recombinase polymerase amplification. A complex is formed between the DNA primers (blue and green) and the recombinase protein (purple), which is then directed to the homologous sequence of the double-stranded target DNA (black). The primer is transferred to the complementary side, which is followed by amplification catalyzed by DNA polymerase (red) while SSB (orange) stabilizes the displaced strand. Image redrawn from this reference 77. Copyright © 2014, Baishideng Publishing Group Inc.

In an equipment-free RPA assay, Lillis *et al.* reported the detection of HIV-1 Proviral DNA using equipment-free RPA assay.⁶² In this work, they conducted the RPA amplification using TwistAmp RPA reaction kit from TwistDx Ltd (UK) at an ambient temperature ranging from 15 to 44 °C. An environment control chamber was used to mimic various room temperature. The amplification was performed in a total volume of 50 µL in a 0.2 mL PCR tube, which was placed

in a metal block at the desired room temperature. During the incubation, the sample in the tubes were mixed by inverting the tubes three times at five minutes. BESt cassette (immuno-chromatographic strip) or gel electrophoresis was used to detect the amplification products. They observed excellent amplification of the target DNA for temperatures between 31 to 43 °C in 20 minutes. At temperatures below 30 °C, false negatives were obtained, and this was attributed to the reduced activity of the enzyme at that temperature. For days when the ambient temperature is not within the range of the assay (31 °C to 43 °C), they developed an exothermal heater using sodium acetate trihydrate at various compositions to produce the right amount of heat leading to the desired temperature.⁶² The proposed amplification platform was fast and worked over a wide range of room temperatures (31 °C to 43 °C) making it amenable to point-of-care analysis in countries where the ambient temperature is above 31 °C.⁷⁸ In countries the room temperature is below 31 °C, which is the case in most of the sub-Saharan Africa countries, this assay cannot be used, therefore limiting its use in countries where they are most needed. Another drawback is the multiple manual steps involved that limits its use as a POC assay.⁶² Additionally, in this report, the author only focused on showing the feasibility of using RPA at a room temperature. The sensitivity and specificity of the assay at various environment mimicking ambient temperatures were not assessed.⁶² These parameters have been addressed in several other reports that focus on the performance of RPA using the TwistAmp kit.⁹⁶

We note that several other studies have indicated that RPA can be performed efficiently at temperatures ranging from 30 to 45 °C RPA.^{63, 95, 97} RPA is also suitable for RNA target by incorporating a reverse transcription step prior to amplification.⁶³

1.4.2.3 Multiple Displacement Amplification

Another isothermal DNA amplification technique that is known to work at a low temperature of 30 °C is multiple displacement amplification (MDA).⁴⁶ Though rare in terms of application in disease diagnosis, MDA has been extensively used for whole genome amplification (WGA), which is particularly useful for genotyping and single nucleotide polymorphism (SNP) detection.⁹⁸⁻¹⁰⁰ This technique offers several advantages compared to other WGA techniques like PCR; for example it exhibits full coverage, very low error rate (99.8% of the genome is retained), and can amplify very small amount of sample including DNA from one cell.^{99, 101} One application of MDA is in forensic laboratories where tiny amount of samples, recovered from a crime scene need to be genotyped.⁹⁹ MDA is commercially available in kits from several companies such as GenomiPhi and TempliPhi from GE Healthcare and Repli-g from Qiagen.⁹⁹

In MDA, the genomic dsDNA is denatured to ssDNA at 95 °C as the first step. The primers are typically hexamers that hybridize at various locations along the ssDNA target in the sample. The amplification process, typically performed at 30 °C for a duration of 16-18 hours, is then facilitated by DNA polymerase that has the capability to displace the downstream DNA.⁴⁶ Lastly, the polymerase is inactivated at 65 °C to terminate the amplification reaction (Figure 1.6).⁴⁶ A few reports have been published for the amplification of the genetic material of infectious diseases using MDA. Wang *et al.* explored the use of MDA as a technique to efficiently expand the low stocks of malaria parasite DNA.¹⁰² George *et al.* has sequenced mycobacteria DNA from sputum samples. They indicated that this was an ideal tool to detect pathogens that are difficult and/or slow to grow in culture (up to 5 to 6 weeks if bacterial load is low for *Mycobacteria Tuberculosis*).¹⁰³ In another report, Liu *et al.* amplified and sequenced the whole genome of ZIKA virus to compare it with other strains of ZIKA virus.¹⁰⁴ In all these reports, MDA was conducted at 30 °C, which is

the upper limit of our room temperature range.¹⁰²⁻¹⁰⁴ For temperature below 30 °C, this technique will not be useful. Additionally, MDA suffers from a long reaction time of 16 – 18 hours, which limits its use at the POC.

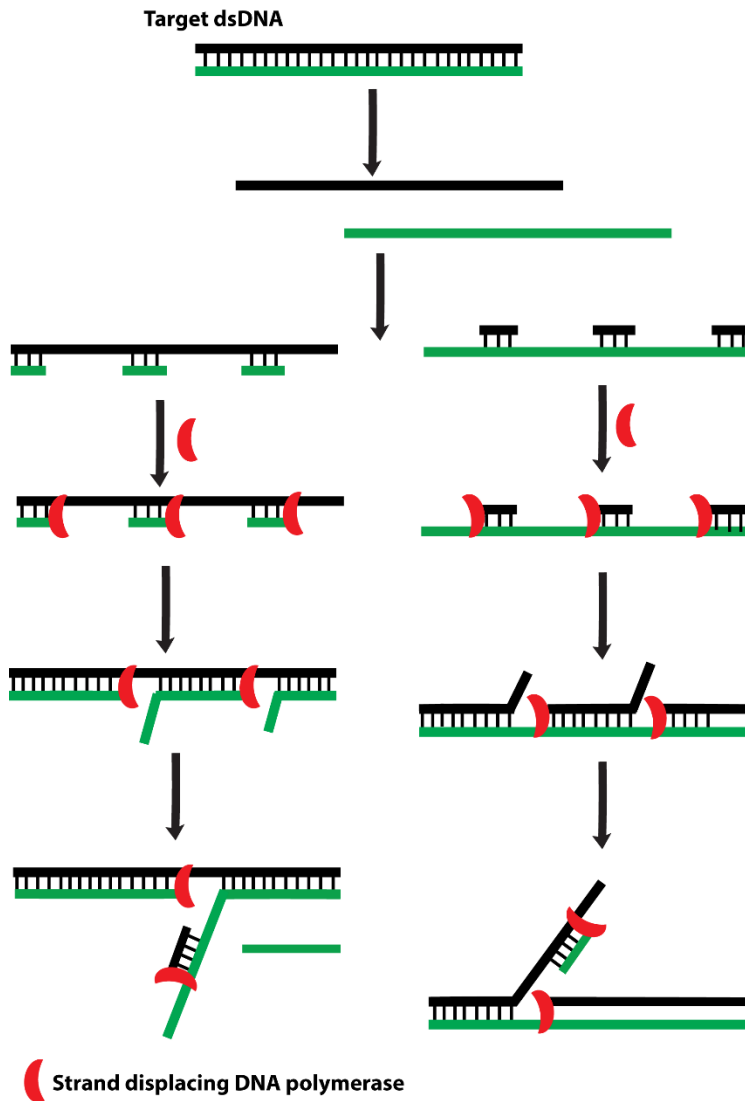


Figure 1.6 Schematic representation of multiple displacement amplification (MDA). The double stranded DNA is denatured into single stranded DNA, which was followed by the annealing of short primers at various locations. DNA polymerase facilitates the extension of the primers along the target DNA sequence while displacing any complementary DNA downstream.

1.4.2.4 Catalytic Hairpin Assembly Coupled with Nicking Endonuclease

Catalytic hairpin assembly (CHA), which is based on the principle of toehold-mediated strand displacement (TMSD) is an enzyme-free nucleic-acid detection method that works by amplifying the signal produced in the presence of a target (non-enzymatic amplification methods will be discussed in Chapter 1.4.3). To achieve real DNA self-replication rather than signal amplification, Dong *et al.* has combined CHA with a nicking endonuclease. Therefore, generating an increased amount of “replicas” bearing the same sequence of the HIV target DNA.⁷⁶ In this CHA/nicking endonuclease platform, the first step involves the opening of hairpin H1 that is triggered in the presence of a target DNA to form HIV target-H1 duplex (Figure 1.7). Another hairpin H2 present in the system, hybridizes with the exposed part of H1 to regenerate the HIV target, which restarts the cycle again (Figure 1.7, Recycling I). The generation of duplex H1-H2 serves two purposes. Firstly, it leads to a fluorescence signal by toehold mediated strand displacement of a fluorophore DNA oligonucleotide from a quencher DNA oligonucleotide. Secondly, the opening of hairpin H3 is triggered, and this open structure hybridizes partially with both the overhangs on H1 and H2. Finally, after hybridization to H1 and H2, the same sequence as the HIV-target DNA is generated by the action of the nicking enzyme, Nt.BsmA1. This newly generated HIV-target sequence dissociates from the H2 sequence owing to the small number of complementary interactions allowing it to enter Recycling I. The remaining fragment of H3 also spontaneously dissociates or is displaced with another H3 continuing Recycling II and generating more copies of the HIV-target DNA sequence. Amplification using this scheme is very fast, requiring only 10 min at 25 °C to detect HIV DNA targets. However, it is unclear whether they used an incubator or performed it on the bench in the laboratory for this work. Despite being extraordinarily versatile and having a low amplification temperature of 25 °C, making it a potential

candidate for room temperature diagnostics, the pre- and post-amplification steps makes less suitable.⁷⁶ For example, the hairpins were prepared prior to using them by heating at 95 °C for 5 min and cooling at room temperature for 3 hours, and the detection was carried out by measuring the fluorescence using a fluorescence spectrometer, which usually requires power-dependent instrumentation. Furthermore, CHA is also known for high background caused by non-specific hybridization and low sensitivity.^{76, 105} The author pointed that when the assay was performed at 37 °C (optimal temperature for Nt.BsmAI activity), high background was observed due to non-targeted CHA.⁷⁶ This indicates that fluctuations in temperature might cause false positives.

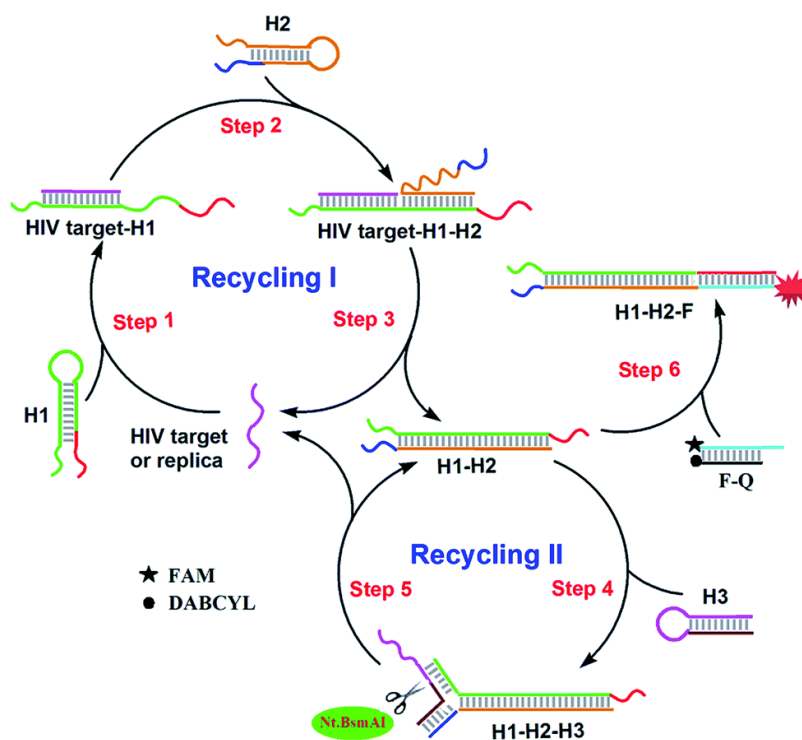


Figure 1.7 Schematic representation of catalytic hairpin assembly. The target hybridizes with the overhang of the hairpin H1 causing its opening and exposing a concealed domain, which triggers the opening of a second hairpin H2. In this process, the target DNA is recycled. Another hairpin H3 bearing a nicking site, hybridizes with the H1:H2 complex. Lastly, the nicking endonuclease

cleaves the DNA at the nicking site to liberate a copy of the target DNA. This scheme was reproduced from reference 76 with permission from the Royal Society of Chemistry (2019).

1.4.3 Non-Enzymatic Room Temperature NAAT

Recently, non-enzymatic strand displacement strategies for exponential amplification of nucleic acids have received major interest, in particular, toehold-mediated strand displacement (TMSD), where CHA is but one example. Developed by Yurke *et al.* in 2000, TMSD has opened a new arena of research in the DNA nanotechnology world.¹⁰⁶ These non-enzymatic systems rely exclusively on hybridization reactions between DNA/RNA and leads to a signal amplification.¹⁰⁵ In signal amplification, the target is indirectly quantified by converting it to a surrogate or tag DNA/RNA sequence, which is in turn amplified.¹⁰⁵ To date, TMSD has been widely applied in various areas of research including nucleic acid amplification testing and has received intense attention because unlike most isothermal amplification techniques, it can be performed without the use of an enzyme and at low temperature. Being enzyme-free significantly simplifies and reduces the cost of the assay, which makes it a promising diagnosis technique for applications at the point-of-care. As shown above in the CHA-containing scheme of Figure 1.7, TMSD involves a duplex (Figure 1.8, blue and purple) with a single-stranded region that can be referred to as a sticky-end, overhang, or toehold hybridizing with a second DNA strand (Figure 1.8, green) that has part of the sequence complementary to the overhang. Following hybridization of part of the green strand to the overhang of the purple strand, the blue strand is displaced. This process is also termed as ‘toehold exchange’¹⁰⁷

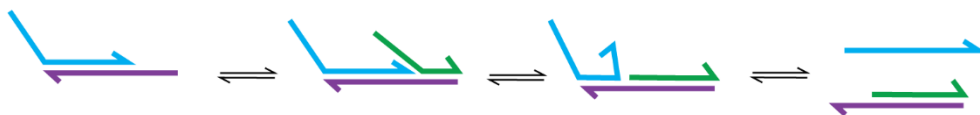


Figure 1.8 Schematic representation of the toehold-mediated strand displacement strategy. This image was redrawn with permission from reference 107. Copyright © 2017, Springer Nature.

TMSD processes based on the opening of hairpin structures were first introduced in 2004, by Dirks and Pierce; they named their target-triggered amplification system the hybridization chain reaction (HCR).¹⁰⁸ A simple representation of HCR is shown in Figure 1.9. The presence of a target strand (or initiator) triggers the opening of a hairpin H1 by hybridizing to an overhang sequence present on H1. Consequently, a hidden domain on H1 is exposed, which in turn interacts with the sticky-end on H2 initiating its opening. As a result, another sequence is exposed bearing the same sequence as the target strand (Figure 1.9). Therefore, by the cross-opening of two DNA hairpins in the presence of a target strand, a nicked DNA concatemer similar to an alternating copolymer is obtained. In the absence of a target, the two hairpins (H1 and H2) are caught in a kinetic trap which allows them to coexist metastably in a reaction mixture.

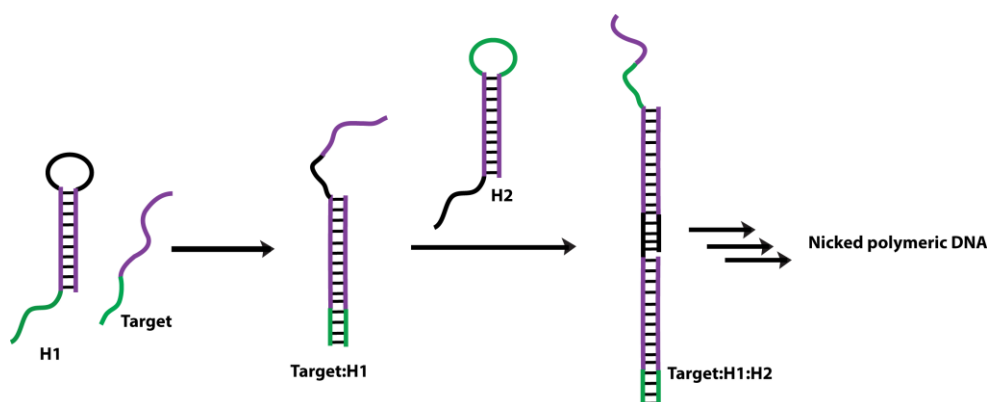


Figure 1.9 Schematic representation of the process of hybridization chain reaction (HCR). DNA hairpin 1 (H1) opens in the presence of an initiator or target nucleic acid bearing a complementary

part with the sticky-end. The newly formed sticky-end triggers the opening of DNA hairpin 2 (H2) via toehold mediated strand displacement. This process of TMSD continues until exhaustion of hairpins H1 and H2.

Earlier this year, Ravan *et al.* developed a novel dual catalytic DNA circuit, based on TMSD, coupled with colorimetric AuNP for the detection of DNA. In the presence of an initiator or target DNA, a cascade of TMSD involving five hairpin structures is triggered as shown in Figure 1.10.¹⁰⁹ During this process, the target and duplex H1-H2 are regenerated for another round of TMSD. Additionally, a three-arm junction structure consisting of three DNA strands, each having a biotin on it, is generated. In the presence of streptavidin-coated gold nanoparticles (SP-AuNP), aggregation occurs resulting in a color change of red to purple. In the absence of a target, the three-arm junction structure is not formed, which leads to no aggregation and thus no color change. For the experiment, the hairpins were heated at 95 °C for 5 min and cooled down to room temperature prior to use. Then the initiator was added, and the reaction was incubated at room temperature (26 °C) for 2 hours. For the colorimetric step, the reaction mixture was added to the SA-AuNPs and allowed to incubate for 45 min at room temperature along with shaking. Subsequently, color change was detected visually or by UV absorbance.¹⁰⁹ TMSD can also be used for the detection of RNA.¹¹⁰⁻¹¹¹ For example, in another report published in 2016 by the same author, a similar strategy was used for the detection of RNA. However, in this case streptavidin-coated wells were used, and the detection was done using an HRP-mimicking DNAzyme and hemin.⁵³ Again, the TMSD reaction was done at room temperature for 2 hours.⁵³ Despite the use of room temperature (25-26 °C), the whole assay procedure is not especially suitable for POC. These assays involve several washing steps, multiple temperatures, and incubation times for the different steps. Furthermore,

they are typically coupled with detection techniques that require instrumentation relying on stable power supply.

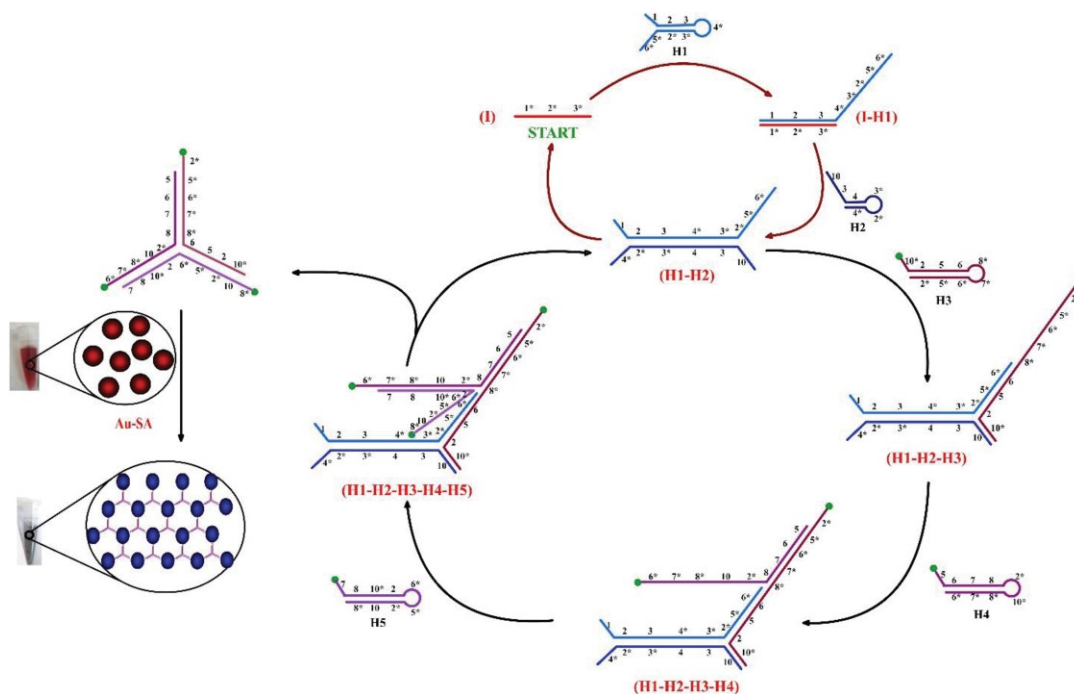


Figure 1.10 Schematic representation of dual catalytic DNA circuit-induced gold nanoparticle aggregation. Brief description in text. Image reproduced with permission from reference 109. Copyright © 2020, Elsevier B.V.

For assays that use HCR as their amplification platform, the temperature at which the reactions are performed is dependent on the stem sequences. If the latter is longer than 24 base-pairs and higher in GC content, 37 °C is preferred, otherwise room temperature (25 °C) is used in most cases.^{56, 108, 112-117} As mentioned earlier being an enzyme-free room-temperature (25 °C) assay, it is well suited for the diagnosis of diseases in low-resource settings as an amplification step in POCT. Yet, reports for the detection of nucleic acids using HCR for POC applications are rare.

Liu *et al.* developed a platform for the detection of DNA targets using HCR and gold nanoparticles.¹¹⁷ In their strategy, two carefully designed hairpins H1 and H2 that coexist in solution were used. H1 and H2 were heated at 95 °C and cooled down to room temperature for 1 hour before use.¹¹⁷ Upon addition of target, the latter hybridizes with the sticky-end of the hairpin H1, which results in the opening of the hairpin. This starts a series of TMSD until exhaustion of the hairpins. Consequently, a long chain-like nicked duplex dsDNA is formed. In the absence of the target, no HCR product is formed (Figure 1.11B). The amplification was performed at 25 °C for 1 hour. Following that, an aliquot of each the targeted and non-targeted samples was added to colloidal AuNP. Upon addition of salt, aggregation of the AuNP which is accompanied with a color change of red to purple is observed. The rationale is that the exposed negatively charged phosphate group of the double helical DNA structures formed by HCR cannot stabilize the AuNP and protect it for salt-induced aggregation. On the other hand, the hairpins containing sticky handles can stabilize them and protect them from aggregating in the presence of high salt concentration as shown in Figure 1.11B.¹¹⁷ Detection was either done visually or using a UV-vis apparatus. Another report by Song *et al.* has used copper nanoparticles for detection of the DNA polymer formed upon HCR triggered by *Escherichia coli* (*E. coli*) DNA (Figure 1.11C). The whole process was performed on streptavidin-modified sepharose beads (cross-linked agarose). The amplification and detection were performed at 25 °C under constant shaking for 2 hours.¹¹⁸ More recently, silver nanoclusters (AgNCs) as fluorescent probes and graphene oxide (GO) have been coupled with HCR for detection of HIV DNA. In the absence of the target HIV DNA biomarker, the DNA-AgNCs fluorescence is quenched on the surface of the GO. On the other hand, upon HCR reaction initiated by target DNA, a DNA nanowire is formed bearing multiple AgNCs that can no more be quenched by the GO (Figure 1.11A). Therefore, fluorescence is obtained as a

positive response indicating the presence of the HIV target.¹¹⁵ The whole process of amplification to detection was around 5 hours with multiple addition steps (5 min at 95 °C, added AgNO₃, room temperature for 30 min, vigorous shaking for 1 min, store in dark at room temperature for 2 hours, added HIV DNA target, HCR for 4 hours at room temperature, added GO, room temperature for 30 min, fluorescence spectroscopy). The HCR step was performed at “room temperature”. However, the author did not precisely define what that meant.¹¹⁵ Lastly, HCR can also be employed for the detection of RNA.¹¹⁹⁻¹²⁰ For example, Bi *et al.* used 4 hairpin structures in a hyperbranched-HCR strategy (Figure 1.11D) to detect miRNA-21, which is a biomarker for different types of cancer at 25 °C.¹²⁰

As seen in these few examples, the ideal temperature for the TMSD-based strategies is 25 °C. However, the reports that are specific for the detection of infectious diseases are found to work at higher temperatures (37 °C).¹²¹⁻¹²³ Although, the signal amplification step is isothermal and can be performed at room temperature, the whole assay, which involves sample preparation, amplification and detection has several heating and cooling steps and laborious detection techniques, which hinders its application in POC diagnostics.¹²⁴⁻¹²⁵ Additionally, the hairpins must be carefully designed so as to minimize background leakage or false positive results.^{105, 125} Several factors such as subtle variations in pH or temperature, as well as nucleic acid impurities or misfolding can contribute to this signal leakage.¹⁰⁵ Finally, TMSD is a very versatile technique and has been used for a variety of targets other than nucleic acids, for example proteins, small molecules, ions and cells.¹⁰⁷ In terms of nucleic acid, the focus is more on genotyping, SNP detection and in the study of tissues and live cells.¹⁰⁵ This technique has a lot of potential to be implemented as a room temperature POC assay. However, further research is still required to circumvent its limitations so as to achieve this goal.

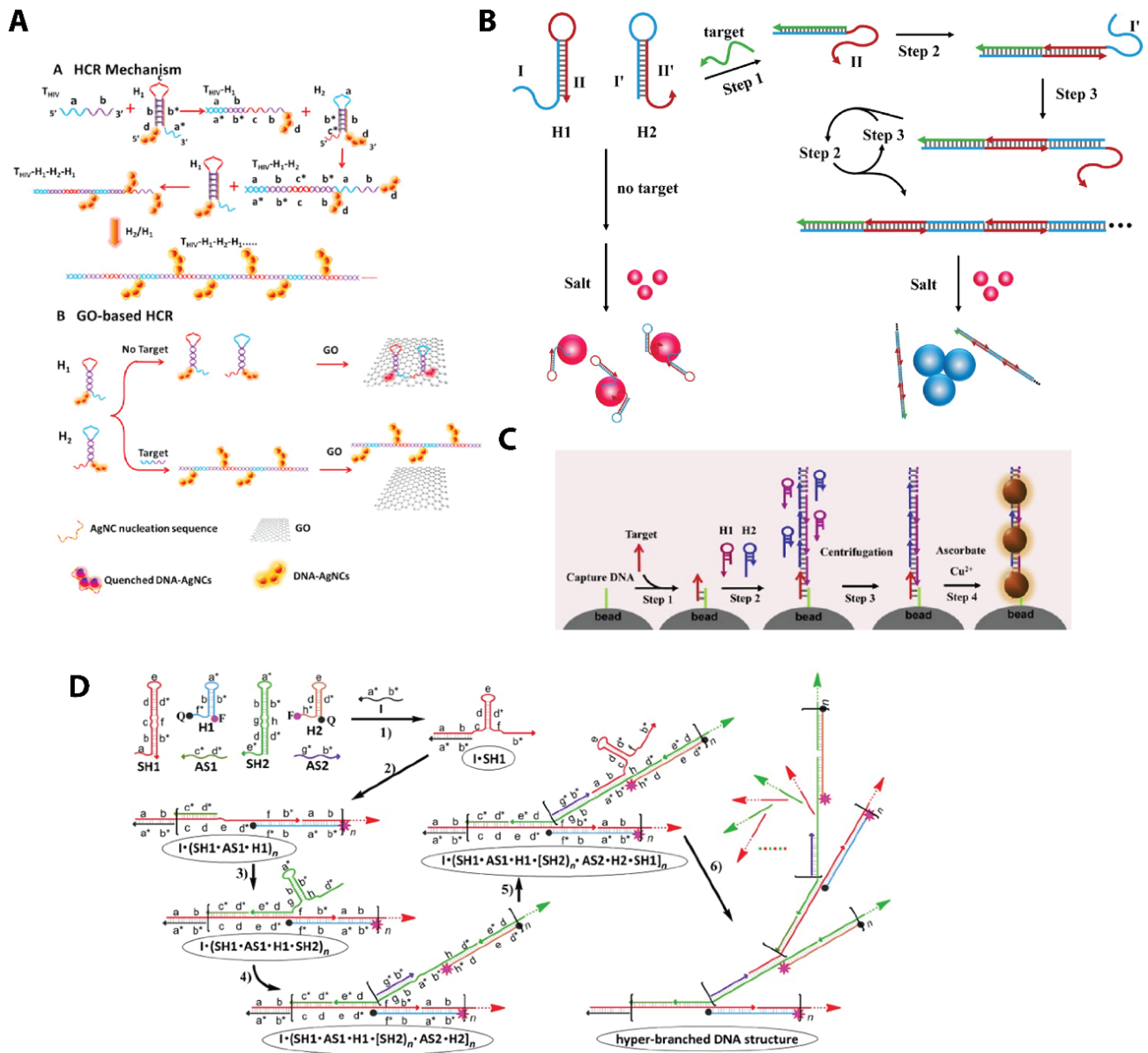


Figure 1.11 Schematic representation of HCR based assays. A) The presence of target DNA triggers the opening of hairpin DNA-AgNCs, H1. Following that, a cascade of TMSD is activated, which forms a DNA polymeric scaffold bearing multiple AgNCs sites that give a fluorescence signal. In the absence of target, the DNA-AgNCs adhere to the GO quenching its fluorescence. B) The target catalyzes the opening of H1 to liberate a hidden DNA sequence. This newly exposed sticky-end nucleates with H2 which again liberate a new piece of DNA that is complementary to part of H1. A cascade of hybridization then occurs with simultaneous opening of H1 and H2 to

form a nicked duplex dsDNA. When colloidal AuNP and salt is added, aggregation occurs. C) A captured DNA attached on a bead hybridizes to a target when present, which then causes the cross opening of two hairpins H1 and H2. A long double-stranded DNA with nicks is formed on the bead. Upon addition of Cu^{2+} and ascorbate, a fluorescence signal is obtained. D) Upon addition of a target, a hybridization chain reaction with the successive opening of four hairpins structure is observed. Images A) B) C) and D) was adapted from reference 115,117,118,120, © 2014 Elsevier B.V., © 2013, American Chemical Society, Weinheim, © 2016, Elsevier B.V. and © 2015, WILEY-VCH Verlag GmbH & Co. KGaA, Weinheim respectively.

1.5 Objectives

The goal of my thesis was to develop a versatile nucleic acid amplification test that is equipment-free and can be performed over a wide range of room temperature. As mentioned earlier, existing isothermal techniques work best at higher temperatures, typically 37 to 65 °C.⁴⁴⁻⁴⁶ Consequently, it is difficult to address the equipment-free criteria of the ASSURED platform implemented by the WHO.¹⁷ Several articles on equipment-free/instrument-free isothermal amplification techniques have been reported where they depend on commercially available or in-house invented heaters that rely on either an exothermic chemical reaction or battery powered system to provide the temperature required.^{25, 42-43, 51, 54, 126} Other systems that work at 37 °C, which is the human body temperature, were demonstrated to work using body heat by placing the amplification tube in the axilla(armpit) or fist.⁴³ Despite these great efforts, these systems still have some limitations.⁴³ Using an individual's body heat is a great idea but it has implications like the safety of the person or simply the uncomfortable situation of having a few tubes in your armpit for few hours.⁴³ Despite being called equipment-free or instrument-free, some of these systems still

involve some instrumentation. A better word to describe these systems would be electricity-free rather than equipment-free since they still involve instrumentation.

Various isothermal NAAT that works at an ambient temperature of 25 °C to 30 °C have been developed as summarized above. Techniques that work below 25 °C are rare. Therefore, the focus of this thesis is to develop a room temperature (17 to 30 °C) assay that works without any complicated equipment. In Chapter 2, I will show how lesion-induced DNA amplification (LIDA), the amplification method developed in our lab,⁷³ was adapted to work over a wide range of room temperatures (18-26 °C). In LIDA, we use a destabilizing group, abasic lesion to achieve isothermal amplification of DNA at 30 °C. Herein, I will discuss the introduction of a second destabilizing element in the system, that is a mismatch in one of the probes. I will show how the presence of different mismatches affects the optimum temperature (T_o) of LIDA. The optimum temperature is the temperature at which there is the greatest difference between the product formed in the presence and absence of target DNA. We first compared LIDA reaction in the presence of one (abasic) and two destabilizing elements (abasic and A:G mismatch) at 26 °C. Following that, we decided to investigate the various mismatches by performing LIDA at different temperatures to determine the optimum temperature. Next, we introduced another abasic lesion at the mismatch site and determined its T_o . Finally, we performed LIDA for one of the systems at room temperature by preparing the amplification sample in an eppendorf tube and placed it on a rack on the bench.⁷¹ Finally, to understand the evolution of simple prebiotic self-replicating systems. We explored the presence of having both probes, containing the mismatch and no mismatch, in one-pot LIDA reaction.

DNA is not the only biomarker for disease as some pathogens have RNA as their genetic material. Also, there is a growing interest towards miRNA as a potential biomarker for several

medical conditions. Therefore, in Chapter 3, I will discuss the potential of using RNA as a target for LIDA. In this chapter, I will show how we reverse transcribed RNA into a cDNA using a simple RNA-templated DNA ligation. We used a toehold-mediated strand displacement strategy to liberate the cDNA, which was used as a template for LIDA. To achieve isothermal and room-temperature amplification, we introduced a mismatch to the system. All the detections were performed using polyacrylamide gel electrophoresis, which is not ideal for POC analysis since it requires trained personal and instrumentation. Therefore, to achieve room-temperature amplification and detection, we coupled the reverse transcription-LIDA (RT-LIDA) to a colorimetric platform previously developed by our group.¹²⁷ I will discuss how the amplicons from the RT-LIDA trigger the rapid disassembly of aggregated AuNP samples, leading to a color change of purple to red. The target RNA from real samples collected from patients is typically present in a sea of random RNA. To address this, we performed RT-LIDA initiated by target RNA spiked in human lungs total RNA and *E. coli* total RNA to mimic the complex environment of real samples, followed by colorimetric detection of the cDNA amplicons. The specificity of the assay will also be discussed by comparing the RT-LIDA of target RNA and that in the presence of a mismatched RNA target and a random RNA target. Finally, we report that performance of reverse transcription-LIDA with colorimetric detection at room temperature (28 °C) on the bench in a complete equipment-free set-up.

One limitation of LIDA is the non-templated background-triggered process, which is observed in both Chapter 2 and Chapter 3. This background-triggered amplification stems from the small amount of target DNA formed when the pseudo-blunt end ligation of the two sets of complementary probes occur. To reduce the background ligation of LIDA, which will ultimately allow us to detect lower amounts of target making the assay more sensitive, in Chapter 4 we

explored the use of different modified ATP in the LIDA system. Fifteen modified ATP cofactors were provided to us by the Hili group. We explored three of them in Chapter 4. Templated and non-templated lesion-induced DNA amplification were performed in the presence of ATP and three ATP derivatives. The results were then compared to each other by an analysis of their point of inflections.

Finally, I will give a conclusion and outlook of all the projects in Chapter 5.

Chapter 2

Achieving Room Temperature DNA Amplification by Dialling in Destabilization

Portions of this chapter are reproduced by the permission

of the Royal Society of Chemistry from:

Alladin-Mustan, B. S.*, Mitran, C. J.*, Gibbs-Davis, J. M. (2015). Achieving Room Temperature DNA Amplification by Dialling in Destabilization. *Chemical Communications*, 51(44), 9101-9104. doi:10.1039/C5CC01548K *Equal contribution

2.1 Introduction

Nucleic acid based diagnostics are the gold standard for the detection of infectious diseases as they offer the greatest specificity and the ability to identify drug responsive or drug resistant strains.¹²⁸⁻¹²⁹ Due to the enormity of disease epidemics like tuberculosis, malaria and HIV including drug-resistant strains especially in the developing countries, there is a global need for assays based on nucleic acid biomarkers that can be performed in resource limited settings.^{38, 130-131} One major challenge facing nucleic-acid based point-of-care (POC) diagnostics is the low concentration of nucleic acid biomarkers in all biologically extracted samples.³⁷ Consequently, a general requirement is to amplify the biomarker target sequence prior to detection.^{37, 132-133} As such, multiple examples of POC diagnostics using enzyme-based isothermal amplification methods have been reported that avoid the expensive instrumentation necessitated by the temperature cycling steps of the polymerase chain reaction.^{37-38, 134}

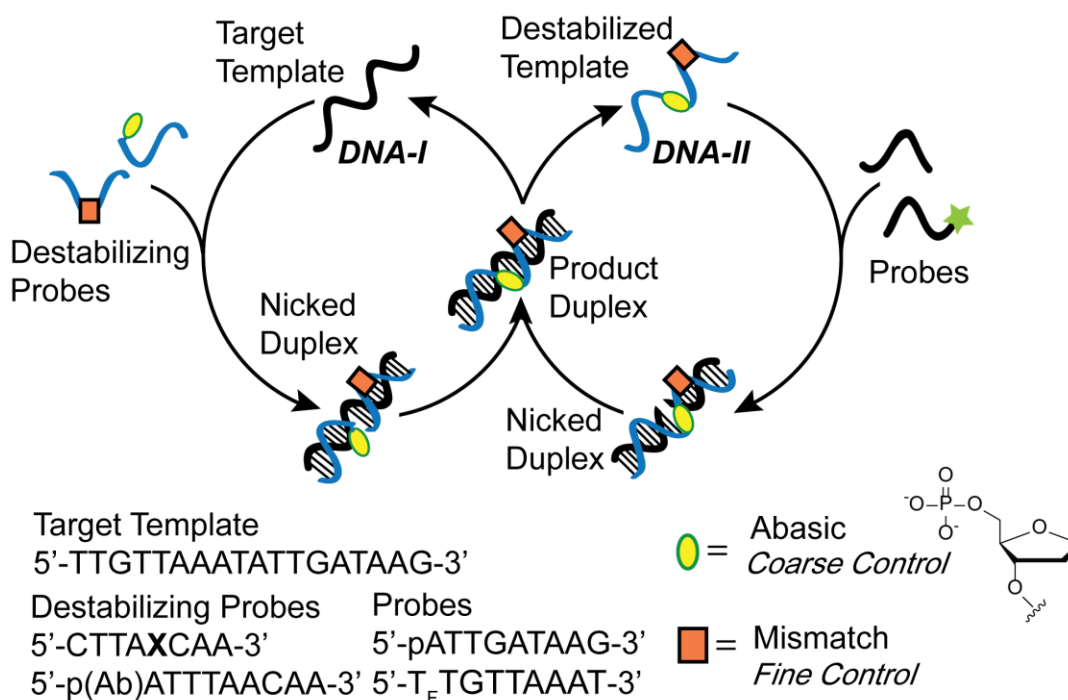
However, virtually all isothermal enzymatic methods with the ability to exponentially amplify the target sequence (key to sensitive detection) operate well above room temperature.¹³⁵⁻¹³⁷ This temperature requirement adds an unfortunate layer of complexity to the assay as heating the sample requires a constant heat source and stable electricity, which is often not available at the point-of-care. Instead, the ideal nucleic acid amplification assay should be operational at room temperature without the need for constant heating. Such an equipment-free test that is also easy to perform by an operator with limited training would address two of the ASSURED criteria of the World Health Organization for ideal POC technologies (affordable, sensitive, specific, user-friendly, robust and rapid, equipment-free and deliverable).^{129, 138} One recent example of an isothermal exponential amplification method that is compatible with lower temperatures is recombinase polymerase amplification, which has been reported to operate at as low as 30 °C.¹³⁹

While this may be suitable for heat-free amplification in certain seasons, it would require a heating element for many days that fall below this temperature. Non-enzymatic nucleic acid circuits have been reported that operate near room temperature like the hybridization chain reaction yet the most sensitive and rapid of these exhibit linear rather than exponential amplification.¹⁴⁰ To address the need for heat-free exponential amplification methods, herein we describe a strategy for tuning the amplification temperature using combinations of destabilizing elements in our simple, yet powerful, amplification by destabilization method.

2.2 Cross-Catalytic Amplification using Two Destabilizing Elements

Our strategy for achieving rapid isothermal DNA amplification involves utilizing destabilization/destabilizing modification to achieve turnover in a ligase chain reaction (Scheme 2.1).⁷²⁻⁷³ We refer to this cross-catalytic process as lesion-induced DNA amplification (LIDA). In the first step of LIDA, the target sequence we wish to amplify, **DNA-I**, hybridizes with two complementary probes (Scheme 2.1, left cycle): one contains a model abasic site (*oval*), the other is perfectly complementary or contains another destabilizing group like a mismatch (*square*). After templated ligation of these probes, the newly formed destabilizing template **DNA-II** dissociates owing to the presence of the destabilizing group or groups. A second reaction then uses this destabilizing strand to template the ligation of two other probes, one of which contains a fluorescent label (**F-DNA-Ia**). The result is a labeled copy of the original target sequence (Scheme 2.1, right cycle). Employing this self-replicating system with only one abasic lesion, we observed rapid exponential amplification of different target sequences using T4 DNA ligase to catalyze ligation.⁷³ Using LIDA, we were able to detect as little as 140 fM of target DNA (2.1 attomoles) based on a two-step serial amplification procedure.⁷³ One aspect that currently limits the sensitivity of this approach, however, is the presence of a background-triggered process when no initial target

is present (discussed in Chapter 4). The background reaction stems from pseudo-blunt end ligation of the probes in the absence of any initial **DNA-I** target, which leads to the formation of **DNA-I** and **DNA-II** *in situ*. These templates are then able to rapidly self-replicate following the LCR cycles. Consequently, to identify the presence of target DNA, we compare the results of the target-initiated reaction with the reaction lacking any initial **DNA-I**. If there is a difference in the amount of **F-DNA-I** formed, then the presence of initial **DNA-I** is confirmed.



Scheme 2.1 Isothermal lesion-induced DNA amplification (LIDA) using different destabilizing elements for coarse and fine temperature control. *Oval*: abasic; *Star* or *T_F*: fluorescein dT; *Square* or *X*: A, G, T or C; *p*: phosphate. Nicked duplexes were ligated in the presence of T4 DNA ligase to form the product duplex.

2.2.1 One Destabilizing Lesion: Abasic Group

Our previous work established that the presence of one abasic group was essential to achieve sigmoidal self-replication of 18 nucleotide target sequences; no self-replication was observed when a mismatch was utilized instead of the abasic group.⁷³ We argued that the mismatch was not sufficiently destabilizing to facilitate turnover based on the observed dissociation temperatures for the corresponding product duplexes containing the complementary nucleotide, a mismatch, or an abasic group. However, combining a mismatch with an abasic group should result in a product duplex that is more destabilized than the abasic-only system, which we hypothesized would lead to enhanced turnover at lower temperatures. To determine whether the ideal temperature could indeed be controlled by tuning the amount of destabilization in our system, we added a mismatch and an abasic group to the destabilizing probe sequences, which resulted in a G across from an A on the target (Scheme 2.1, X = G).

2.2.2 Two Destabilizing Lesion: Abasic and A:G Mismatch

2.2.2.1 Single Turn-Over Reaction

Single turn-over reaction is the stoichiometric ligation reaction between the target **DNA-I** and reactive complementary probes **F-DNA-IIb(X)** and **DNA-IIa**. Fluorescein label is used in one of the probes to be able to follow the ligation reaction via polyacrylamide gel electrophoresis (PAGE). The ligation reaction was performed at 16 °C with different mismatches. In Figure 2.1 C, the percent yield increased with decreasing temperature, which indicates that the amount of product formed is proportional to the amount of nicked duplex present at that temperature. As the association constants increase with decreasing temperature, the percent yield of ligation is expected to increase. These results suggest that the intrinsic rate of ligation is similar for the

different mismatches, so the rate is most affected by the amount of nicked duplexes present, which in turn depends on the value of their equilibrium constant at a given temperature.

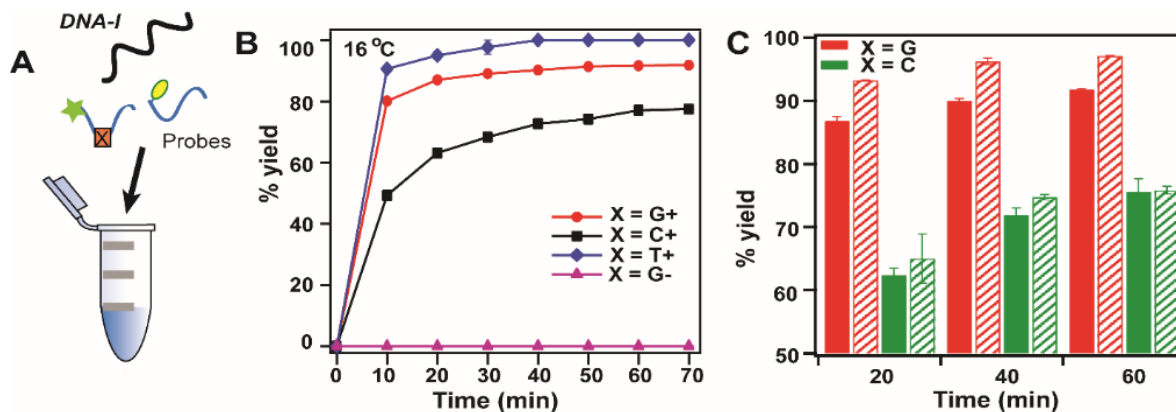


Figure 2.1 A) Scheme illustrating the four components in the single-turnover experiment (*Oval*: abasic; *Star*: fluorescent label; Square or *X* = A, G, C or T). B) The formation of **F-DNA-II(X)** at 16 °C for ligations initiated by 1.4 μM (+) or 0 μM (-) **DNA-I**. C) The % yield of **F-DNA-II(X)** formed at 16 °C (solid) and 12 °C (striped). *Experimental conditions*: 1.4 μM **DNA-I**, 1.4 μM **F-DNA-IIb(X)**, 2.8 μM **DNA-IIa**, 300 Cohesive End Unit (CEU) T4 DNA ligase, 50 mM TRIS-HCl, 10 mM MgCl_2 , 1 mM ATP, pH 7. Cohesive End Unit (CEU), the unit of enzyme activity is a measure of the amount of enzyme needed to get 50% ligation of sticky-end of lambda DNA generated by the restriction enzyme HindIII in 30 min at 16 °C. The corresponding gel images shown in Figure 2.18.

2.2.2.2 Cross-Catalytic Reaction

Figure 2.2 exhibits cross-catalytic formation of the labeled **F-DNA-I** target with time in LIDA reactions initiated with 14 nM or 0 nM **DNA-I**, using probes with either an abasic (only) or both an abasic and a mismatch. By incorporating the additional mismatch, we observed that the

rate of amplification was greatly enhanced at 26 °C ($X = G$), when compared with the system that lacked the mismatch ($X = T$). With respect to target detection, the optimum temperature (T_o) is defined as the temperature where we observed the greatest difference in **F-DNA-I** formed between the target-initiated and background-triggered reactions (Δ **F-DNA-I**). Therefore, this T_o value of 26 °C for the abasic + A:G mismatch system was four degrees less than the T_o for the abasic only system,⁷³ which indicated that incorporating mismatches did allow us to tune the optimum replication temperature. Interestingly we observed that the nicked duplex of the A:G mismatch system formed in the first cycle had a dissociation temperature (T_m) of 11.4 °C, which was four degrees lower than that of the abasic only system (Figure 2.3).⁷³ The strong similarity between trends in T_o and nicked duplex T_m for the two systems suggested that the thermal stability of the nicked duplex was a good predictor of optimum replication temperature.

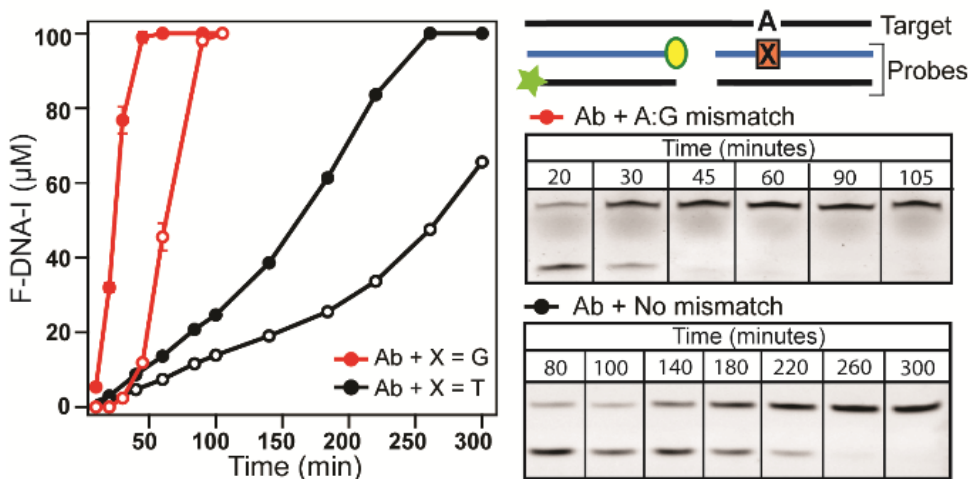


Figure 2.2 *Oval*: abasic lesion; *Star*: fluorescent label. Comparison of LIDA with one destabilizing element (abasic only, where $X = T$) or two destabilizing elements (abasic and mismatch, where $X = G$). Kinetics of **F-DNA-I** formation at 26 °C for cross catalysis initiated by 14 nM (solid circles) or 0 nM (open circles) **DNA-I** with the abasic only system ($X = T$, black traces) or the abasic+mismatch system ($X = G$, red traces). Polyacrylamide gel image of the **DNA-I** initiated

reaction at different time points corresponding to the black and red solid circles. *Top band*: **F-DNA-I** product; *bottom band*: **F-DNA-Ia** fluorescently labelled probe. Comparison of isothermal lesion-induced DNA amplification with an abasic destabilizing group and both abasic and mismatch destabilizing groups. *Oval*: abasic lesion; *Star*: fluorescent label.

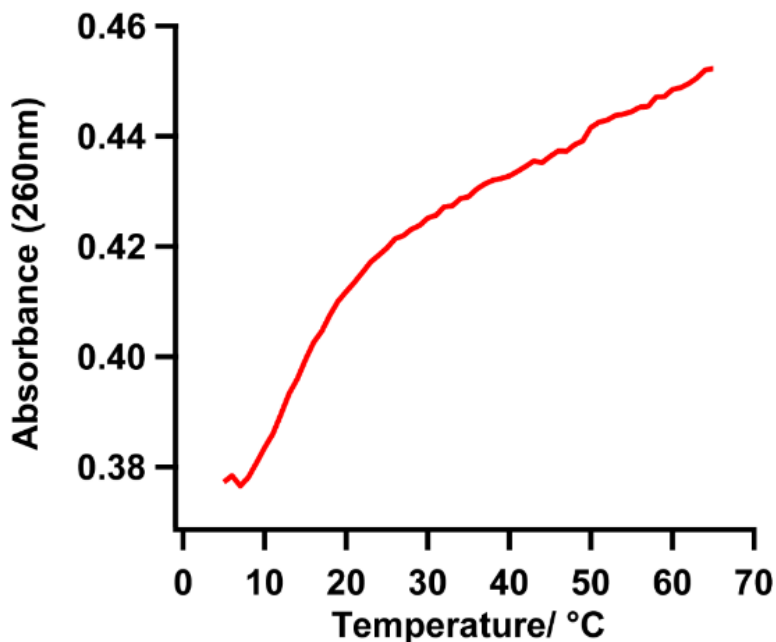


Figure 2.3 Melting profile of the nicked duplex corresponding to **DNA-I: DNA-IIa: DNA-IIb(G)**. A melting temperature of 11.8 °C was observed. *Experimental conditions*: 1.3 μ M of each DNA strand in 10 mM $MgCl_2$, 10 mM PBS, pH 7.

Moreover, similar to our original work,⁷³ the A:G mismatch system was easily able to discriminate as little as 140 pM (2.1 femtomoles) of **DNA-I** in a single amplification experiment, which corresponded to a target-initiated turnover number (TON) of 800 ± 100 (Figure 2.4). This similarity in sensitivity revealed that the addition of the mismatch did not compromise the ability of LIDA to detect the target DNA.

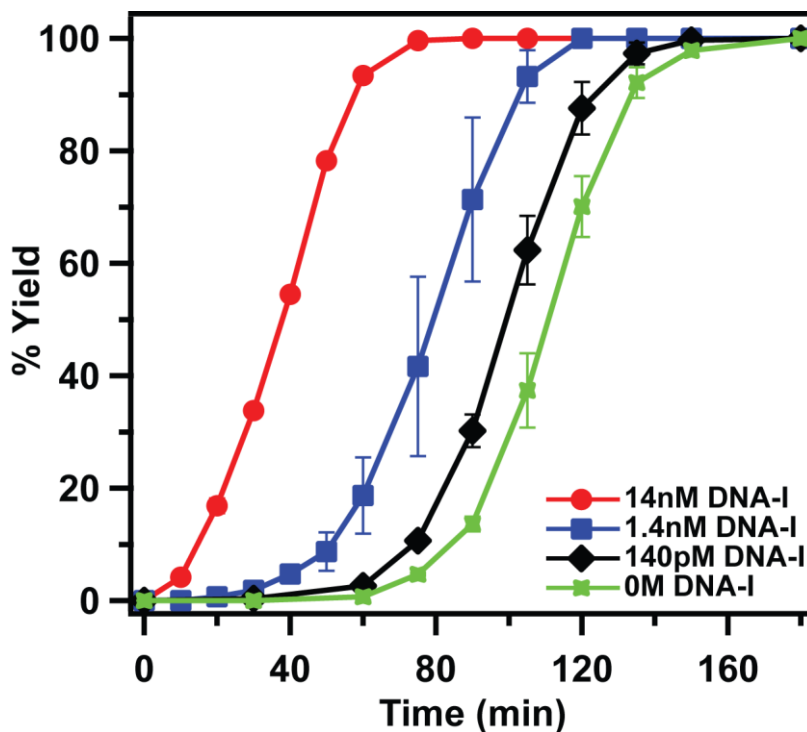


Figure 2.4 The % yield of **F-DNA-I** formed as a function of time with different concentrations of initial **DNA-I** template and lower replicator concentrations than standard conditions. *Experimental conditions:* 14 nM, 1.4 nM, 140 pM or 0 nM **DNA-I**; 0.7 μ M **F-DNA-Ia**; 1.4 μ M **DNA-Ib**; 1.4 μ M **DNA-IIa** (M = Ab); 1.4 μ M **DNA-IIb(G)**; 26 °C.

2.2.3 Influence of Abasic + Different Mismatches on T_0

To determine the influence of the second destabilizing element on T_0 we performed LIDA at multiple temperatures using destabilizing probes with X = G, C, A and abasic (Ab) and compared these results with that of the original system where X was complementary to the target (X = T) (Figure 2.5). Using different mismatches, we were able to tune the optimum temperature from 22 – 26 °C. Specifically, the A:G mismatch led to a T_0 of 26 °C whereas the T_0 for the A:A and A:C mismatch systems was 22 °C, indicating that these mismatches led to similar destabilization of the product duplex. Our observed trends in optimum replication temperature

were similar to the trend in stability observed for central A:X mismatches in DNA:DNA duplexes,¹⁴¹ which revealed that the temperature could be tuned in a highly predictable manner by considering the destabilizing effect of the mismatch (*vide supra*). Importantly, the maximum ΔF -DNA-I observed, and in turn the turnover number, was similar for the different mismatches, indicating that the identity of the mismatch also did not impact sensitivity (Figure 2.5). Moreover, all of the four examined systems exhibited a relative insensitivity to the temperature as excellent turnover was observed at $T_0 \pm 2$ °C, which may provide an advantage in point-of-care applications with limited temperature control.¹³⁹ Finally, as expected, incorporating two abasic groups reduced the optimum temperature most dramatically to 18 °C. The observed temperature dependence of these combinations indicated that mismatches provide fine control for temperature tuning, whereas incorporating abasic groups lead to coarse control. This ability to make small or large jumps in the optimum temperature of replication by varying the combination of destabilizing elements results in unprecedented tunability of the amplification temperature of a particular target sequence.

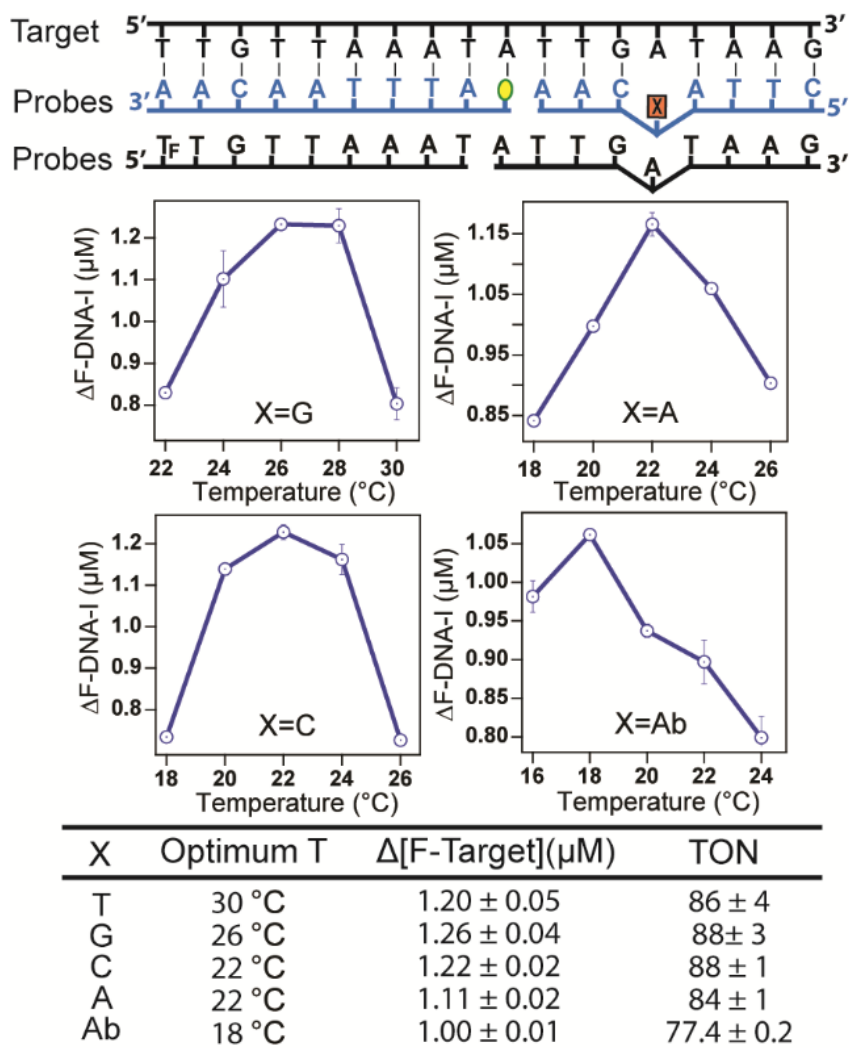


Figure 2.5 Temperature-dependent LIDA for two destabilizing element systems containing an abasic group and various mismatches. *Oval*: abasic lesion; *T_F*: fluorescein-labeled T; *X* or *Square*: A, G, C or Ab. The maximum difference of **F-DNA-I** formed between the target-initiated and the background-triggered cross-catalytic reaction at various temperatures using destabilizing probes that resulted in different A:X mismatches. The optimum temperature corresponds to the highest point of each plot (the maximum $\Delta[F\text{-DNA-I}]$ value). Table: the $\Delta[F\text{-DNA-I}]$ value and the corresponding turnover number (TON) at each system's optimum temperature for the complementary system ($X = T$) and the systems having different A:X mismatches.

2.2.4 Correlation Between Stability of Mismatch Versus T_o

To quantify the relationship between stability of the A:X pair and the optimum replication temperature, we determined the contribution of each A:X mismatch to the overall $\Delta G_{\text{dissociation}}$ from the work of Gaffney and Jones.¹⁴¹ (Owing to the low stability of the X = A, C and Ab systems, we were unable to determine the T_m values of the corresponding nicked duplexes, which should lie around or below 10 °C). A plot of $\Delta\Delta G$ ($\Delta G_{\text{A:T}} - \Delta G_{\text{A:X mismatch}}$) versus T_o for the corresponding mismatch revealed a linear correlation ($T_o = 0.00217\Delta\Delta G + 30.171$; $r^2 = 0.97$; Figure 2.6), which supports that the optimum replication temperature can indeed be predicted based on the destabilizing effect of the mismatch. Future work will aim to create a more refined model for predicting T_o that will also take into account the influence of the flanking base identity on mismatch stability.¹⁴²⁻¹⁴³

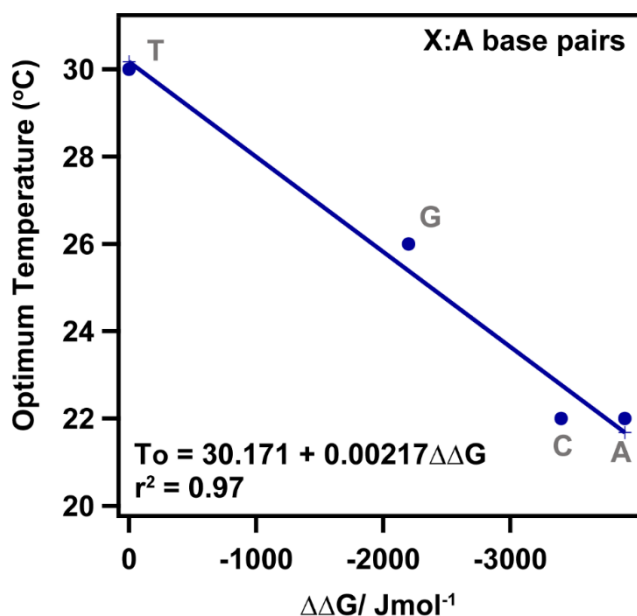


Figure 2.6 Linear fit of $\Delta\Delta G$ against the optimum replication temperature for the corresponding matched or mismatched base. The ΔG of the matched and mismatched systems were obtained from

the work of Gaffney and Jones.¹⁴¹ $\Delta\Delta G$ is the difference between the corresponding ΔG values of the matched and the mismatched system for a series of A:X mismatches.

2.3 LIDA using Abasic + A:C Mismatch at Room Temperature

Thus far, we had utilized a thermal incubator for maintaining a constant temperature for each amplification reaction. The performance of the C-mismatch + abasic system, however, indicated that it should operate at the ambient temperature of the lab (typically between 21-24 °C) without the need for an incubator. Figure 2.7 reveals the rapid amplification exhibited at ~21 °C by simply combining all the DNA probes, the target, and the T4 DNA ligase master mix in an Eppendorf and placing the Eppendorf in a tube holder on the bench. Within less than an hour the reaction mixture containing target showed 100-fold amplification while the control lacking template displayed much less target sequence formation. The error bars shown in Figure 2.7A are based on the standard deviation of two data sets measured at the same lab temperature, but we note that this system was even faster and equally discriminating on a warmer lab day at 24 °C (Figure 2.8).

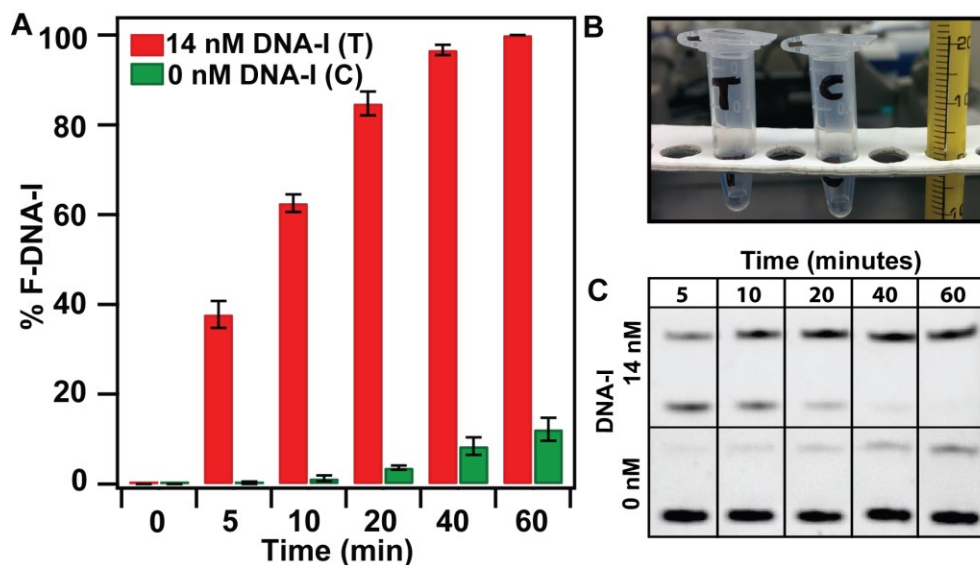


Figure 2.7 A) LIDA performed on benchtop at room temperature (21 °C) with two destabilizing elements (abasic (Ab) + mismatch (X = C)) B) LIDA on benchtop with T, templated reaction and C, background-triggered ligation reaction. C) Polyacrylamide gel image of the **DNA-I** initiated reaction at different time points corresponding to the red and green bar graph. *Top band: F-DNA-I* product; *bottom band: F-DNA-Ia* fluorescently labeled probe.

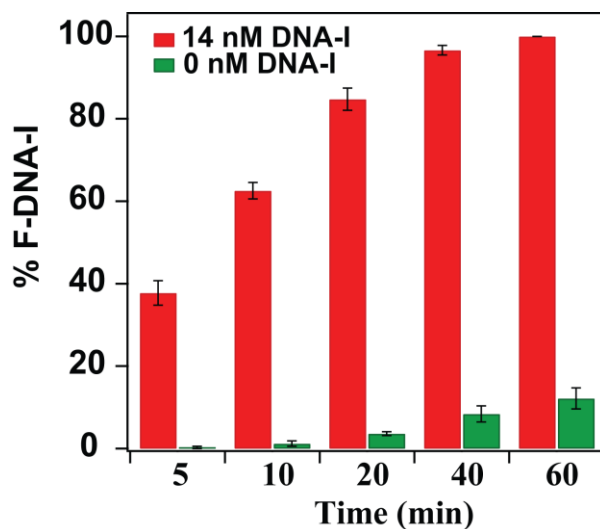


Figure 2.8 LIDA performed on benchtop at room temperature (24 °C) with two destabilizing elements (abasic (Ab) + mismatch (X = C)). * Reaction was performed only once.

2.4 Competing Ligation Reaction

The requirement for temperature cycling presents a challenge for point-of-care diagnostics and adds difficulty in understanding the evolution of simple prebiotic self-replicating systems. One source of temperature cycling on early earth proposed by Szostak and co-workers is the cycling of vesicles containing genomic material towards and away from volcanic vents in the ocean.³¹ A simpler alternative involves isothermal nucleic acid replication based on lesion-induced destabilization of the replicating complexes. To see whether systems select the destabilizing element, we designed probes that had different degrees of destabilization and allowed them to compete head-to-head. To evaluate this competition reaction the product resulting from the more destabilizing probe needed to be distinguishable from that of the less destabilizing probe. Consequently, in these experiments we monitored the formation of the destabilizing template (**DNA-II**) instead of the target sequence (**DNA-I**) using two different destabilizing probes of different lengths. Specifically, the probe lacking a mismatch, which resulted in a destabilizing template containing only the abasic lesion was made 9 bases long, while the probe containing the A:G mismatch was made 11 bases long. Thus, the destabilizing template that contained only an abasic lesion could be distinguished from that containing an abasic lesion and the A:G mismatch.

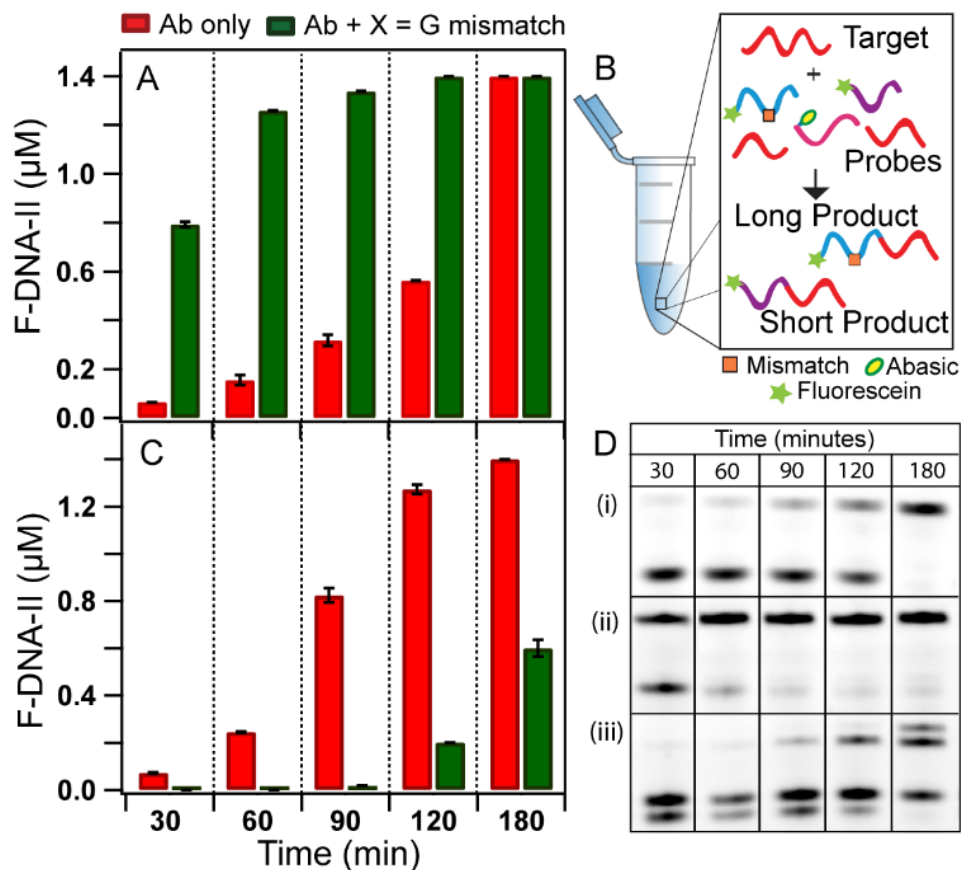


Figure 2.9 Comparison of LIDA with one and two destabilizing elements (abasic (Ab) and abasic + mismatch, respectively). A) Cross-catalytic amplification of the destabilizing template (**F-DNA-II**) at 26 °C for the Ab and Ab + mismatch systems, performed separately. B) Scheme showing the competition reaction between the fluorescently labeled probes that have or lack a mismatch, resulting in a longer or shorter **DNA-II** product, respectively. Both systems are initiated by **DNA-I** (Target) and use three common probes, one of which contains the abasic group. C) Competitive cross-catalytic amplification of the short **F-DNA-II** (Ab only) and the long **F-DNA-II** (Ab + mismatch) at 26 °C with all probes present as described in (B). D) PAGE images of: (i) LIDA of **DNA-II** for the Ab only system; (ii) LIDA of **DNA-II** for the Ab + mismatch system; (iii) competition reaction as shown in (B). The highest band corresponds to the longer product (Ab + mismatch) and the second highest band corresponds to the shorter product (Ab only).

As shown in Figure 2.9A, when the systems were kept separate at 26 °C, the rate of amplification of the longer destabilizing template **DNA-II**, corresponding to the abasic and A:G mismatch, was much greater than that of the shorter **DNA-II**, corresponding to the abasic only. This result was consistent with what we observed for **DNA-I** formation at 26 °C when comparing the system with just an abasic group versus an abasic and A:G mismatch (Figure 2.2). Next, we monitored which **DNA-II** was made preferentially when the two processes were in direct competition with one another as shown in Figure 2.9B. The system then had the choice of amplifying the sequence with the mismatch and the abasic or only the abasic. Despite being at the optimum temperature for the mismatch and abasic, the system preferentially amplified the sequence that contained only the abasic lesion (Figure 2.9C). These results reveal that replication favors formation of the most faithful complement even if it slows down the replication. Consequently, we reason that lesion-induced DNA amplification could only have played a significant role in prebiotic replication if the destabilizing elements preceded the presence of the perfectly complementary elements. Alternately, additional processes may have occurred that trapped out the complementary products from those that contained lesions, allowing the latter to dominate in the replication process.³² Finally, we note that the rate of amplification of the abasic **DNA-II** was faster for the competition reaction than the separate reactions (Figure 2.9C, red and 2.9A, red, respectively) despite being at virtually the same concentrations. This interesting result suggests that competition may enhance the amplification rate of the winner.

2.5 Conclusion

In summary, we found that the introduction of a mismatch led to further destabilization in our lesion-induced DNA amplification system, which allowed us to tune the optimum amplification temperature. Depending on the destabilizing effect of the additional mismatch or

lesion, the T_0 of amplification for a given sequence ranged from 18 to 26 °C, while the T_0 of the system with only the abasic lesion was 30 °C. From a point-of-care diagnostic perspective, this tunability is ideal in achieving simple and efficient nucleic-acid based detection of diseases in settings where there is poor temperature control. Moreover, this strategy of controlling temperature can be combined with other approaches like serial LIDA to access lower sub picomolar target concentrations.⁷² Future work will address other important factors of ASSURED for successful POC detection: sample preparation and enzyme stabilization¹⁴⁴⁻¹⁴⁶ to afford a robust amplification platform that is insensitive to storage temperature and can be operated with minimal training at the point-of-care. Finally, we note developing a non-enzymatic LIDA system would avoid utilizing sensitive enzymes. Such a system may have advantages over current examples of non-enzymatic auto-catalytic and cross-catalytic replication at constant temperature^{132, 140, 147-149} that have specific sequence requirements¹⁵⁰ or exhibit slow turnover or high background.¹⁵¹⁻¹⁵³ Lastly, we also demonstrated that there is selectivity towards the more complementary system when LIDA was performed in the presence of both perfect and mismatched probes in addition to the probe with an abasic lesion. This selectivity is somewhat surprising given the faster amplification rate of the less complementary system and sheds light on the influence of competition in prebiotic nucleic acid replication.

2.6 Experimental

2.6.1 General

All DNA synthesis and purification reagent: nucleotides, CPGs and Glen-Pak cartridges were purchased from Glen Research (Sterling,VA). DNA was synthesized using an Applied Biosystems Model 392 DNA/RNA solid phase synthesizer. DNA concentrations and thermal dissociation profiles were determined using an HP 8453 diode-array spectrophotometer equipped

with a HP 89090A Peltier temperature controller. The DNA oligonucleotides were characterized by MALDI-TOF using a Voyager Elite (applied Biosystems, Foster City, CA) time-of-flight mass spectrometer. StainsAll reagent (Aldrich cat #E9379) was used to assess the purity of the synthesized DNA oligos. Polyacrylamide gel electrophoresis (PAGE) was used to monitor the kinetics of single turn over and cross catalysis. 15% PAGE gels were made using urea (99%, Fisher, BP169212), tris base (Fisher, BP1521), TEMED (Fisher, BP15020), 40% acrylamide/bis solution 19:1 (Bio-Rad, 161-0144) and ammonium persulphate (BioShop, AMP 001). Gel imaging was done using ImageQuant RT ECL Imager from GE Healthcare Life Science (with fluorescein filter). The temperatures for the DNA ligation experiments were maintained using a Torrey Pines Scientific Echotherm Chilling/Heating Plate Model IC22. The high concentration enzyme T4 DNA ligase (2,000,000 Cohesive End Unit (CEU)/mL, catalog #M020T) and the corresponding ligase buffer were purchased from New England Biolabs. PAGE gel was performed using the Bio-Rad Mini-PROTEAN Tetra Cell System (catalog #165-8000). 30% ammonium hydroxide was purchased from Fisher Sci. (catalog #A669500). Ultrapure water was obtained from a Milli-Q Ultra-Pure Water System. Autoclave tips, water, and buffers were used for all the experiments.

2.6.2 Preparation of Oligonucleotides

Applied Biosystems Model 392 DNA/RNA synthesizer was used for the synthesis of all oligonucleotides using standard phosphoramidite reagents and CPGs. Special modifications (Figure 2.10) were used for the synthesis of some oligonucleotides: Fluorescein-dT phosphoramidite (catalog #10-1056-95), dSpacer CE phosphoramidite (catalog #10-1914-90) and chemical phosphorylation reagent II (catalog #10-1901-90) was used to incorporate a fluorescein, an abasic group and a phosphate group, respectively. The synthesis was performed under DMT-on option and upon completion, the synthesized strands were incubated overnight in 30%

ammonium hydroxide at room temperature to remove protecting groups and the solid support. The purification was done following the manufacturer's instruction using Glen-Pak cartridges. DNA concentration was determined, and purity was assessed by StainsAll. The DNA sequences are listed in Table 2.1.

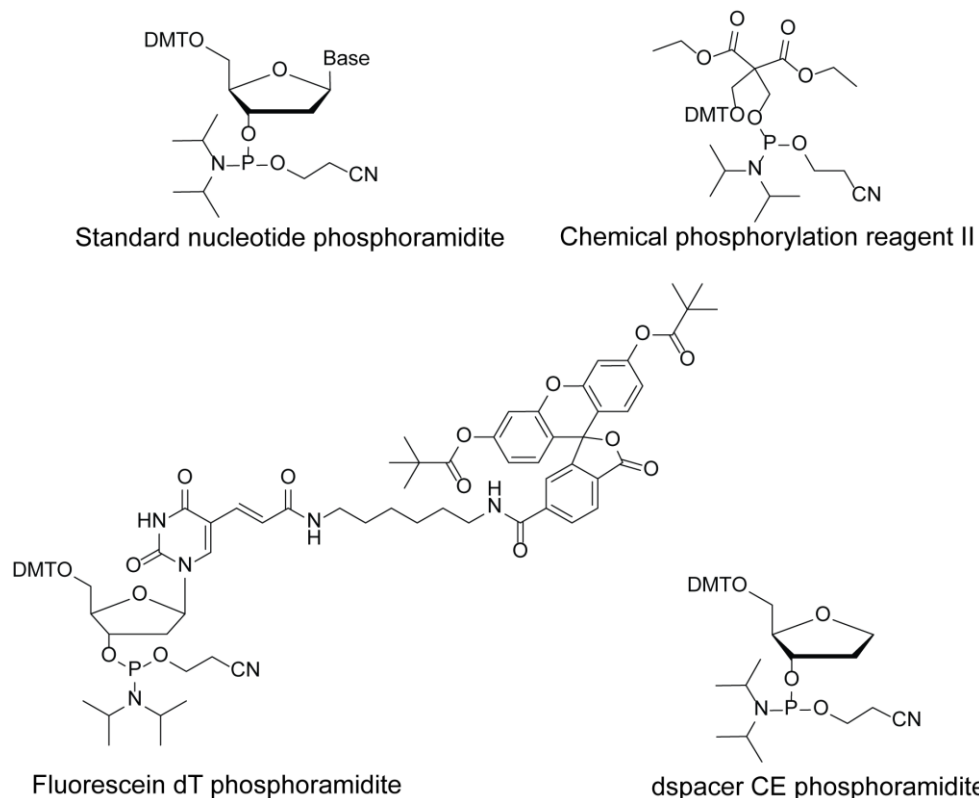


Figure 2.10 Chemical structures of the phosphoramidites used in this study. DMT is 4,4'-dimethoxytrityl.

2.6.3 StainsAll Preparation for Strand's Purity

The purity of all the synthesized oligonucleotides were assessed by running 1.3 nmol of each DNA strands on a 15% denaturing PAGE gel, which is then stained for 15 min in a StainsAll solution (25 mL of water, 25 mL of formamide, and 3 mg of StainsAll). The gels were

immediately imaged on the imager. Single band in each lane for each synthesized strand confirmed the purity. Multiple bands would suggest the presence of impurities.

Table 2.1 DNA sequences used in this project.

Temperature Tuning Reaction		
Sequence name	DNA sequence	
DNA-I	5'-TTGTTAAATATTGATAAG-3'	
F-DNA-I	5'-T _F TGTTAAATATTGATAAG-3'	
F-DNA-Ia	5'-T _F TGTTAAAT-3'	
DNA-Ib	5'-pATTGATAAG-3'	
DNA-IIa	5'-p(Ab)ATTTAACAA-3'	
DNA-IIb(G)	5'-CTTAGCAA-3'	
DNA-IIb(C)	5'-CTTACCAA-3'	
DNA-IIb(A)	5'-CTTAACAA-3'	
DNA-IIb(Ab)	5'-CTTA(Ab)CAA-3'	
F-DNA-IIb(T)	5'-T _F CTTATCAA-3'	
F-DNA-IIb(G)	5'-T _F CTTAGCAA-3'	
F-DNA-IIb(C)	5'-T _F CTTACCAA-3'	
Competition Reaction		
Sequence name	DNA sequence	
DNA-I	5'-TTGTTAAATATTGATAAG-3'	
F-DNA-II(T)	5'-T _F CTTATCAA(Ab)ATTTAACAA-3'	<i>Short Product</i>
F-DNA-II(G)	5'-T _F ATCTTAGCAA(Ab)ATTTAACAA-3'	<i>Long Product</i>
DNA-Ia	5'-TTGTTAAAT-3'	

DNA-Ib	5'-pATTGATAAG-3'
DNA-IIa	5'-p(Ab)ATTTAACAA-3'
F-DNA-IIb(T)	5'-T _F CTTATCAA-3'
F-DNA-IIb(G)	5'-T _F ATCTTAGCAA-3'

T_F: fluorescein-modified thymidine, p: phosphate, Ab: abasic lesion

2.6.4 MALDI Characterization

All the DNA strands were characterized by MALDI-TOF. About 5 nmol of each of the synthesized DNA strands were dissolved in triethylammonium acetate (0.1 M TEAA, pH 7.0) and desalted using C18 Ziptip pipette tips (ZTC18S096, Millipore) according to their procedure. After the desalting procedure, the DNA was eluted with 5 μL of 1:1 ACN/H₂O. The latter was then mixed in a 1:1 ratio with a matrix solution consisting of a 9:1 mixture of 3-hydroxypicolinic acid (25 mg/mL) and ammonium citrate solution (25 mg/mL). 1 μL of the DNA/matrix mixture was spotted on a MALDI target plate and allowed to dry. The plate was loaded on the instrument and measurements were taken on a Voyager Elite (Applied BioSystems, Foster City, CA, USA) time of flight-mass spectrometer in linear negative mode.

Table 2.2 MALDI-TOF of DNA sequences.

DNA sequence name	Calculated mass	Measure mass
DNA-I	5552	5552
F-DNA-Ia (fluorescein modified)	3240	3241
DNA-Ib (5'-phospahte):	2842	2842
DNA-IIa (abasic group, 5'-phosphate)	2966	2966
DNA-IIb(T):	2369	2368

F-DNA-IIb(T) (fluorescein modified)	3185	3187
DNA-II(G)	2394	2394
DNA-IIb(C)	2354	2354
DNA-IIb(A)	2378	2379
DNA-IIb(Ab)	2244	2243
F-DNA-IIb(T)	3185	3187
F-DNA-IIb(G)	3827	3829

2.6.5 Thermal Dissociation Experiment

DNA-I (1.3 nmol), **DNA-IIa** (1.3 nmol), and **DNA-IIb(G)** (1.3 nmol), which form the nicked duplex were combined in 1.0 mL of PBS buffer (10 mM MgCl₂, 20 mM PBS, pH 7.0).

The mixture was hybridized in the fridge for 1 hour before transferring into a quartz cuvette with a stirring bar. The cuvette was capped and then immediately placed on an HP 8453 diode-array spectrophotometer with an HP 89090A Peltier temperature controller instrument. The melting profile was collected at a temperature range of 8 to 65 °C with a 1 °C increment, while stirring at 200 rpm.

2.6.6 15% Denaturing Polyacrylamide Gel Electrophoresis

Polyacrylamide gel electrophoresis (PAGE) is a technique used to separate nucleic acids based on their electrophoretic mobility. In our case, a lower band indicates the smaller fluorescent probe (8mer) and an upper band indicates the ligated fluorescent product (18mer) as shown in Figure 2.11.

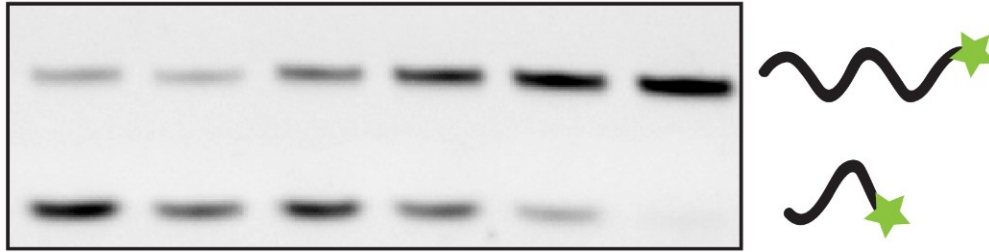


Figure 2.11 Polyacrylamide gel electrophoresis image of a ligation reaction. *Lower band*: small fluorescent probe and *upper band*: ligated fluorescent product.

2.6.6.1 Sample Preparation for PAGE

The ligation reaction was performed in a total of 15 μL mixture. At various time points 1.8 μL of the ligation mixture was pipetted into a labelled microtube containing 2 μL of running dye solution. The running dye is a mixture of 0.25% w/v bromophenol blue in 80% w/v sucrose in 0.5 M ethylenediaminetetraacetic acid (EDTA). The bromophenol provides the visual color to monitor the reaction on the gel and sucrose provides viscosity to the sample allowing the settling down in the well of the PAGE gel. EDTA was used to stop the ligation reaction by chelating the magnesium ions, which is a cofactor for T4 DNA ligase. The aliquots collected at the various data points were loaded on a 15% PAGE gel.

2.6.6.2 Preparation of 15% PAGE

Firstly, urea (4.8 g) was weighed into a 100 mL graduated cylinder. Concentrated Tris/Borate/EDTA buffer (5x TBE, 1mL) and 40% Acrylamide/Bis-Acrylamide solution 19:1 (3.75 mL) were added to the cylinder. The mixture was top-up to 10 mL with MilliQ water followed by stirring until all the urea was dissolved. Then 80 μL of aqueous ammonium persulfate (APS, 10% w/v) and 10.7 μL tetramethyl ethylenediamine (TEMED) were added to initiate polymerization. The gel mixture was immediately pipetted into the gel casting system and was

allowed to polymerize for one hour. The prepared gels were 0.75 mm thick with 10 wells. After one hour the gels were either stored in a sealed Ziplock bag at room temperature for a maximum of two days or immediately used.

2.6.6.3 Running PAGE Gel

The gels were washed to remove extra polymerized gel on the plates and then assembled in a Bio-Rad Mini-PROTEAN Tetra Cell, which was then filled with running buffer (1x TBE). Prior to loading the gels, the wells were rinsed with a syringe containing running buffer to remove excess accumulated urea. The reaction/running dye (3 μ L) mixture was loaded into each well. The gel was run for 75 min at 175 V until the bromophenol blue band reached the bottom. The gel was immediately imaged on an ImageQuant RT fluorescent imager with trans-UV illumination and a fluorescein filter (Filter #4). The fluorescence intensity of each band on the gels was quantified in terms of percentage using an ImageQuant TL analysis software. The lower band indicates the % yield of the fluorescent reactant probe, while the upper band represents the longer fluorescent product (ligated DNA strand).

2.6.6.4 Quantifying Ligation Yields and Turnover Numbers (TON)

The data in each Figure represents the average of at least two ligation reactions and the error bars represent the standard deviation. The % yield (% conversion) for every ligation reaction was quantified from PAGE images. The following equation was used to calculate the % yield of the product at each data point:

$$\% \text{ Yield} = \frac{\text{Intensity (Product Band)}}{\text{Intensity (Product Band + Reactant Band)}} \times 100\%$$

By multiplying this percentage with the concentration of the fluorescently labeled probe (the limiting fragment = 1.4 μM), the concentration of the product was obtained. The turnover was calculated according to the equation below.

$$\text{TON} = \frac{\Delta[\text{F-DNA-I}]}{[\text{Template}]}$$

The maximum difference of **F-DNA-I** is calculated as follows:

$$\Delta[\text{F-DNA-I}] = [\text{F-DNA-I}(\text{Template})] - [\text{F-DNA-I}(\text{Control})]$$

2.6.7 DNA Ligation Experiments

2.6.7.1 Single Turn-Over Reaction

Phosphate probe **DNA-I** (20 pmol), fluorescent probe **F-DNA-IIb(X)** (20 pmol), and **DNA-IIa** probe (40 pmol) were added in a 600 μL microcentrifuge. The volume was top up to 10 μL with MilliQ water. The reaction mixture was placed in a heat incubator set at 12 or 16 $^{\circ}\text{C}$. In the meantime, a master mix containing T4 DNA ligase (300 CEU, 2 μL), ligation buffer (3 μL) and MilliQ water (5 μL) was prepared in another 600 μL microtube. The latter was vortexed, centrifuged and 5 μL was immediately added to the 10 μL DNA solution. A timer was started. The final volume was 15 μL and final concentration was 1.4 μM for 20 pmol DNA. Data points were collected by aliquoting 2 μL from the ligation mixture into 2 μL of EDTA/sucrose/dye mixture to stop the ligation reaction at various time points. After collecting samples at all the time points, they were all run on a 15% PAGE gel.

2.6.7.2 Cross Catalysis

For the DNA cross-catalysis ligation experiments, the reaction set up was exactly like the single turn over experiment except that there were 4 probes rather than two and the enzyme used was 2000 CEU T4 DNA ligase (New England Biolabs). Total volume was 15 μ L. Final concentration was 14 nM, 1.4 nM, 140 pM or 0 nM target **DNA-I**; 1.4 μ M limiting fluorescent probe **F-DNA-I** and 2.8 μ M for the other probes (**DNA-Ib**, **DNA-IIa** and **DNA-IIb(X)**) except for the template concentration variation studies where the fluorescent probe was 0.7 μ M while the other probes were 1.4 μ M. . X=T for a matched probe and X=G, C, A or Ab for mismatched probe. A temperature range of 16 to 30 $^{\circ}$ C was stated in the caption of each Figure.

2.6.8 Gel Images

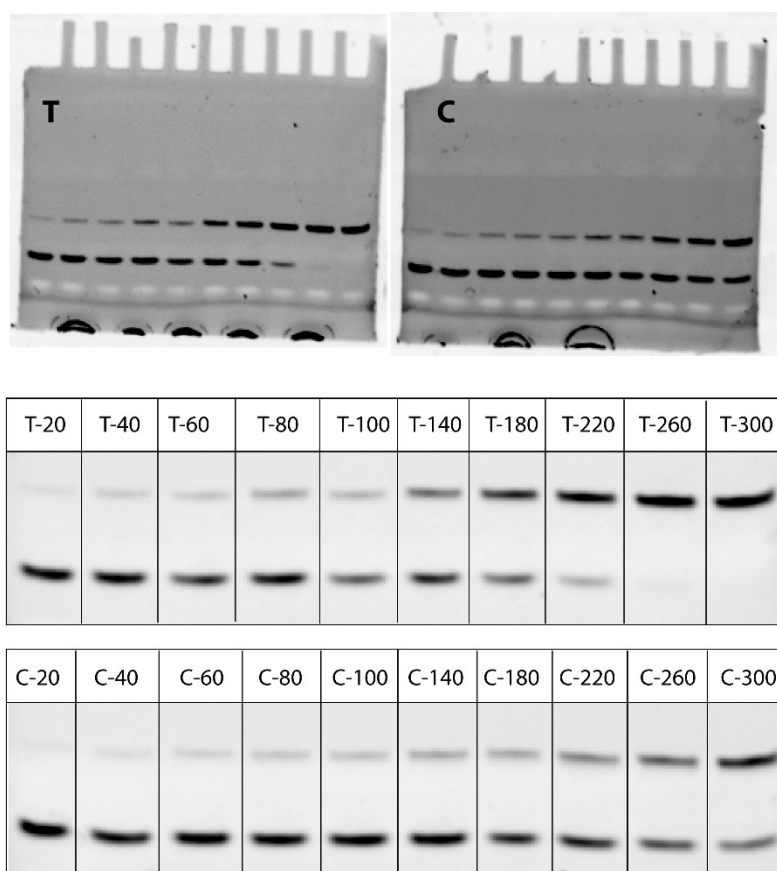


Figure 2.12 Gel images representing the ligation reaction using destabilizing probes (Ab and no mismatch) as a function of time in minutes (shown in Fig. 2.2, Ab + X = T, black trace). T and C

refers to the presence or absence of 14 nM of initial target **DNA-I**, respectively. *Top band: F-DNA-I; bottom band: F-DNA-Ia*. *Experimental conditions: 14 or 0 nM DNA-I; 1.4 μM F-DNA-Ia; 2.8 μM DNA-Ib; 2.8 μM DNA-IIa; 2.8 μM DNA-IIb(T); 26 °C.*

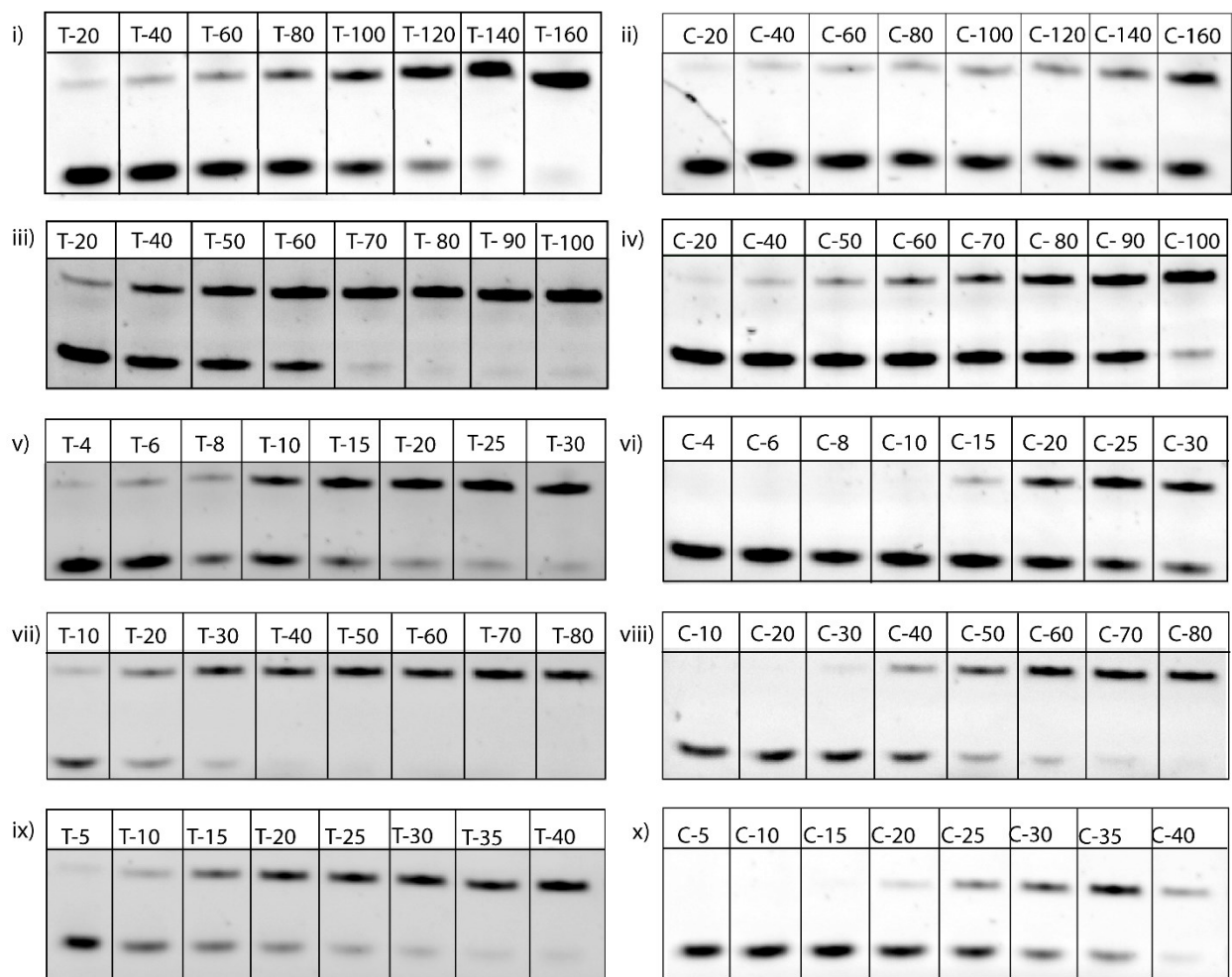


Figure 2.13 Gel images representing ligation reactions using destabilizing probes containing the abasic and mismatch as a function of time and at different temperatures. These data are exhibited in Figures 2.2 and 2.5 ($Ab + X = G$). Experiments shown in i) iii) v) vii) ix) were done in the presence of initial target (14 nM **DNA-I**) and ii) iv) vi) viii) x) were performed with no initial target (0 nM **DNA-I**). *Top band: F-DNA-I; bottom band: F-DNA-Ia*. *Experimental conditions: 14*

or 0 nM **DNA-I**; 1.4 μ M **F-DNA-Ia**; 2.8 μ M **DNA-Ib**; 2.8 μ M **DNA-IIa**; 2.8 μ M **DNA-IIb(G)**;
 i) and ii) 22 °C; iii) and iv) 24 °C; v) and vi) 26 °C; vii) and viii) 28 °C; ix) and x) 30 °C.

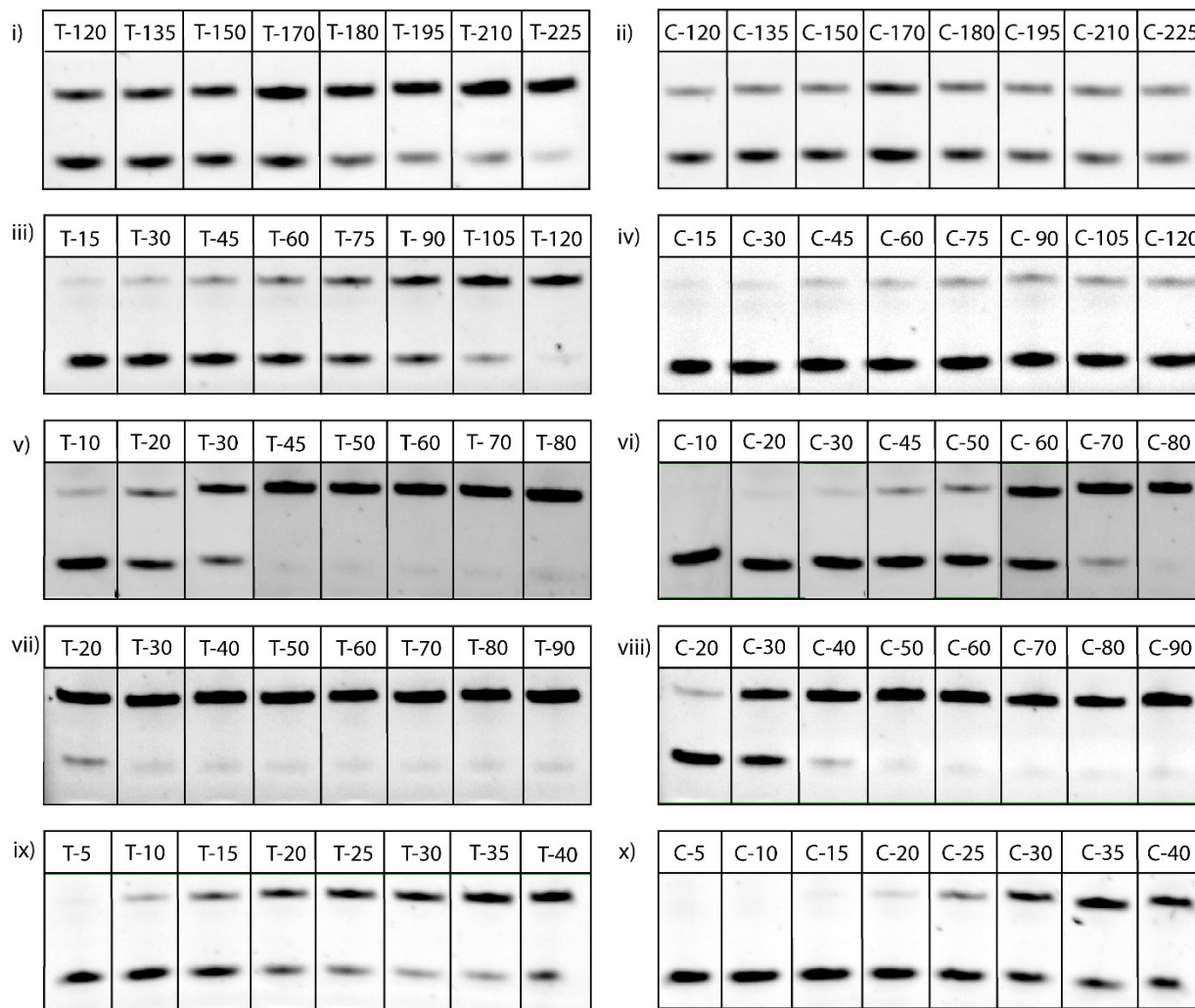


Figure 2.14 Gel images representing ligation reactions using destabilizing probes containing the abasic and mismatch as a function of time and at different temperatures. These data are exhibited in Figures 2.5 ($Ab + X = C$). Experiments shown in i) iii) v) vii) ix) were done in the presence of initial target (14 nM **DNA-I**) and ii) iv) vi) viii) x) were performed with no initial target (0 nM **DNA-I**). *Top band: F-DNA-I; bottom band: F-DNA-Ia. Experimental conditions: 14 or 0 nM*

DNA-I; 1.4 μM **F-DNA-Ia**; 2.8 μM **DNA-Ib**; 2.8 μM **DNA-IIa**; 2.8 μM **DNA-IIb(C)**; i) and ii) 18 °C; iii) and iv) 20 °C; v) and vi) 22 °C; vii) and viii) 24 °C; ix) and x) 26 °C.

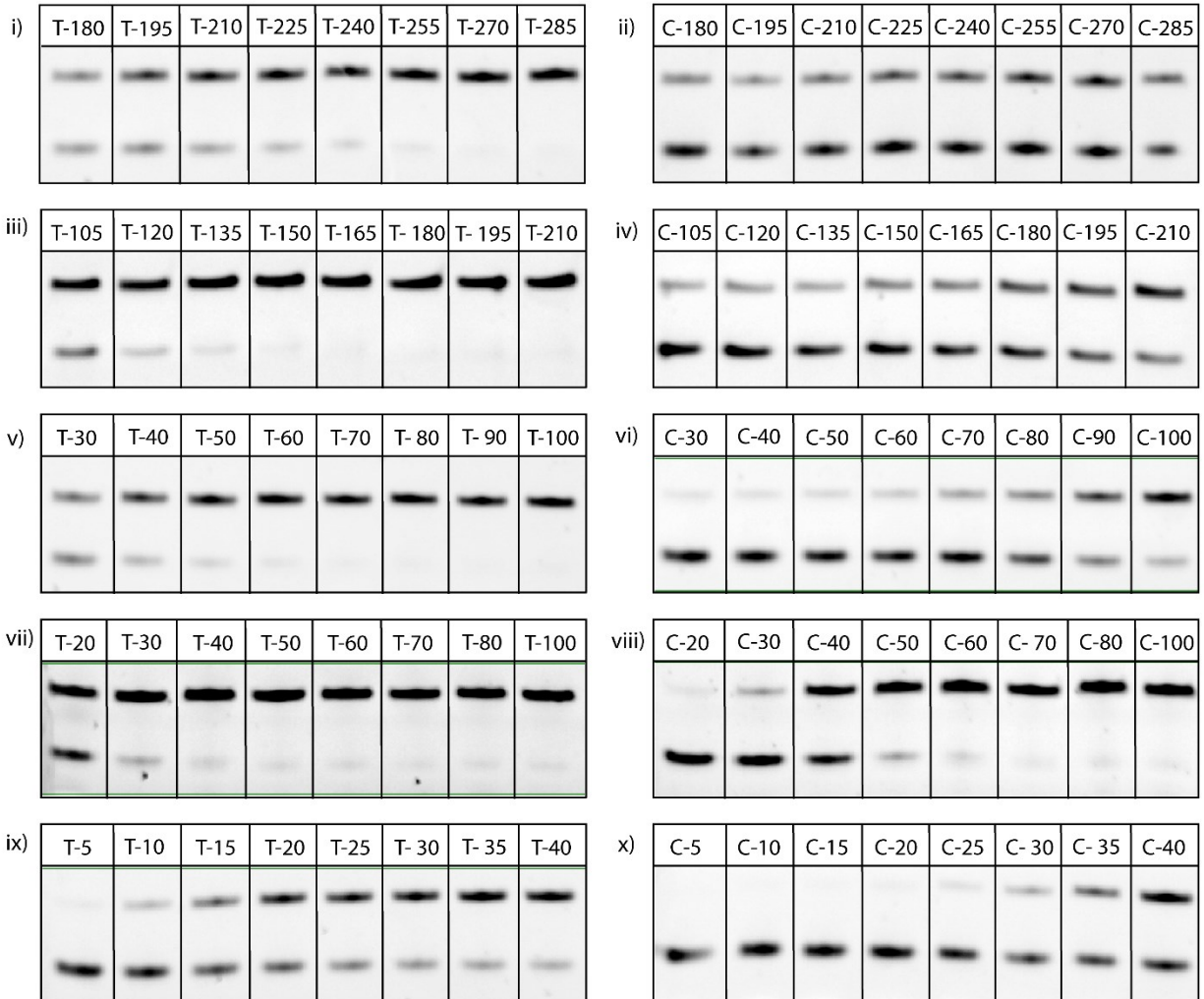


Figure 2.15 Gel images representing ligation reactions using destabilizing probes containing the abasic and mismatch as a function of time and at different temperatures. These data are exhibited in Figure 2.5 ($\text{Ab} + \text{X} = \text{A}$). Experiments shown in i) iii) v) vii) ix) were done in the presence of initial target (14 nM **DNA-I**) and ii) iv) vi) viii) x) were performed with no initial target (0 nM **DNA-I**). *Top band: F-DNA-I; bottom band: F-DNA-Ia. Experimental conditions: 14 or 0 nM **DNA-I**; 1.4 μM **F-DNA-Ia**; 2.8 μM **DNA-Ib**; 2.8 μM **DNA-IIa**; 2.8 μM **DNA-IIb(A)**; i) and ii) 18 °C; iii) and iv) 20 °C; v) and vi) 22 °C; vii) and viii) 24 °C; ix) and x) 26 °C.*

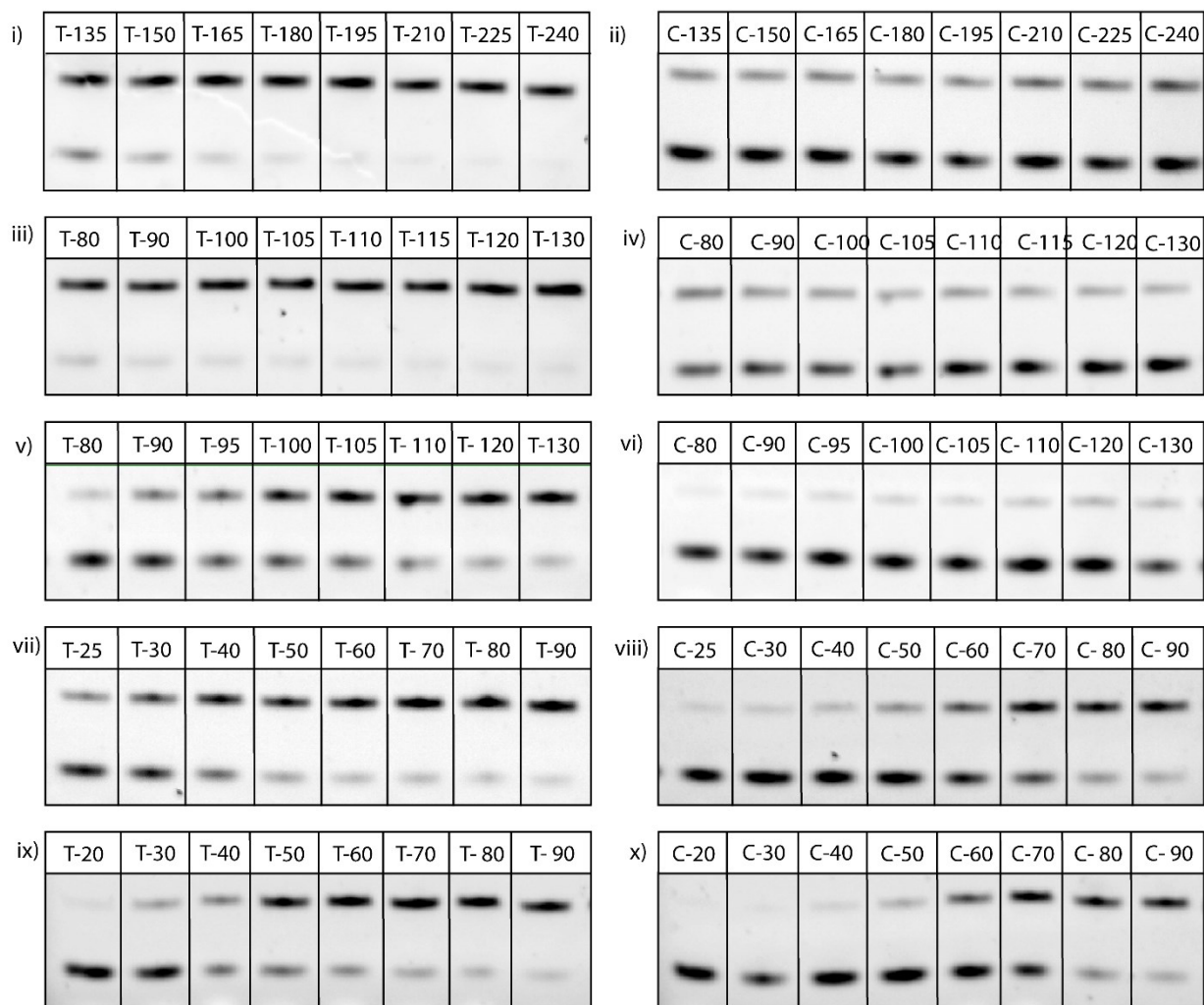


Figure 2.16 Gel images representing ligation reactions using destabilizing probes containing the abasic and mismatch as a function of time and at different temperatures. These data are exhibited in Figure 2.5 ($Ab + X = Ab$). Experiments shown in i) iii) v) vii) ix) were done in the presence of initial target (14 nM **DNA-I**) and ii) iv) vi) viii) x) were performed with no initial target (0 nM **DNA-I**). *Top band: F-DNA-I; bottom band: F-DNA-Ia.* *Experimental conditions:* 14 or 0 nM **DNA-I**; 1.4 μ M **F-DNA-Ia**; 2.8 μ M **DNA-Ib**; 2.8 μ M **DNA-IIa**; 2.8 μ M **DNA-IIb(Ab)**; i) and ii) 16 °C; iii) and iv) 18 °C; v) and vi) 20 °C; vii) and viii) 22 °C; ix) and x) 24 °C.

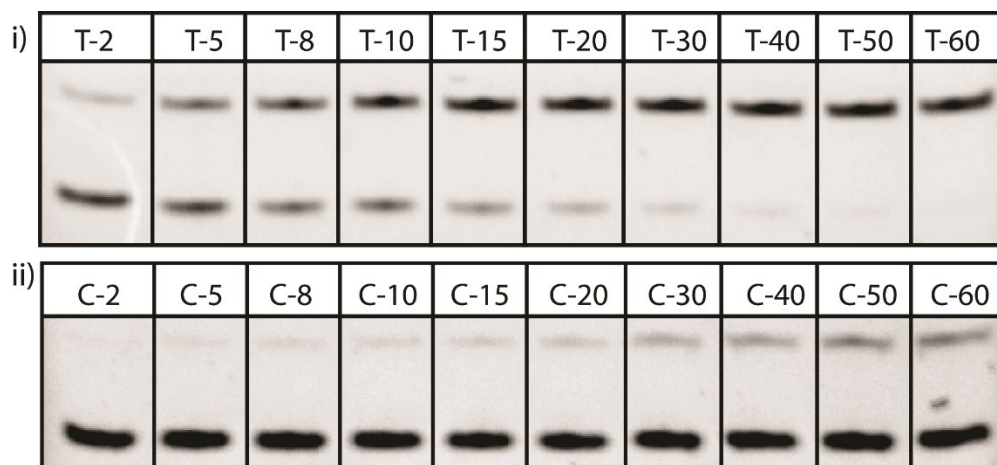


Figure 2.17 Gel images representing the ligation reaction done on the bench top using destabilizing probes containing the abasic and mismatch as a function of time in minutes and at room temperature (shown in Figure 2.7). T and C refers to the presence or absence of 14 nM of initial target **DNA-I**, respectively. *Top band: F-DNA-I; bottom band: F-DNA-Ia.* *Experimental conditions:* 14 or 0 nM **DNA-I**; 1.4 μ M **F-DNA-Ia**; 2.8 μ M **DNA-Ib**; 2.8 μ M **DNA-IIa**; 2.8 μ M **DNA-IIb(C)**; 21 °C.

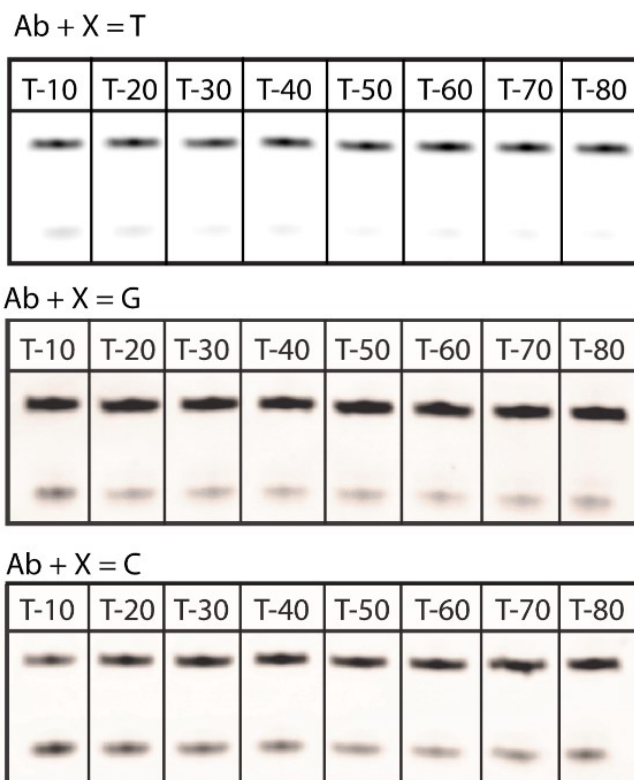


Figure 2.18 Gel images representing the single turnover ligation reaction using destabilizing probes (Ab and X=T/G/C mismatch) as a function of time in minutes (shown in Figure 2.1) T refers to the presence of initial of 14 μM target **DNA-I**. *Top band: F-DNA-II; bottom band: F-DNA-IIb(X)*. *Experimental conditions: 14 μM DNA-I; 1.4 μM F-DNA-IIb(X); 2.8 μM DNA-IIa; 16 $^{\circ}\text{C}$.*

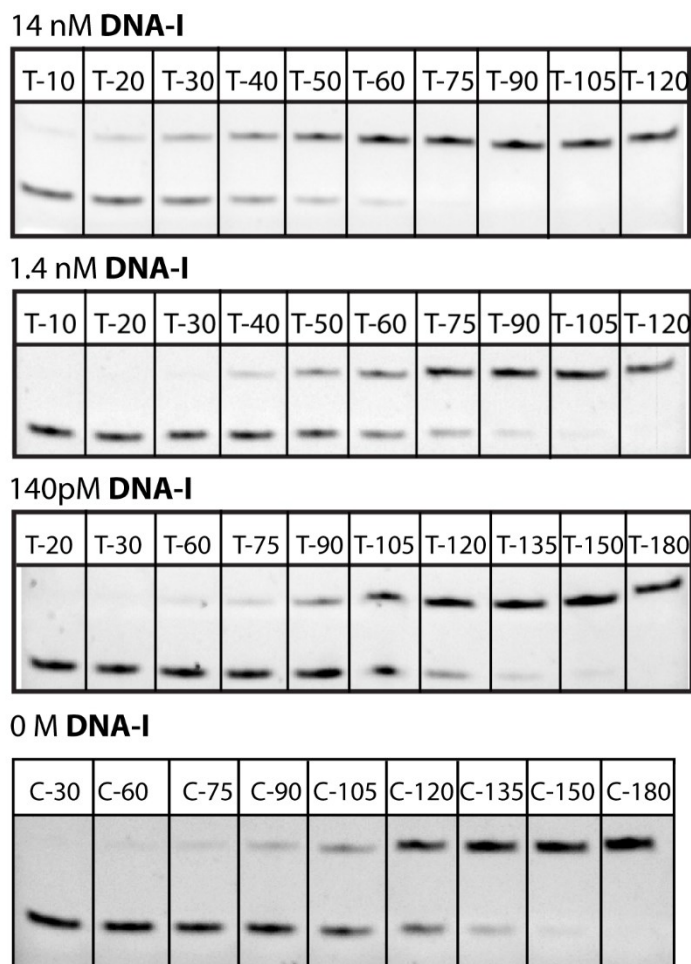


Figure 2.19 The concentration of **F-DNA-I** formed as a function of time with different concentrations of initial **DNA-I** template and lower replicator concentrations than standard conditions (shown in Figure 2.4). T and C refers to the presence or absence of initial target **DNA-I**, respectively. *Top band: F-DNA-I; bottom band: F-DNA-Ia*. *Experimental conditions: 14 nM, 1.4 nM, 140 pM or 0 nM DNA-I; 0.7 μM F-DNA-Ia; 1.4 μM DNA-Ib; 1.4 μM DNA-IIa; 1.4 μM DNA-IIb(T); 26 °C.*

Chapter 3

Reverse Transcription Lesion-Induced DNA Amplification:

An Instrument-Free Isothermal Method to Detect RNA

3.1 Introduction

The use of ribonucleic acid (RNA) sequences as a biomarker for the diagnosis of a range of diseases has gained attention over the last few decades.¹⁵⁴⁻¹⁵⁵ For example, many infectious viruses such as HIV¹⁵⁶, Ebola¹⁵⁷, hepatitis C¹⁵⁶, Zika¹⁵⁷⁻¹⁵⁸, Covid-19^{2, 10} have RNA as their genetic material rather than DNA. Additionally, messenger RNA (mRNA) are present in a larger abundance than DNA in bacterial cells,¹⁵⁴ thus mRNA can be a useful biomarker for bacterial detection.¹⁵⁹⁻¹⁶⁰ Moreover, as protein expression levels are mirrored by mRNA concentration, mRNA biomarkers are also useful for detecting cell abnormalities.¹⁶¹⁻¹⁶² Finally, microRNA (miRNA) is a class of naturally occurring RNA of short length,¹⁶³ and the abundance of specific sequences can be correlated with various diseases such as cancer, heart failure, and diabetes mellitus amongst others.^{56, 155, 164-165} Thus, the development of a simple, rapid, and sensitive RNA detection platform that can be performed with minimal training and in limited resource settings is key for early disease diagnosis, prognosis, and treatment especially in low income countries where infectious diseases are more prevalent.¹⁶⁶ However, one major problem of nucleic acid based diagnostics is the low concentration of nucleic acids biomarker in the biological samples i.e., blood, urine, saliva etc.^{37, 56, 163} Therefore, a key step prior to detection of the biomarker is to amplify the nucleic acid.³⁷ Although equipment- or instrument-free platforms are ideal for point-of-care (POC) diagnostics as outlined by the World Health Organisation,^{25, 28} methods for the enzymatic amplification of nucleic acids without the use of a heating element are rare.^{54, 125}

Many techniques for RNA biomarker-triggered nucleic acid amplification have been developed but reverse transcription polymerase chain reaction (RT-PCR) remains the gold standard.¹⁵⁶⁻¹⁵⁸ It is a two-step process that relies on transcribing the RNA into a complementary DNA (cDNA) using the reverse transcriptase enzyme followed by that cDNA undergoing

exponential enzymatic amplification by a PCR reaction. RT-PCR has shown great sensitivity but it requires multiple steps, two enzymes, highly trained personnel, and a thermocycler which makes it time consuming and expensive.^{158, 164, 167-168} This method is also not suitable for the detection of short sequences such as that of miRNA, which are typically 19 – 23 bases long, so complex primers have to be designed to accommodate the short target.^{55, 164, 167, 169} As such efforts have been made to develop ways to lengthen the RNA or cDNA prior to the PCR step adding another layer of complexity and cost of the assay.^{55, 163, 170-171} To simplify the instrumentation requirements, researchers are now focusing on the development of isothermal amplification techniques like RT-loop mediated isothermal amplification (LAMP)^{52, 55} and rolling circle amplification (RCA)⁵⁸ for POC diagnostics.

One challenge of isothermal methods like RT-LAMP and RCA commonly used in POC applications, is that they often require more than one enzyme and higher temperatures, the latter necessitating the use of heating instrumentation.^{52, 58, 82} For example, RT-LAMP, like RT-PCR, utilizes reverse transcriptase in the first step to transcribe RNA into cDNA,⁵² while for RCA an RNA-templated DNA ligation is performed with ligase to generate a circular template.^{58, 82} Next the cDNA is liberated from the RNA by digestion or nicking enzymes followed by amplification by polymerase.^{52, 162} These sequential steps of forming and amplifying cDNA often lead to the use of multiple temperatures even when isothermal amplification methods are employed¹⁷². To overcome these problems and present a complementary approach to RT-polymerase based methods, we describe a simple, instrument-free method for detecting RNA that is completely performed at room temperature, uses only one enzyme (a ligase) and colorimetric detection. Although examples exist for sensitive RNA detection that require no heating element,¹⁷³ the

detection step often requires significant instrumentation unlike our method that requires only eppendorf tubes and reagents to proceed.

Previously we reported the development of lesion-induced DNA amplification (LIDA), which was capable of rapid, exponential amplification of different 18 nucleotide DNA target sequences by incorporating a destabilizing abasic lesion into one of the target-complementary primers, or probes, in a ligase chain reaction.⁷¹⁻⁷³ With this approach, as little as 140 fM (2.1 attomoles) of target DNA was detected following a two-step serial amplification procedure.⁷³ In more recent work, it was revealed that adding a second destabilizing lesion consisting of a mismatch or another abasic group allowed the replication temperature to be tuned from 18-30 °C for a particular target sequence. Using the optimal probe sequences, target DNA was amplified on the benchtop without any heating source or equipment.⁷¹ Regarding the visualization step, our group has also developed a rapid, room-temperature method for detecting single-stranded DNA using DNA-modified gold nanoparticle aggregate disassembly.¹²⁷ Herein we combine these two approaches and add an additional step to facilitate both amplification and detection triggered by a RNA target sequence. This RNA-triggered LIDA uses only one enzyme and proceeds entirely at 28 °C. Using this modified LIDA followed by cDNA-initiated nanoparticle disassembly, we can distinguish 105 amol target RNA in the presence of cellular RNA within three hours by colorimetric detection.

3.2 Design of Isothermal RNA Transcription Lesion-Induced DNA Amplification

To achieve rapid isothermal RNA detection using LIDA, the RNA is first transcribed into a cDNA using a ligation strategy rather than a reverse transcription (as compared to RT-PCR or RT-LAMP). In the second step, the cDNA is amplified in a cross catalytic fashion using lesion-induced turnover in a ligase chain reaction as shown in Figure 3.1. Specifically, in step A, the

target RNA hybridizes with two complementary DNA primers, or probes, (**DNA-IIa** and **DNA-IIb**) to form an RNA-**cDNA** nicked duplex, which is then ligated by T4 DNA ligase, the same enzyme used for DNA amplification by LIDA (Figure 3.1). The denaturation of RNA-**cDNA** product duplex can be achieved using various strategies like applying heat,¹⁷⁴ using a nuclease enzyme (example DSN or RNase H)^{115, 175-176} or by toehold-mediated strand displacement⁵⁸. Since the goal was to have a simple, cost effective and isothermal assay, the latter option was selected. Displacement DNA (**ddDNA**) was designed to hybridize with the RNA target sequence, including an overhang region (i.e. toehold) that stemmed from the use of DNA primers in the first step that were shorter than the RNA target (Figure 3.1). As the resulting RNA-**ddDNA** duplex was designed to be more stable than the RNA-**cDNA** duplex, displacement should be spontaneous. Once liberated, the **cDNA** sequence can hybridize to two complementary probes (Figure 3.1, cycle B): one that contains an abasic site (*oval*) and the other a mismatch (*square*) as well as a fluorescent label (*star*). After templated ligation of these probes, the newly formed destabilizing template DNA (referred to as **F-DNA** as it contains a fluorescent label) spontaneously dissociates from the **cDNA** due to the presence of the destabilizing groups. A second reaction (Figure 3.1, cycle C) then uses this destabilizing strand to template the ligation of two other probes (the same probes in step A). The result is a copy of the **cDNA** (Figure 3.1, cycle C). This cross-catalytic replication of **cDNA** and **F-DNA** continues until all the probes are consumed.

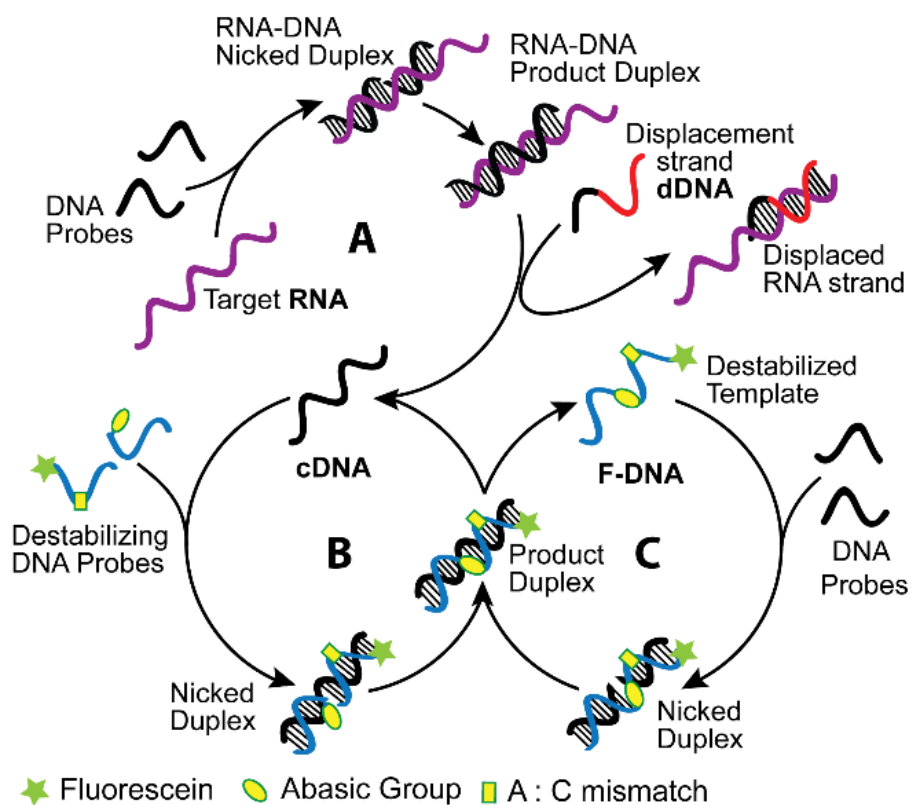


Figure 3.1 Schematic of reverse transcription lesion-induced DNA amplification (RT-LIDA). First the RNA target is transcribed into a **cDNA** strand, which is then amplified isothermally by LIDA after strand displacement by **dDNA**. *Black probes: DNA-IIa and DNA-IIb; Blue destabilizing probes: DNA-Ia and DNA-Ib; Oval: abasic lesion; Square: A:C mismatch; Star: fluorescein label.*

3.3 Optimization of RNA Transcription-Lesion Induced DNA Amplification

3.3.1 Influence of ATP Concentration in the RNA-Templated Synthesis of cDNA

Landegren and coworkers reported that RNA-templated ligation using T4 DNA ligase works best at low ATP concentration ($\sim 10 \mu\text{M}$).¹⁷⁷ In contrast, our normal LIDA reaction is performed at an ATP concentration of 1 mM. Thus, to optimize the concentration of ATP, the RNA-templated ligation step (Figure 3.1, step A) was investigated separately for different ATP

concentrations: 10 μM , 100 μM and 1 mM. For proof of concept, a 27-base long synthetic RNA sequence mimicking a miRNA (1.4 μM) was incubated at 28 $^{\circ}\text{C}$ with 2.8 μM of **DNA-IIa** and 1.4 μM of fluorescently labelled **DNA-IIb** at varying ATP concentrations. As expected, >90% ligation was observed within 90 minutes using 10 μM ATP based on polyacrylamide gel electrophoresis (PAGE) as compared to 100 μM and 1 mM ATP, which gave only 46% and 23% ligation, respectively (Figure 3.2A). The time course of the ligation reaction with 10 μM ATP based on PAGE analysis is shown in Figure 3.2. These results confirmed that a lower concentration of ATP was required for RNA-templated DNA ligation as compared with the DNA-templated reaction to avoid premature AMP reloading of the enzyme owing to the slower ligation rate in presence of RNA template.¹⁷⁷

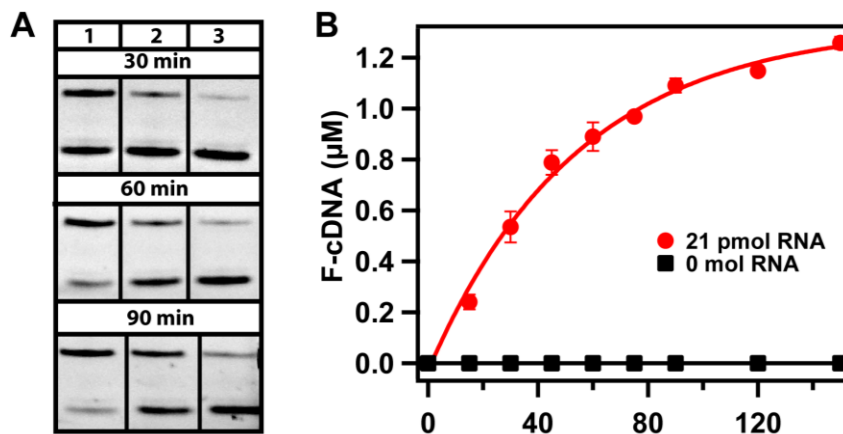


Figure 3.2 A) Polyacrylamide gel image of the RNA-templated DNA ligation at different ATP concentrations and time points. Lane 1: 10 μM ATP; Lane 2: 100 μM ATP; Lane 3: 1 mM ATP; Top band: **F-cDNA** product; bottom band: **F-DNA-IIb** fluorescent labelled probe. B) Kinetics of **F-cDNA** formation at 28 $^{\circ}\text{C}$ initiated by 21 pmol (red trace) and 0 pmol (black trace) RNA template. *Experimental conditions:* RNA (21 pmol or 0 mol), fluorescent probe **F-DNA-IIb** (21 pmol) and 5'-phosphate terminated probe **DNA-IIa** (42 pmol), 2000 CEU T4 DNA ligase, 50 mM Tris-HCl (pH 7.5), 10 mM MgCl_2 and 100 μM ATP, final volume 7.5 μL , 28 $^{\circ}\text{C}$.

3.3.2 Tuning the Temperature of the cDNA-Initiated LIDA

To have an isothermal assay, both the RNA-templated ligation and LIDA of cDNA should work at the same temperature, ideally room temperature. However, the cross catalysis of this cDNA sequence by LIDA works best at 37 °C when only one destabilizing group was incorporated into the probe sequence (Figure 3.3A). As mentioned, our previous work showed that the replication temperature in LIDA can be tuned by the introduction of a mismatch to the system, which is less destabilizing than an abasic group.⁷¹ Thus, a T base was switched into a C base in one of the probes (**DNA-Ia**) that resulted in an A:C mismatch (square, Figure 3.1). This combination of destabilizing elements allowed us to lower the temperature from 37 °C to 28 °C (Figure 3.3B), which is the same optimal temperature as the RNA-templated ligation step. Figure 3.3B illustrates the sigmoidal formation of DNA with time in LIDA reactions initiated by 105 fmol (red trace) or 0 mol (black trace) of cDNA using the abasic and an A:C mismatched probes (**DNA-Ib** and **DNA-Ia**, respectively). The background process, which also leads to **F-DNA** sequence amplification in the absence of initial RNA is due to a pseudo-blunt end ligation reaction of the four primers that is used in the LIDA system (Figure 3.3 and 3.4, black trace).⁷³

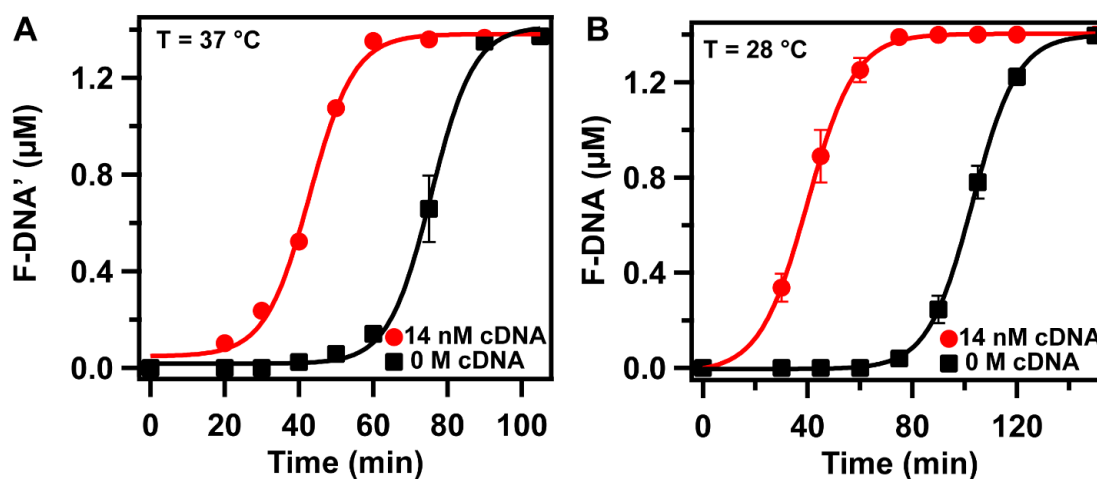


Figure 3.3 A) Kinetics of LIDA using the probe without the A:C mismatch (perfectly matched probe is **F-DNA-Ia'** which yields **F-DNA'**). **F-DNA'** formation at 37 °C for cross catalysis

initiated by 14 nM (circles) or 0 nM (squares) **cDNA** with the abasic-only system. B) Kinetics of cross-catalytic formation of **F-DNA** at 28 °C initiated by 14 nM (circles) or 0 nM (squares) **cDNA** with the abasic + A:C mismatch system (mismatch-containing probe is **F-DNA-Ia** which yields **F-DNA**). *Experimental conditions:* 14 nM **cDNA**, 1.4 μM **F-DNA-Ia** or **F-DNA-Ia'**, 2.8 μM **DNA-Ib**, 2.8 μM **DNA-IIa**, 2.8 μM **DNA-IIb**. We followed the experimental procedure described in our previous work.⁷³

3.3.3 Combining RNA Transcription and LIDA

The RNA-templated ligation step was merged with LIDA of **cDNA** via strand displacement to link both steps and maintaining a constant temperature. First, RNA-templated DNA ligation was initiated by 105 fmol (14 nM) of target RNA in the presence of two probes (**DNA-IIa** and **DNA-IIb**), T4 DNA ligase, and 10 μM of ATP. We also explored the background-triggered process that leads to spontaneous LIDA in the absence of any target⁷³ by combining the two probes, enzyme, and ATP and allowing them to incubate for 15 minutes (Figure 3.4, 0 fmol RNA). After various wait times for the reaction mixtures containing target RNA as well as the negative control, more ATP was added to make up a concentration of ~1 mM ATP along with the two destabilizing probes (**F-DNA-Ia** and **DNA-Ib**) and the **ddDNA** to liberate the **cDNA** from the RNA:**cDNA** duplex. The time trace of the resulting cross-catalytic formation of **F-DNA** (the complement of **cDNA**) by LIDA was monitored by PAGE (Figure 3.4). With 105 fmol of RNA target and various wait times for the first step, LIDA proceeded faster than in the absence of RNA target (Figure 3.4, 105 fmol vs 0 fmol). This suggests that the **cDNA** was successfully generated, displaced from the RNA:**cDNA** product duplex, and engaged in the cross-catalytic reaction. Moreover, there was no significant difference in the LIDA kinetic profiles for 15-, 30- and 60-minutes wait time.

Therefore, 15 minutes were taken as our optimized wait time for the reverse transcription step. As a control experiment, we performed the two-step process under the same conditions but the strand displacement DNA (**ddDNA**) was not added at the beginning of the second step, and only background-triggered LIDA was observed, indicating that no liberation of **cdDNA** occurred in the absence of **ddDNA** (Figure 3.5).

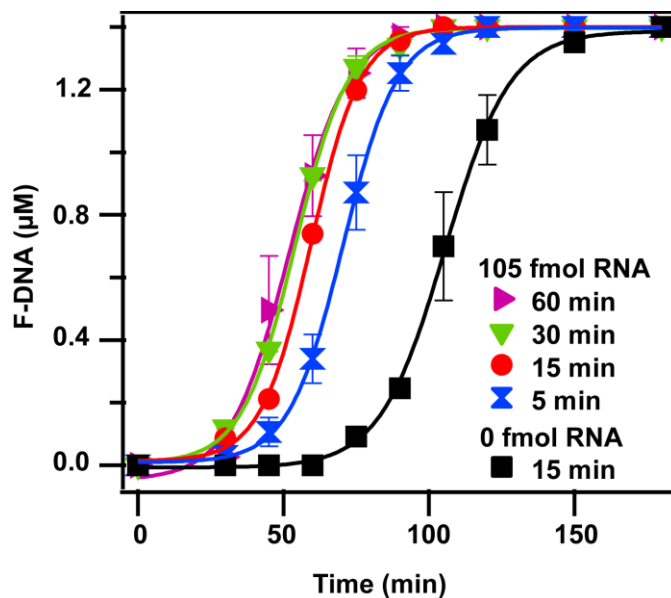


Figure 3.4 Kinetics of cross-catalytic formation of **F-DNA** at 28 °C initiated by **cdDNA** formed from the templated ligation of 105 fmol (purple, green, red, blue traces) or 0 fmol (black trace) RNA target. The legend refers to the reaction time of step one in RT-LIDA, the RNA-templated ligation step. *Probe concentrations:* 1.4 μM **F-DNA-Ia**; 2.8 μM **DNA-Ib**; 2.8 μM **DNA-IIa**; 2.8 μM **DNA-IIb**; 1.4 μM **ddDNA**.

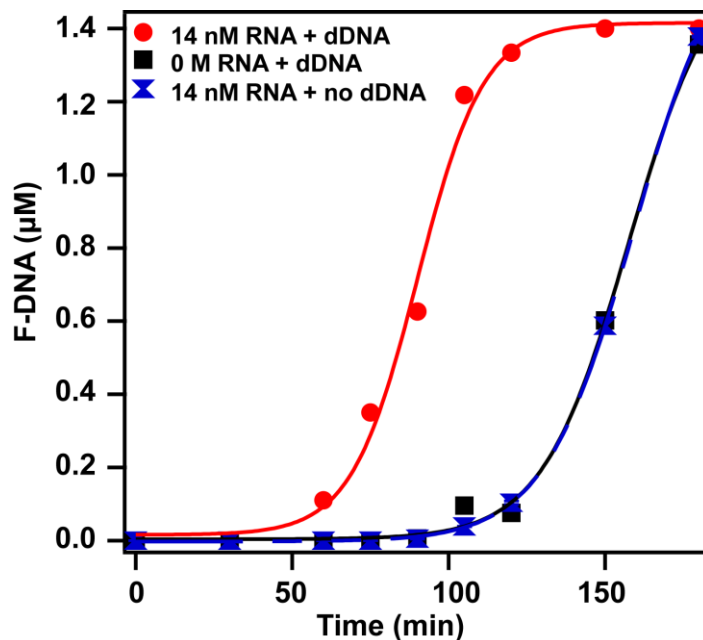


Figure 3.5 Kinetics of cross-catalytic formation of F-DNA at 28 °C initiated by 14 nM (red and blue trace) or 0 nM (black) RNA. *Experimental conditions:* 14 or 0 nM RNA; 1.4 μM F-DNA-Ia; 2.8 μM DNA-Ib; 2.8 μM DNA-IIa; 2.8 μM DNA-IIb; red trace and black trace was done in the presence of 1.4 μM dDNA, while blue trace was performed in the absence of dDNA.

3.4 Sensitivity of RT-LIDA

With these optimized conditions, reverse transcription LIDA was performed with different initial concentrations of RNA (Figure 3.6A), albeit at lower probe concentrations, which has been shown to slow down the background reaction compared with the templated process.⁷³ To determine the sensitivity of our assay, we determined the point-of-inflection (POI) from a sigmoidal fit to each kinetic trace. We then took the difference between the POI for the kinetic trace with RNA target and that from the reaction containing no RNA target (i.e., the background-triggered process) (Figure 3.6A). The Δ POI versus the logarithm of initial RNA concentration ($-\log C$) gave a linear trend with a line-of-best fit of Δ POI = $7.3 \pm 0.3 - 0.65 \pm 0.03 (-\log C)$, (r^2 -value

= 0.99). From the line of best fit, we calculated a $-\log C$ value of 11.2 ± 0.7 for ΔPOI of 0 (the x-intercept) which corresponds to the concentration when the templated reaction cannot be distinguished from the background-triggered process. The red arrow in Figure 3.6B marks the upper limit of this value ($-\log C$ of 10.5) which is equal to a concentration of 32 pM (240 amol) and is a conservative estimate of the limit of detection using PAGE and RT-LIDA. We note, however, that we could discriminate as low as 14 pM (105 amol) initial RNA target and the background-triggered process based on a discernable ΔPOI (Figure 3.6B).

These results suggest that reverse transcription lesion-induced DNA amplification has a similar sensitivity to our DNA-based assay indicating that transcribing the RNA into **cDNA** did not impact the overall cross catalysis reaction.⁷³ This similarity also implies that a serial ligation amplification procedure could be used to detect as low as 2 amol of initial RNA as shown in our previous work.⁷³ However, this procedure does add time to the assay. As our current sensitivity is suitable for microRNA target concentrations relevant to disease states (vide infra),¹⁷⁸ we did not optimize it any further.

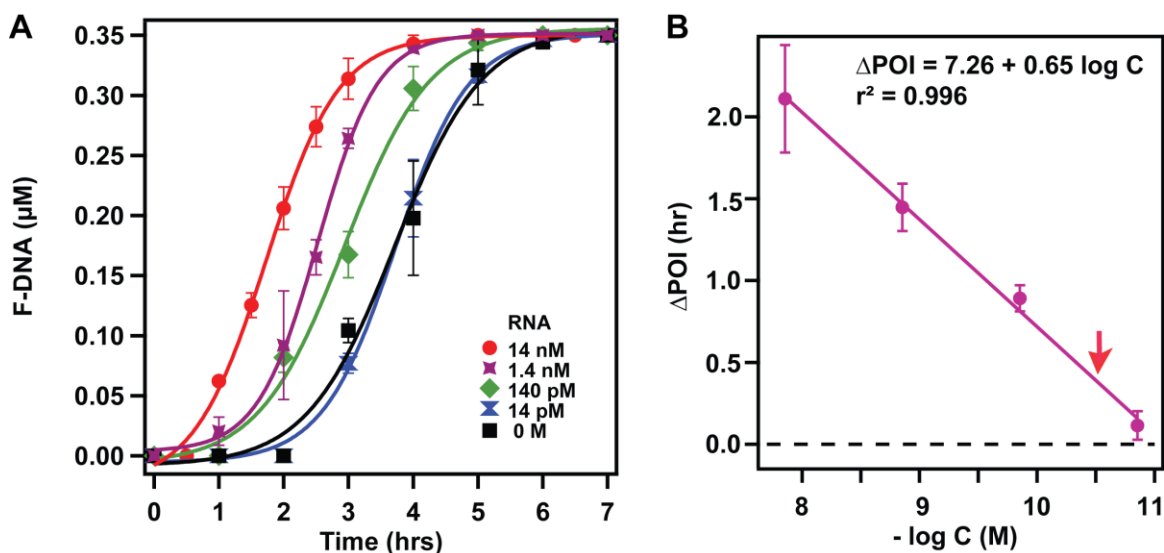


Figure 3.6 A) Kinetics of cross-catalytic formation of **F-DNA** at 28 °C initiated by 14 nM (105 fmol), 1.4 nM (10.5 fmol), 140 pM (1.05 fmol), 14 pM (105 amol) and 0 M RNA using lower probe concentration. B) Δ POI as a function of different target RNA concentrations using a lower probe concentration. *Experimental conditions:* 0.35 μ M **F-DNA-Ia**; 0.7 μ M **DNA-Ib**; 0.7 μ M **DNA-IIa**; 0.7 μ M **DNA-IIb**; 1.4 μ M **ddDNA**; 28°C.

3.5 Selectivity of RT-LIDA

To assess the selectivity of the assay, we compared RNA-triggered LIDA using three different RNA sequences including the complementary target RNA (matched), a one-base mismatched RNA, and a random RNA sequence of the same length. Figure 3.7A shows the kinetic trace of the formation of **F-DNA** with time and Figure 3.7B displays the concentration of **F-DNA** formed at 60 minutes, 75 minutes and 90 minutes initiated by these different RNA sequences. As expected, there was a significant difference in **F-DNA** formed between the matched RNA strand (Figure 3.7, red trace) compared to the mismatched (Figure 3.7, blue trace) and random (Figure 3.7, green trace) target. Moreover, the results from the mismatched and random strand were within error to that of the experiment that had no RNA target (Figure 3.7, black trace) for all of the three time points. This suggested that only background (blunt end) ligation leading to the background-triggered LIDA as opposed to RNA-templated ligation in the presence of the non-target RNA strands. Additionally, a ligation reaction in which matched, mismatched, and random RNA were mixed in one tube was conducted (Figure 3.7A, purple trace). A concentration of **F-DNA** similar to that of the matched RNA was observed, indicating the presence of random strands at these concentrations did not affect our assay.

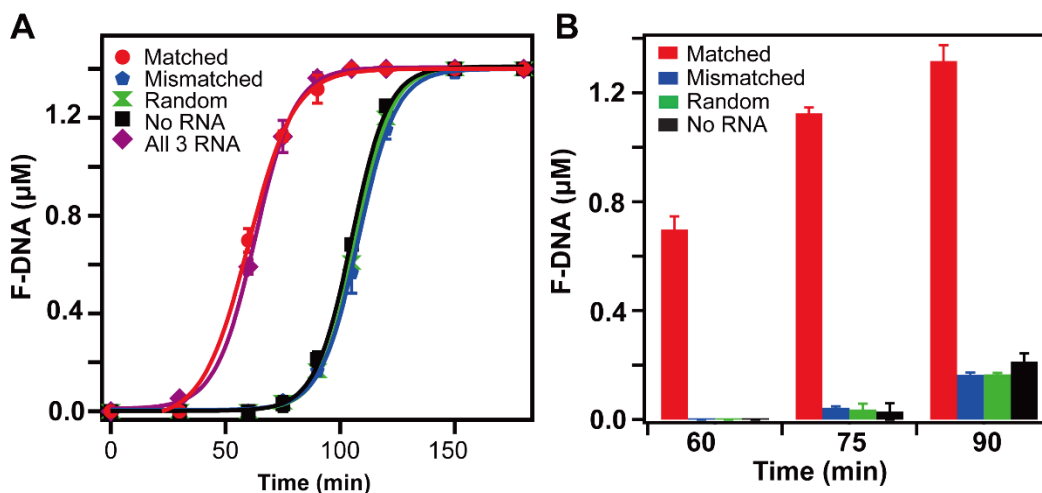


Figure 3.7 Specificity of reverse transcription LIDA. A) Kinetics of **F-DNA** formation at 28 °C for cross catalysis initiated 14 nM; (105 fmol) of various targets: Matched RNA (red trace), mismatched RNA (blue trace), random RNA (green trace). Purple trace represents all three targets together and black trace represents no RNA target. B) Formation of **F-DNA** initiated by various targets represented in red, blue and green after 60 minutes, 75 minutes and 90 minutes time point of the LIDA reaction. *Experimental conditions*: 14 or 0 nM RNA; 1.4 µM **F-DNA-Ia**; 1.4 µM **dDNA**, 2.8 µM **DNA-Ib**; 2.8 µM **DNA-IIa**; 2.8 µM **DNA-IIb**.

3.6 Detection of RNA Target Spiked in Total RNA Samples

Biological fluids such as blood, saliva, and urine are typically used for the detection of diseases.^{37, 56, 163} The cells in those samples are purified and lysed to collect cellular extract that contains the target RNA as well as all the cellular RNA. Therefore, to determine the capability of our assay in detecting target RNA in the presence of realistic amounts of other RNA sequences, we conducted RT-LIDA in the presence of human lungs total RNA (HLTR) and *E. coli* total RNA (EcTR) to mimic the complexity of biological samples. Specifically, 105 fmol of matched target RNA was spiked into both the HLTR and EcTR (4 µg/15 µL). At this target concentration, the

reaction was not hindered by the presence of total RNA for either sample (Figure 3.8). Also, both the templated (solid red and blue bar) and the non-templated (faint red and blue bars) reaction were the same within error despite the total RNA being from two completely different cell types.

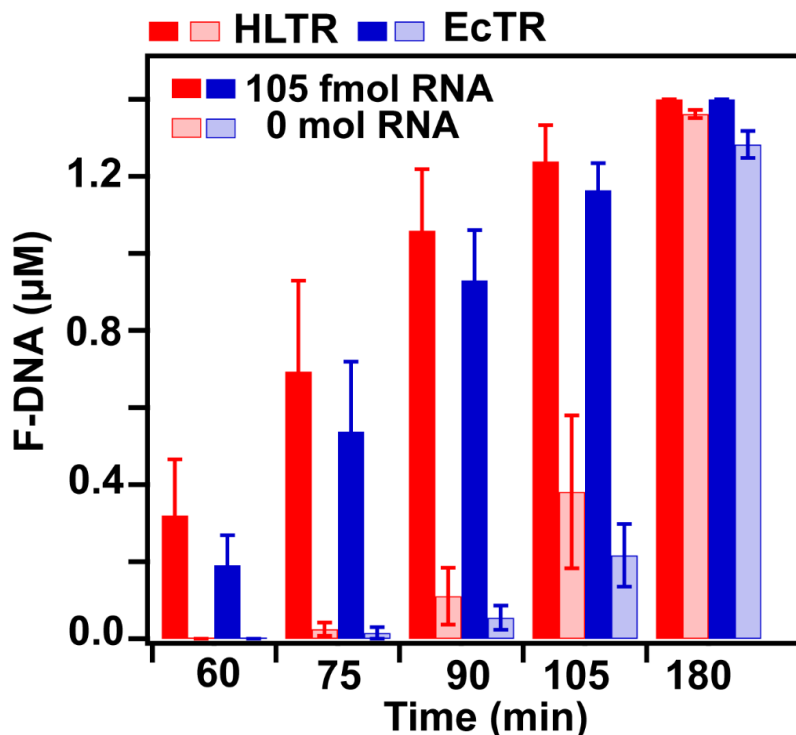


Figure 3.8 Formation of F-DNA initiated by 105 fmol matched RNA (solid trace) and 0 mol matched RNA (faint trace) in the presence of human lungs total RNA (red traces) and *E. coli* total RNA (blue traces) at various time points. *Experimental conditions*: 14 or 0 nM target RNA; 1.4 μM F-DNA-Ia; 1.4 μM dDNA, 2.8 μM DNA-Ib; 2.8 μM DNA-IIa; 2.8 μM DNA-IIb; 4 μg of HLTR or EcTR, 28 °C.

As mentioned previously, to increase the sensitivity of LIDA by further suppressing the background-triggered process, which will allow us to detect lower initial target concentrations, we typically lower the probe concentration. However, when we performed RT-LIDA at these lower probe concentrations with samples spiked in a pool of random RNA, the overall RNA templated

LIDA was slowed down significantly (Figure 3.9A). Therefore, we decided to use a higher concentration of probes while determining the limit of detection in spiked samples (Figure 3.9B). Based on these conditions we could detect as low as 14 pM target RNA in 4 $\mu\text{g}/15 \mu\text{L}$ of cellular RNA. This corresponds to the detection of 105 attomoles in 4 μg of total RNA, which falls into the range of sensitivity required for real samples.¹⁷⁸⁻¹⁸¹ For example, Zhang *et al.* reported that the amount of miR-21 in 8 cancerous tissue samples from patients having cervical cancer was $\sim 0.95 - 1.58 \text{ fmol}/\mu\text{g}$.¹⁷⁸

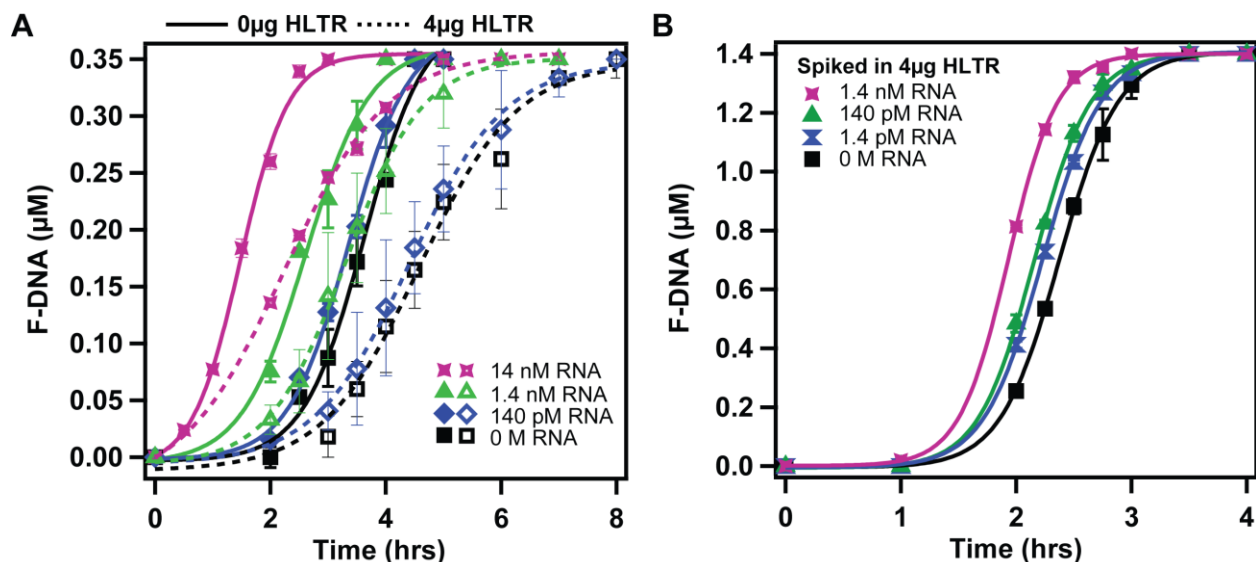


Figure 3.9 Kinetics of F-DNA formation at 28 °C for cross catalysis initiated by various concentration of target RNA using lower probe concentration in the absence of HLTR and when spiked in 4 μg of HLTR. *Experimental conditions:* A) 14 nM, 1.4 nM, 140 pM and 0M RNA; 0.35 μM F-DNA-Ia; 0.7 μM dDNA, 0.7 μM DNA-Ib; 0.7 μM DNA-IIa; 0.7 μM DNA-IIb, 28°C. B) 1.4 nM, 140 pM, 14 pM and 0M RNA; 1.4 μM F-DNA-Ia; 1.4 μM dDNA, 2.8 μM DNA-Ib; 1.4 μM DNA-IIa; 1.4 μM DNA-IIb, 28 °C.

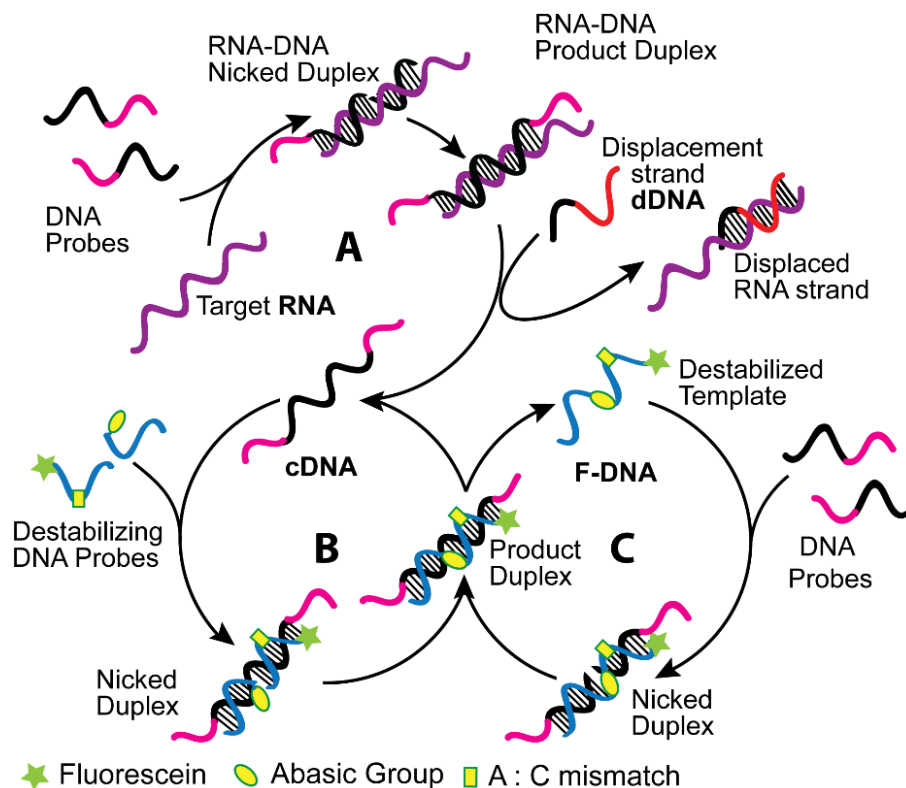


Figure 3.10 Reverse transcription lesion-induced DNA amplification (RT-LIDA) depicting overhangs on probes that lead to an overhang on the cDNA, which is the target for DNA-AuNP disaggregation.

3.7 Colorimetric Detection

3.7.1 RT-LIDA Followed by Colorimetric Detection at Room Temperature

Finally, to achieve instrument-free room-temperature colorimetric amplification and detection, we combined our colorimetric method previously reported by our group with RT-LIDA. This method is based on the rapid target-triggered disassembly of aggregated DNA-modified gold nanoparticles (AuNPs), leading to a striking color change from blue precipitate to red solution.¹²⁷ Our previous work revealed that incorporating five single-stranded polyA regions at the 3'- and 5'- termini of the linker DNA that held the AuNPs together via hybridization allowed for rapid target-triggered disassembly by toehold mediated strand displacement over a range of temperatures

that encompass room temperature including 28 °C. Consequently, probes were prepared that resulted in **cdNA** with 5 polyTs appended to the 3' and 5' ends, which would initiate toehold-mediated strand displacement (Figure 3.10). Using these new probes, LIDA was performed with the optimized conditions on a sun-exposed lab bench (Figure 3.11). The temperature recorded at that location throughout the assay was 27-30 °C. After specific time points, 3 µL of the amplified sample was aliquoted from tube (+) which was initiated by 105 fmol of RNA target and tube (-) which was initiated by 0 mol of RNA target into another set of microtubes containing aggregated DNA modified gold nanoparticles. These aggregates were stored as lyophilized samples for approximately ten days on the bench top and were rehydrated using 10 µL of nuclease-free water immediately prior to use. As shown in Figure 3.12B, after 60 minutes of the LIDA step the aliquot from the sample containing RNA target led to disaggregation and rapid color change to red. On the other hand, the aliquot from the negative control (no initial RNA template) led to no color change until the LIDA step had proceeded to 75 minutes, which was consistent with the amount of time required for the background reaction to trigger amplification of **cdNA**. Interestingly, we observed that the addition of just the probes that comprised the **cdNA** could trigger aggregate disassembly.¹⁸² Fortunately, this probe-triggered process did not occur when both sets of probes were present presumably because of competition between the probes that are complementary to one another, and the linker DNA sequence.

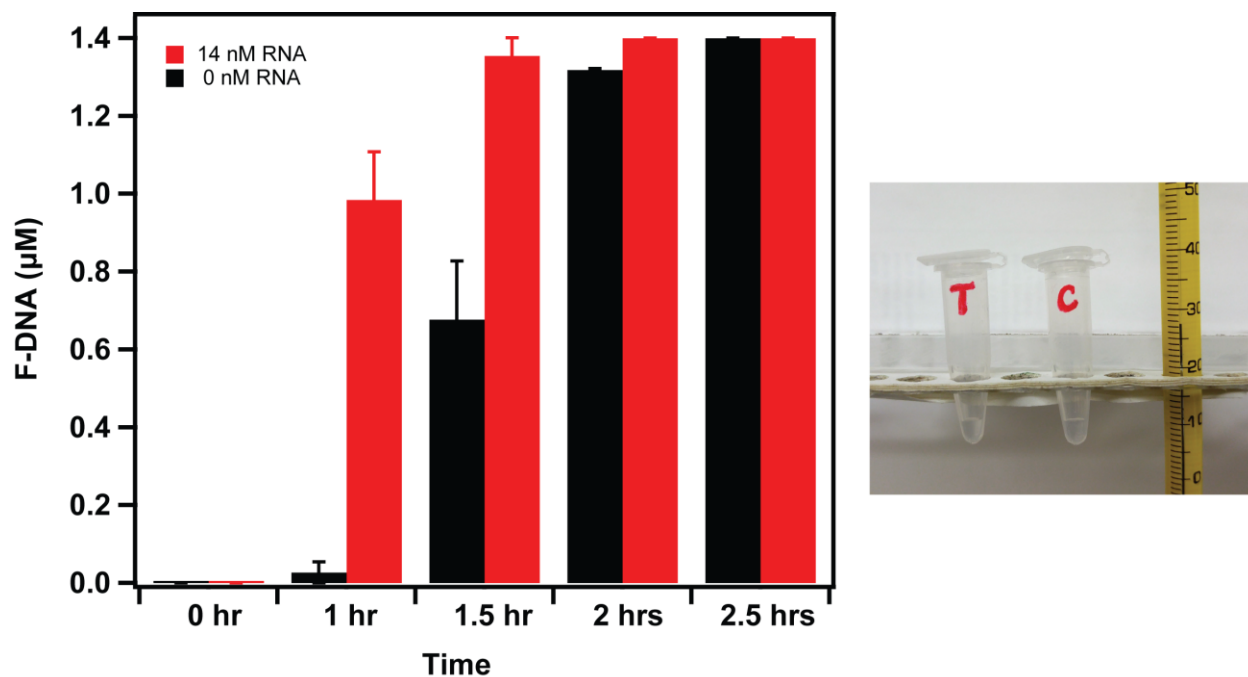


Figure 3.11 Left: Bar graph representing bench-top RNA triggered LIDA performed at room temperature. Red bar represents the concentration of **F-DNA** formed with 14 nM of RNA target while black bar represents **F-DNA** formation with no RNA target. Right: Reverse transcription LIDA on benchtop with T, templated reaction and C, background-triggered ligation reaction. *Experimental conditions:* 14 or 0 nM target RNA; 1.4 µM **F-DNA-Ia**; 1.4 µM **ddNA**, 2.8 µM **DNA-Ib**; 2.8 µM **DNA-IIa**; 2.8 µM **DNA-IIb**; 27-30 °C.

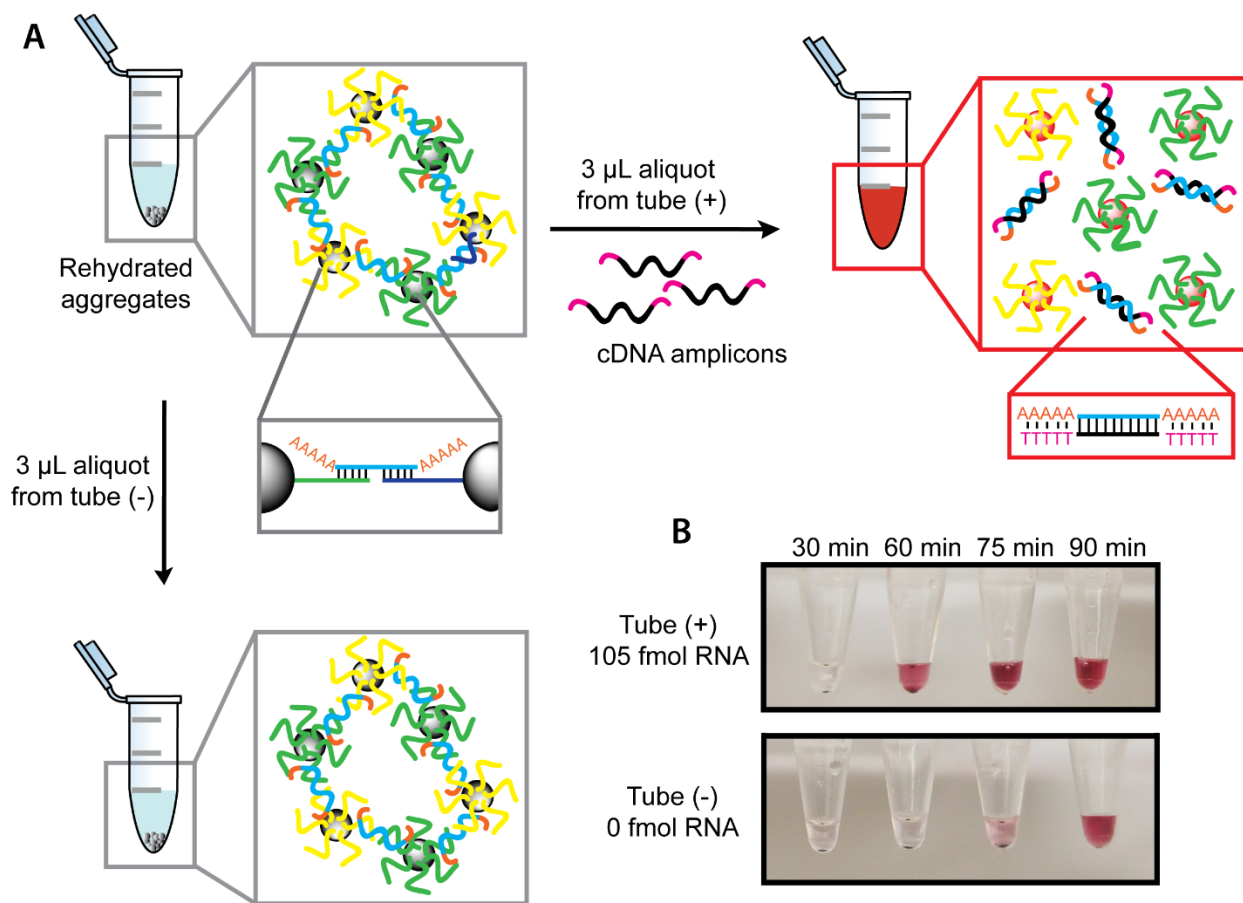


Figure 3.12 Room temperature colorimetric detection of amplicons using toehold mediated DNA-modified gold nanoparticles. A) Scheme representing toehold mediated target disassembly of AuNP. B) Image of DNA-AuNP aggregates after the addition of 3 μ L aliquots of the RT-LIDA reaction performed at room temperature initiated by 105 fmol RNA (tube T) or 0 mol RNA (tube C) added at various time points. The picture was taken 15 minutes after adding the aliquot of the LIDA step to the aggregates.

3.7.2 RT-LIDA in the Presence a Mismatched and Random RNA

We successfully used our colorimetric approach to detect the cDNA amplicons in the presence of mismatched and random RNA sequences under conditions similar to those shown in

Figure 3.7. After 75 minutes of the amplification step, a rapid color change to red was observed upon the addition of 3 μL from the tube that contains the matched target (Figure 3.13, right). On the other hand, no color change was observed when 3 μL of aliquot was added from the tubes containing the mismatched RNA, the random RNA, and no RNA. At 90 minutes and 105 minutes, we observed a faint color change for the control (Figure 3.13, right). Surprisingly, no color change was found in the presence of the random DNA at both time points, while a faint color change was visible at 105 minutes for the mismatched RNA. We hypothesized that the presence of the mismatched and random RNA interferes with the $(\text{T}_5)\text{cDNA}(\text{T}_5)$, which is key for triggering the disaggregation of AuNP.

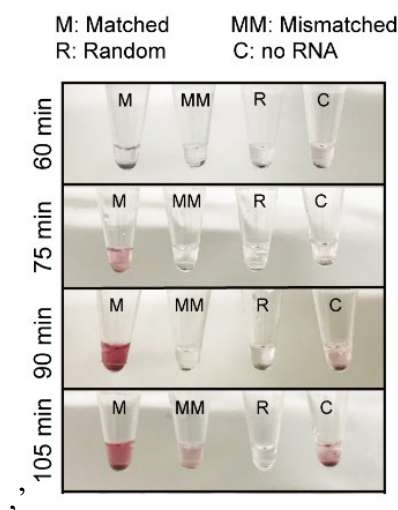


Figure 3.13 Image of DNA-AuNP aggregates after the addition of 3 μL aliquots of the RT-LIDA reaction initiated by 14 nM (105 fmol) of various targets: matched RNA (M), mismatched RNA (MM) and random RNA (R) and 0 mol RNA (C) added at various time points. The picture was taken 15 minutes after adding the aliquot of the LIDA step to the aggregates. *Experimental conditions for RT-LIDA:* 1.4 μM **F-DNA-Ia**; 1.4 μM **ddDNA**, 2.8 μM **DNA-Ib**; 2.8 μM **DNA-IIa(T₅)**; 2.8 μM **(T₅)DNA-IIb**, 28 °C.

3.7.3 RNA Spiked in HLTR Samples

Target RNA (105 fmol) in the presence of HLTR was also successfully detected colorimetrically as shown in Figure 3.14 (right). We could observe rapid color change to red at 90 minutes of LIDA in presence of 105 fmol of target. In contrast, the reaction lacking target RNA showed no color change at 90 minutes. In this case, disaggregation of the DNA-AuNP was observed at 105 minutes, which is consistent with the kinetic data at which the background reaction is triggered (Figure 3.14, left).

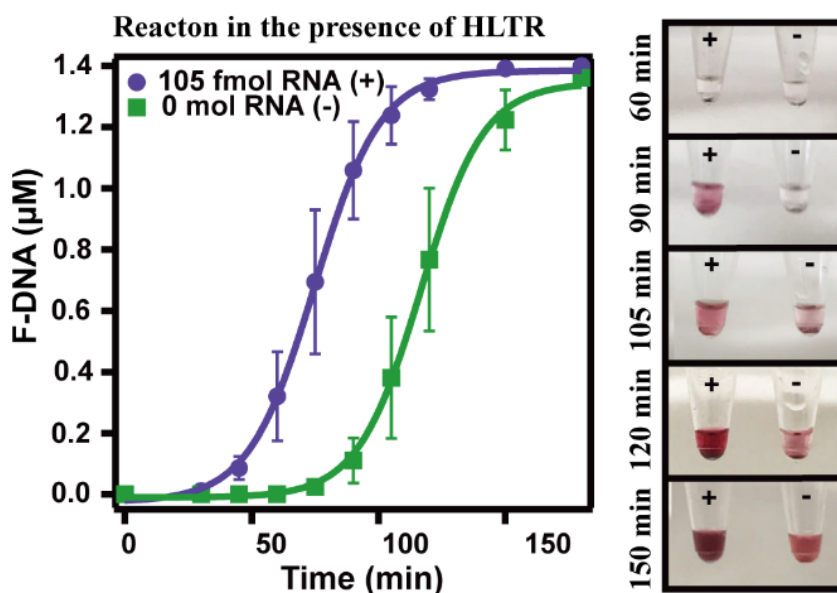


Figure 3.14 Left: Kinetics of cross-catalytic formation of F-DNA at 28 °C initiated by 105 fmol and 0 mol target RNA in the presence and absence (4 μg) of HLTR. *Probe concentrations:* 1.4 μM F-DNA-Ia; 1.4 μM ddDNA, 2.8 μM DNA-Ib; 2.8 μM DNA-IIa; 2.8 μM DNA-IIb. Right: Images of DNA-AuNP aggregates after the addition of 3 μL aliquots of the RT-LIDA reaction performed in 4 μg HLTR initiated by 105 fmol RNA (tube '+') or 0 mol RNA (tube '-') added at various time points. The picture was taken 15 minutes after adding the aliquot of the LIDA step to the aggregates. *Experimental conditions:* 14 or 0 nM target RNA; 1.4 μM F-DNA-Ia; 1.4 μM ddDNA, 2.8 μM DNA-Ib; 2.8 μM DNA-IIa(T₅); 2.8 μM (T₅)DNA-IIb; 4 μg of HLTR, 28 °C.

However, to achieve more sensitive detection, we reduced the amount of aggregates used in our visualization step. Under these conditions, 3 pmol of **cDNA** led to a clear color change while 2 pmol did not (Figure 3.15A). Using these smaller aggregate samples, we could successfully detect 105 amol (14 pM) of target RNA after 2.5 hours of amplification in the presence of cellular RNA (Figure 3.15B), thereby achieving the same sensitivity as our point-of-inflection analysis using PAGE to monitor the reaction profiles. Having a colorimetric read-out, however, is far superior for POC applications and only requires 15 minutes to perform.

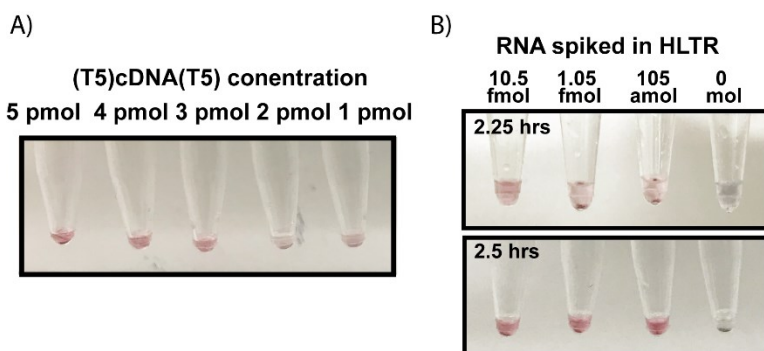


Figure 3.15 Reduced DNA-AuNP aggregates (33.3%) A) Tubes representing the disaggregation of the DNA-AuNP in the presence of 5 pmol, 4 pmol, 3 pmol, 2 pmol and 1 pmol of **(T5)cDNA(T5)**. B) Tubes representing DNA-AuNP aggregates when 7.5 μL aliquot of RNA LIDA solution initiated by 10.5 fmol, 1.05 fmol, 105 amol RNA or 0 mol RNA were added at 2.25 hours and 2.5 hours time points. The picture was taken 15 minutes after adding the aliquot of the LIDA step to the aggregates.

3.8 Conclusion

In summary, this work demonstrated that RNA can be amplified and detected isothermally without instrumentation by combining a reverse transcription step with our lesion-induced DNA amplification system. The addition of an RNA strand displacement step and a mismatch to LIDA

allowed us to lower the assay temperature to 28 °C and perform it on the bench in our lab. Furthermore, the incorporation of target-triggered disaggregation of gold nanoparticles resulted in colorimetric visualization of the target without requiring any heating element. A detection range of 14 pM to 14 nM with a limit of detection of 32 pM (240 amol) was achieved based on an analysis of the point-of-inflection of kinetic amplification traces. However, we were visually able to discriminate 14 pM (105 amol) of target RNA based on the colorimetric read-out. Our assay is simple, instrument-free and utilizes a small number of reagents and simple reaction vessels (eppendorf tubes). Moreover, this process is ideal for the detection of short strands of RNA like miRNA (18- 23 bases) providing an advantage to other techniques like RT-PCR where amplifying short sequences compromises the sensitivity and the specificity of the assay. Future work will address incorporating instrument-free methods for sample preparation including RNA isolation from biological samples.

3.9 Experimental

3.9.1 General

Urea (catalog #9912), tetramethylethylenediamine (TEMED), ammonium persulphate (catalog #AMP 001), tris base (catalog #BP1521), sodium dodecyl sulfate (SDS), and sodium azide were purchased from Fisher. Gold (III) chloride trihydrate, sodium chloride, sodium citrate tribasic dihydrate and dithiothreitol were bought from Sigma Aldrich. For polyacrylamide gel synthesis, the 40% acrylamide/bis solution 19:1 (catalog #161-0144) was purchased from Bio-Rad. Nuclease free water (NFW) was purchased from Integrated DNA Technologies and was used for all experiments. All RNA oligonucleotides were bought from Integrated DNA Technologies (IDT, Iowa, USA) and all DNA oligonucleotides were synthesized using CPGs, phosphoramidites and reagents from Glen Research (Sterling, VA). The enzyme, T4 DNA ligase was bought from

New England Biolabs, while the human lungs total RNA (#AM7968) and *E. coli* total RNA (#AM7940 from Fisher Scientific).

3.9.2 Synthesis and Characterization of DNA

All DNA oligonucleotides were synthesized following the manufacturer's instruction using an Applied Biosystems Model 392 DNA/RNA Synthesizer. Some of the DNA strands had special modifications: fluorescein, 5'-phosphate, 5' or 3' thiol and the abasic lesion. Fluorescein-dT phosphoramidite and 3' thiol modifier C3 S-S CPG were used to incorporate the fluorescein and the 3' thiol, respectively, while chemical phosphorylation reagent II and thiol modifier C6 were used to add the 5'-phosphate group and the thiol group on the 5'-end of the DNA oligonucleotide, respectively. Furthermore, the abasic group was incorporated using a dSpacer CE phosphoramidite.

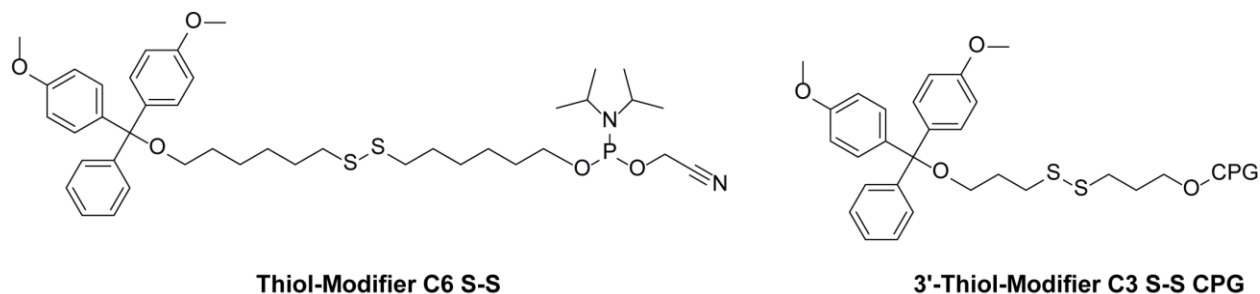


Figure 3.16 Structure of thiol-modifier C6 S-S and 3'-thiol-modifier C3 S-S CPG used to synthesize **Probe A** and **Probe B**. CPG means controlled pore glass.

All synthesized DNA were purified with the DMT-On protocol using Glen-Pak cartridges according to the manufacturer's instruction. Characterization and purity of the DNA was assessed by MALDI-TOF and StainsAll as described in Chapter 2.

Table 3.1 DNA and RNA sequences.

Sequence name	RNA/DNA sequence
RNA	5'-UGU CAG UUG <u>UUG UUC GAU UGA UUC CAU</u> -3'
nm RNA	5'- UGA GAC CCU AAC UUG UGA UGU UUA CCG-3'
mm RNA	5'-UGU CAG UUG <u>UUG UUC GAU GGA UUC CAU</u> -3'
cDNA	5'-ATG GAA TCA ATC GAA CAA-3'
DNA-IIa	5'-pATC GAA CAA-3'
DNA-IIb	5'-ATG GAA TCA-3'
F-DNA-IIb	5'-T _F ATG GAA TCA-3'
F-DNA-Ia'	5'-T _F TG TTC GA-3'
F-DNA-Ia	5'-T _F TG TCC GA-3'
DNA-Ia	5'-TTG TCC GA-3'
DNA-Ib	5'-p(Ab) TGA TTC CAT-3'
dDNA	5'- <u>TC GAA CAA</u> CAA CTG ACA-3'
F-DNA'	5'-T _F TG TTC GAT (Ab) TGA TTC CAT-3'
DNA-I	5'-TTG TTC GAT TGA TCC CAT-3'
F-DNA	5'-T _F TG TTC GAT (Ab) TGA TCC CAT-3'

Table 3.2 DNA sequences for colorimetric detection with DNA-modified AuNPs.

Sequence name	DNA sequence
Probe A	5'-(HS)AAA AAA AAA AAT GG AAT CA-3'
Probe B	5'-ATC GAA CAA AAA AAA AAA A(SH)-3'
(A ₅)Linker(A ₅)	5'-AAAAA TTG TTC GAT TGA TTC CAT AAAAA-3'

(T ₅)cDNA(T ₅)	5'-TTTTT ATG GAA TCA ATC GAA CAA TTTTT-3'
DNA-IIa(T ₅)	5'-pATC GAA CAA TTTTT-3'
(T ₅)DNA-IIb	5'-TTTTT ATG GAA TCA-3'
DNA-Ia	5'-TTG TCC GA-3'

T_F: fluorescein-modified thymidine, p: phosphate, Ab: abasic lesion

Table 3.3 MALDI characterization.

Sequence name	Calculated mass	Measure mass
cDNA	5525	5526
DNA-IIa	2795	2795
DNA-IIb	2747	2748
F-DNA-IIb	3563	3565
F-DNA-Ia'	2928	2928
F-DNA-Ia	2912	2917
DNA-Ib	2948	2949
dDNA	5156	5157
Unreduced Probe A	6206	6208
Unreduced Probe B	6091	6091
(A ₅)Linker(A ₅)	8602	8602
(T ₅)cDNA(T ₅)	8567	8566
DNA-IIa(T ₅)	4316	4316
(T ₅)DNA-IIb	4268	4267
DNA-Ia	2401	2402

3.9.3 Preparation of DNA-Modified AuNPs

DNA functionalized gold nanoparticles were prepared according to our previous work with some modifications.¹²⁷ Specifically, for each batch of DNA-modified gold nanoparticles, the thiolated DNA probe strand (15 nmol) after deprotection by DTT following the manufacturer's protocol was immediately added to a citrate-capped gold nanoparticle suspension (1 mL of the synthesized gold nanoparticles). This mixture was then salted up to 0.2-0.3 M NaCl following our previous work¹²⁷ while maintaining a constant concentration of 10 mM phosphate buffer (0.01 wt% SDS, 0.05 wt% NaN₃, pH 7). Both DNA-modified AuNPs (150 fmol) and linker DNA (6 pmol) were combined and topped up to 10 μ L with 0.2 M NaCl in the above mentioned 10 mM phosphate buffer and allowed to aggregate overnight. Newly synthesized DNA and AuNP aggregates were aliquoted and lyophilized. For the low target concentration assay, a reduced DNA-AuNP was prepared: 50 fmol of DNA-modified AuNP and 2 pmol of linker DNA were used.

3.9.4 RNA-Transcription LIDA Protocol

For all the RNA target-triggered experiments except for the target-variation experiments, the following procedure was used. Single-stranded RNA (105 fmol), probe **DNA-IIb** (41 pmol) and **DNA-IIa** (41 pmol), 2000 CEU T4 DNA ligase, 50 mM TRIS-HCl, 10 mM MgCl₂ and 10 μ M ATP were combined in a 600- μ L microtube (total volume of 7.5 μ L). The reaction was allowed to continue at 28 °C for 15 minutes unless otherwise stated. The non-templated reaction, which is the control (C or (-)) was performed similarly without the target (NFW was used instead of RNA solution). Following 15 minutes wait time, 7.5 μ L of a master mix comprising of **DNA-Ib** (41pmol), **ddDNA** (20.5 pmol), **F-DNA-Ia** (20.5 pmol), ATP (3 μ L, 100 mM) and T4 DNA ligase buffer (3 μ L, from New England Biolabs) was added to the reaction tubes. After vortexing and centrifugation, they were quickly placed in the thermal incubator again at 28 °C unless otherwise

noted. Aliquots of the bulk reaction were then collected at several time points. Reaction was stopped in each aliquot with 2 μL of 0.5 M EDTA/sucrose/bromophenol blue mixture. Finally, the data points were collected, and the samples were run through 15% denaturing PAGE.

For target variation experiments a lower concentration of probes was used as this has been shown to increase our ability to discriminate from the background-triggered process.⁷³ Specifically, various concentrations of RNA in the first step were 14 nM (105 fmol), 1.4 nM (10.5 fmol), 140 pM (1.05 fmol) and 14 pM (105 amol) while the final concentration of the fluorescent probe, **F-DNA-Ia** after both steps was 0.35 μM (5.38 pmol per 15 μL) and all other probes had a final concentration of 0.7 μM (10.3 pmol per 15 μL) unless otherwise stated. Also, a longer wait time of 1 hour was employed for the RNA templated ligation.

3.9.5 Preparation and Running of Denaturing Polyacrylamide Gel Electrophoresis

Refer to Chapter 2.

3.9.6 Quantifying Ligation Yields and ΔPOI

The data in each Figure represent the average of at least two ligation reactions and the error bars represent the standard deviation. The % yield (% conversion) for every ligation reaction was quantified from polyacrylamide gel images. The following equation was used to calculate the % yield of the product at each data point:

$$\% \text{ Yield} = \frac{\text{Intensity (Product Band)}}{\text{Intensity (Product Band + Reactant Band)}} \times 100\%$$

The equation below was used to calculate the difference in POI between the LIDA with and without target.

$$\Delta\text{POI} = \text{POI}(\text{Target}) - \text{POI}(\text{No target})$$

3.9.7 Gel Images

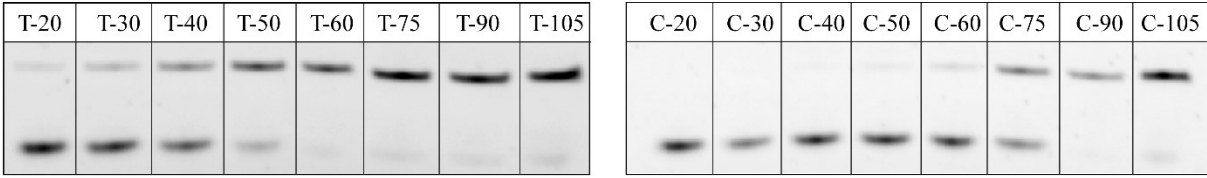


Figure 3.17 Gel images representing the ligation reaction using destabilizing probes (Ab and no mismatch) as a function of time in minutes (data shown in Figure 3.3A). T and C refers to the presence or absence of 14 nM of initial target **cDNA**, respectively. *Top band: F-DNA-I'*; *bottom band: F-DNA-Ia*. *Experimental conditions: 14 or 0 nM cDNA; 1.4 μ M F-DNA-Ia'; 2.8 μ M DNA-Ib; 2.8 μ M DNA-IIa; 2.8 μ M DNA-IIb; 37°C.*

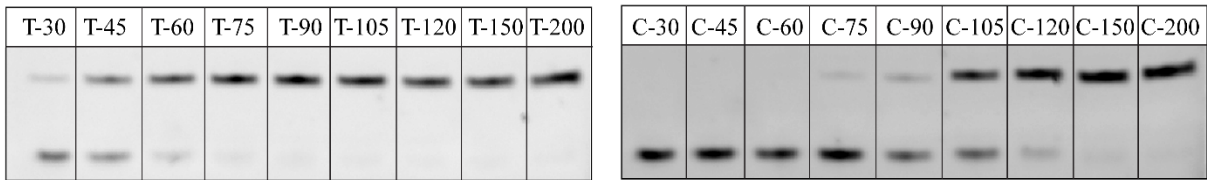


Figure 3.18 Gel images representing the ligation reaction using destabilizing probes (Ab and A:C mismatch) as a function of time in minutes (data shown in Figure 3.3B). T and C refers to the presence or absence of 14 nM of initial target **cDNA**, respectively. *Top band: F-DNA-I*; *bottom band: F-DNA-Ia*. *Experimental conditions: 14 or 0 nM cDNA; 1.4 μ M F-DNA-Ia; 2.8 μ M DNA-Ib; 2.8 μ M DNA-IIa; 2.8 μ M DNA-IIb; 28 °C.*

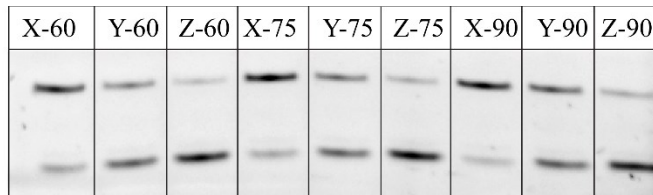


Figure 3.19 Gel images representing the single stoichiometric ligation reaction initiated by 1.4 μM RNA at various ATP concentrations at time points 60 minutes, 75 minutes and 90 minutes. X, Y and Z refers to ATP concentration of 10 μM , 100 μM and 1 mM respectively. *Top band: F-DNA-I; bottom band: F-DNA-Ia.* *Experimental conditions: 1.4 μM RNA; 1.4 μM F-DNA-IIa; 2.8 μM DNA-IIb; 28 $^{\circ}\text{C}$.*

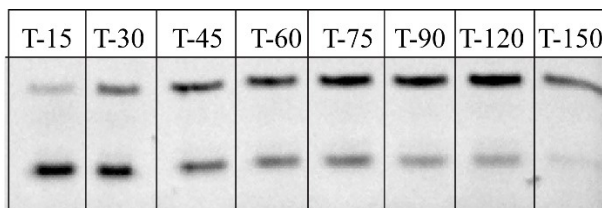


Figure 3.20 Gel images representing the single stoichiometric ligation reaction initiated by 1.4 μM RNA at 10 μM ATP. These data are exhibited in Figures 3.2B. *Top band: F-DNA-I; bottom band: F-DNA-Ia.* *Experimental conditions: 1.4 μM RNA; 1.4 μM F-DNA-IIa; 2.8 μM DNA-IIb; 28 $^{\circ}\text{C}$.*

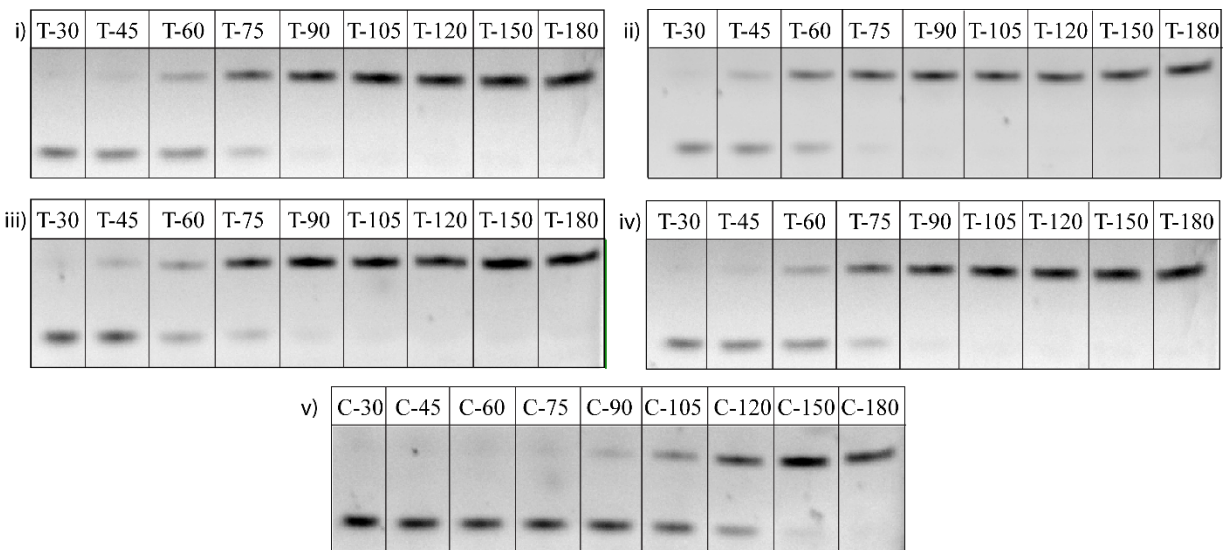


Figure 3.21 Gel images representing ligation reactions with various wait times for the RNA templated DNA ligation reaction as a function of time. These data are exhibited in Figure 3.4. T and C refers to the presence or absence of 14 nM of initial target RNA, respectively. *Top band: F-DNA; bottom band: F-DNA-Ia.* *Experimental conditions:* 14 or 0 nM RNA; 1.4 μ M F-DNA-Ia; 1.4 μ M ddDNA; 2.8 μ M DNA-Ib; 2.8 μ M DNA-IIa; 2.8 μ M DNA-IIb; 28 °C; i) 60 minutes, ii) 30 minutes, iii) 15 minutes, iv) 5 minutes, v) 15 minutes.

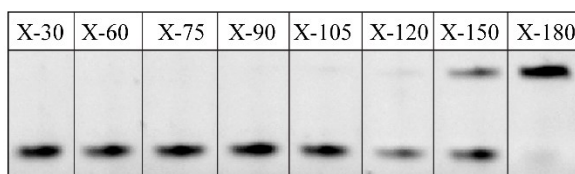


Figure 3.22 Gel images representing control experiment initiated by 14 nM RNA but in the absence of ddDNA as a function of time. These data are exhibited in Figure 3.5, blue trace. *Top band: F-DNA; bottom band: F-DNA-Ia.* *Experimental conditions:* 14 M RNA; 1.4 μ M F-DNA-Ia; 1.4 μ M ddDNA; 2.8 μ M DNA-Ib; 2.8 μ M DNA-IIa; 2.8 μ M DNA-IIb; 28 °C.

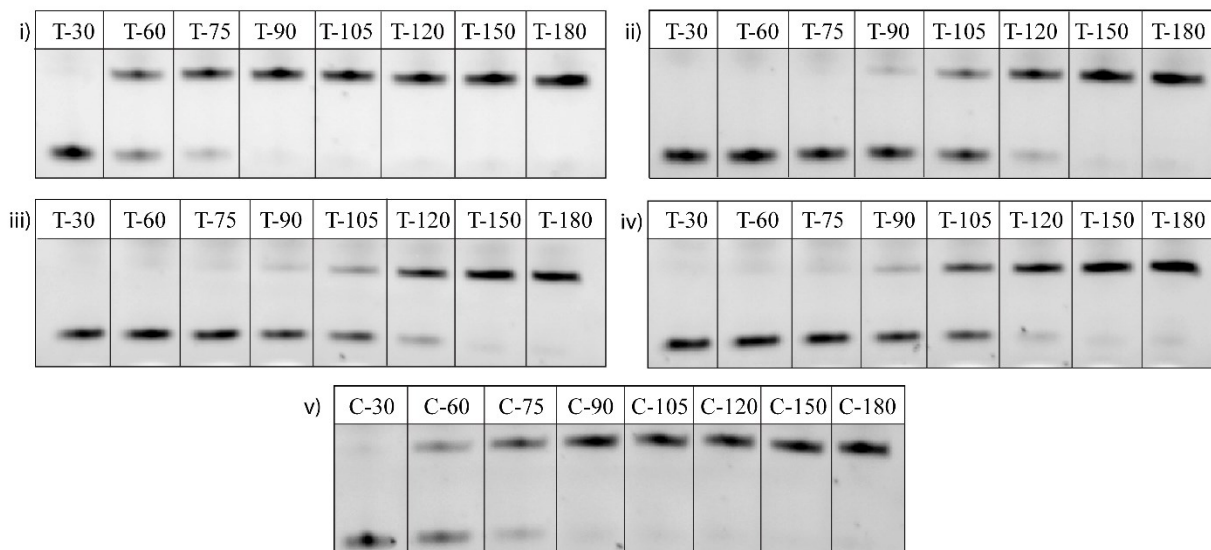


Figure 3.23 Gel images representing ligation reactions with various targets for the RNA templated DNA ligation reaction as a function of time. These data are exhibited in Figure 3.7 and 3.13. T and C refers to the presence or absence of 14 nM of initial target RNA, respectively. *Top band: F-DNA; bottom band: F-DNA-Ia.* *Experimental conditions:* 14 or 0 nM target RNA; 1.4 μ M F-DNA-Ia; 1.4 μ M dDNA; 2.8 μ M DNA-Ib; 2.8 μ M DNA-IIa; 2.8 μ M DNA-IIb; 28 °C; i) matched RNA, ii) random RNA, iii) one-base mis-matched RNA, iv) no RNA, v) all three RNA together.

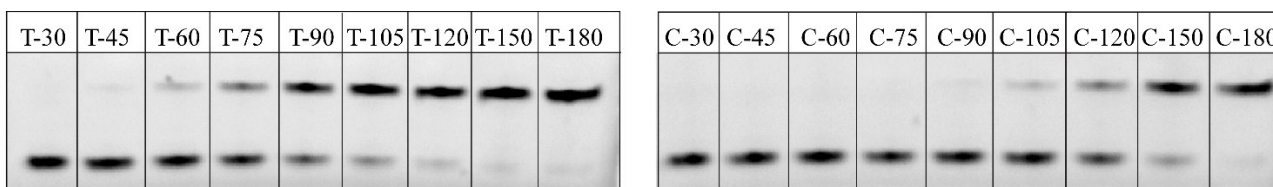


Figure 3.24 Gel images representing ligation reactions in the presence of human lung total RNA (HLTR) as a function of time. These data are exhibited in Figure 3.8 (red bars). T and C refers to the presence or absence of 14 nM of initial target RNA, respectively. *Top band: F-DNA; bottom band: F-DNA-Ia.* *Experimental conditions:* 14 or 0 nM RNA; 1.4 μ M F-DNA-Ia; 1.4 μ M dDNA; 2.8 μ M DNA-Ib; 2.8 μ M DNA-IIa; 2.8 μ M DNA-IIb; 4 μ g HLTR; 28 °C.

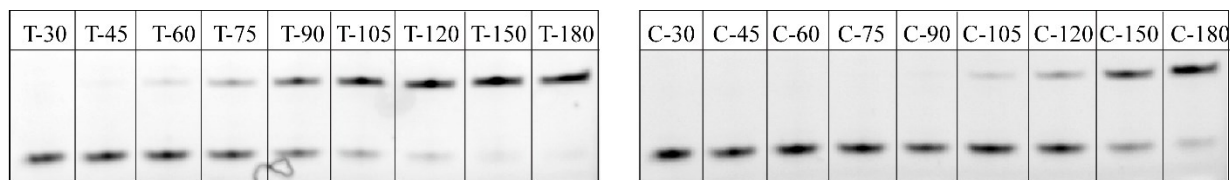


Figure 3.25 Gel images representing ligation reactions in the presence of *E. coli* total RNA (EcTR) as a function of time. These data are exhibited in Figure 3.8 (blue bars), blue traces. T and C refers to the presence or absence of 14 nM of initial target RNA, respectively. *Top band: F-DNA; bottom*

band: F-DNA-Ia. Experimental conditions: 14 or 0 nM RNA; 1.4 μM F-DNA-Ia; 1.4 μM dDNA; 2.8 μM DNA-Ib; 2.8 μM DNA-IIa; 2.8 μM DNA-IIb; 4 μg EcTR; 28 °C.

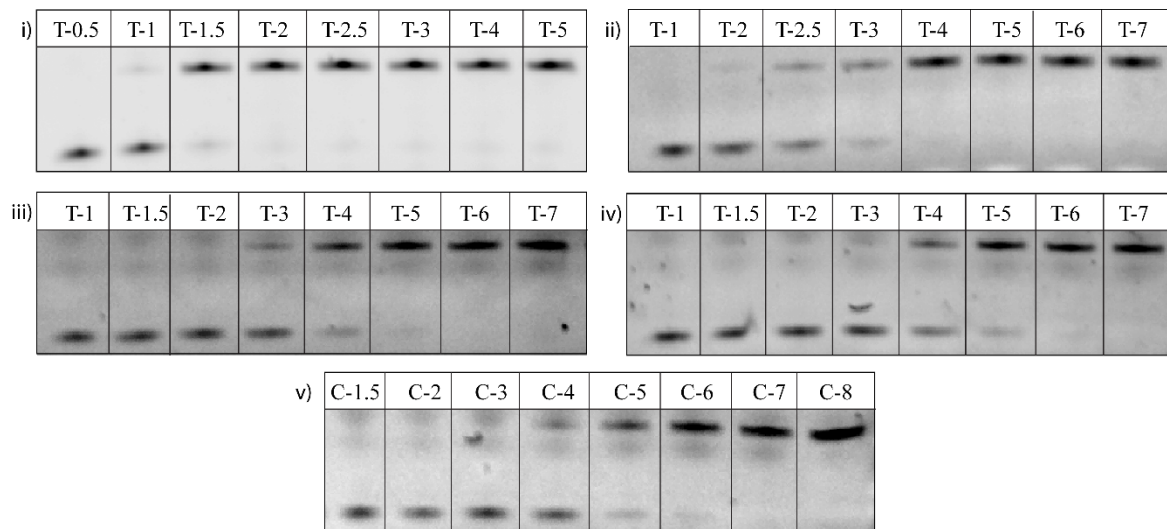


Figure 3.26 Gel images representing ligation reactions with various RNA target concentration. as a function of time in hours. T and C refers to the presence or absence of initial target RNA, respectively. These data are exhibited in Figure 3.6. *Top band: F-DNA; bottom band: F-DNA-Ia. Experimental conditions: RNA concentration in step 1: i) 14 nM; ii) 1.4 nM, iii) 140 pM, iv) 14 pM, v) 0 M.; 0.7 μM F-DNA-Ia; 1.4 μM dDNA; 1.4 μM dDNA, 1.4 μM DNA-Ib; 1.4 μM DNA-IIa; 1.4 μM DNA-IIb; 28 °C.*

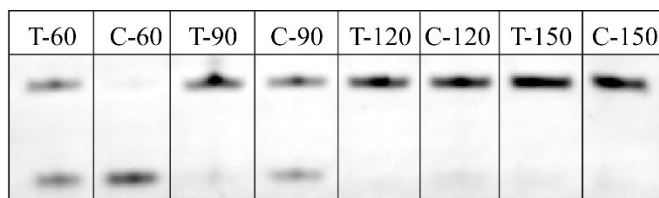


Figure 3.27 Gel images representing the ligation reaction done on the bench top as a function of time in minutes and at room temperature (shown in Figure 3.11). T and C refers to the presence or

absence of 14 nM of initial target **RNA**, respectively. *Top band: F-DNA; bottom band: F-DNA-Ia.* *Experimental conditions:* 14 or 0 nM **RNA**; 1.4 μ M **F-DNA-Ia**; 1.4 μ M **ddDNA**; 2.8 μ M **DNA-Ib**; 2.8 μ M **DNA-IIa**; 2.8 μ M **DNA-IIb**; room temperature (27-30 °C).

Chapter 4

Influence of the ATP Derivatives on Lesion-Induced DNA Amplification

4.1 Introduction

As seen in the previous chapters, the sensitivity of lesion-induced DNA amplification (LIDA) is affected by the background-triggered process.⁷¹⁻⁷³ When template is not initially present, the four probes in the system form a 'pseudo-blunt end' (as explained below) that leads to the slow formation of the template DNA resulting in sigmoidal amplification albeit at a longer time than the target-initiated process. Therefore, decreasing the background-triggered process should lead to a lower limit of detection in LIDA. Several strategies have been attempted by previous group members to reduce this background-triggered amplification. Former group members showed that this background-triggered process was slowed down more than the target-initiated process by the reduction of the probe concentration.⁷³ Specifically, by reducing the concentration of the probes, 14 pM of target DNA was able to be detected.⁷³ Further reducing the probe ratio in a serial ligation strategy, the background-triggered reaction was further suppressed and a higher sensitivity (140 fM) was obtained.⁷³ In Abu Kausar's thesis, he further explored the use of various ligase enzymes in an attempt to reduce the background-triggered reactions.¹⁸³ Three enzymes known to give less or no blunt end ligation, which is the source of our background-triggered reaction, were used: T7 DNA ligase, *E. coli* ligase and T3 DNA ligase enzymes.¹⁸⁴⁻¹⁸⁶ He reported a slower background-triggered LIDA when using T7 DNA ligase and *E. coli* ligase. However, despite resulting in a better sensitivity, the background-triggered process was not completely shut down.¹⁸³

An alternative way to selectively inhibit blunt end ligation reported in the literature is to vary the concentration of ATP.¹⁸⁷⁻¹⁸⁸ In ligation reactions using T4 DNA ligase to catalyze the formation of a phosphodiester bond between a 5'-phosphate and 3'-hydroxy strand termini ATP is required as a cofactor,¹⁸⁸ yet Kausar found that increasing to 4.2 mM ATP, had little effect on the difference in the kinetic profile of LIDA initiated with and without target.¹⁸³ Recently, Hili and

coworkers showed that modified ATP affected the rate of templated ligation.¹⁸⁹ Therefore, in this chapter, we will discuss our attempt to control the ligation rates of the target-initiated versus the pseudo-blunt end reaction responsible for background-triggered LIDA by taking advantage of the characteristics of the modified ATP. Our goal was to assess the impact on LIDA of 15 different ATP derivatives, provided to us by the Hili group, that have been modified on either their adenine, ribose or phosphate groups.¹⁸⁹ We hypothesized that some of these derivatives would delay or shut down the background-triggered process (pseudo-blunt end ligation) while having minimal or low impact on the templated reaction, ultimately improving the sensitivity of LIDA.

4.2 Source of Background-Triggered LIDA

In LIDA, four probes are employed as shown in Figure 4.1 (red square). When a target (black) is present, the two complementary blue probes that contain at least one destabilizing abasic modification hybridize with the latter. Upon ligation in the presence of T4 DNA ligase, a ligated blue target is formed, which in turn hybridizes with two complementary probes (short black) that together make up the same sequence as the template (long black). These two short black oligonucleotides are complementary to the blue probes. Therefore, in the absence of template, the four probes can hybridize with each other to form two small DNA duplexes as shown in Figure 4.1B. Occasionally, when the two duplexes come close to each other to form a ‘pseudo-blunt end’, ligation can occur by T4 DNA ligase to generate a catalytic amount of target, which in turn triggers the process of LIDA. This is where the background-triggered amplification originates, and consequently the ability of T4 DNA ligase to join short DNA duplexes bearing a blunt end or sticky-end at the ligation site plays a significant role in LIDA sensitivity (ability to discriminate between LIDA initiated by small amounts of target and no target).^{188, 190-191}

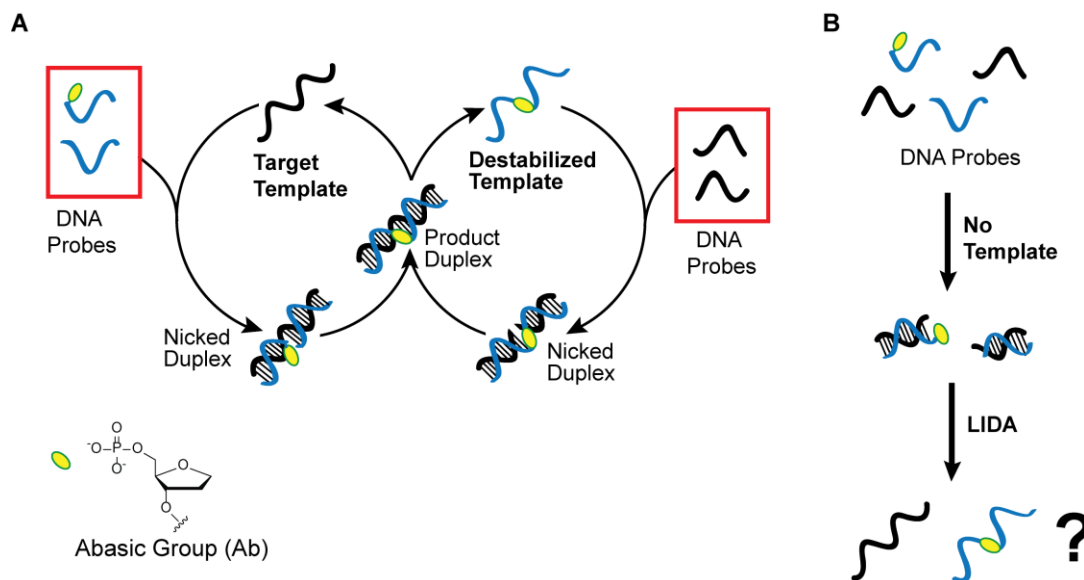


Figure 4.1 Background-triggered lesion-induced DNA amplification. A) Schematic representation of lesion-induced DNA amplification in the presence of a template. B) The duplex formation of probes in the absence of a template.

Blunt end is defined as two short duplexes that have no overhangs (extra bases unhybridized at a strand terminus) and therefore there is only transient interactions between them in the absence of the ligase as shown in Figure 4.2A.¹⁸⁸ On the other hand, sticky-ends also known as cohesive ends are duplexes that have one or more extra unpaired nucleotides on one end that are complementary to another overhang (Figure 4.2B).¹⁸⁸ Thus, in solution, the overhang recruits its complementary part, which causes the two DNA duplexes to be held together by hydrogen bonding and π -stacking prior to ligation.¹⁸⁸ Some ligases like T4 DNA ligase are known to efficiently perform both sticky-end and blunt end ligation.¹⁸⁴ In our LIDA system, we have a sticky-end with one base overhang. However, there is no base interaction as on one side there is an adenosine, while on the other there is an abasic nucleotide (**D/Ab**) as shown in Figure 4.2 (C and D). As a result, no hydrogen bonding occurs between the terminal adenine and the terminal

abasic of the sticky end. We refer to this structure as a pseudo-blunt end. Based on the presence of a background-triggered process, we indirectly know that this pseudo-blunt end structure is ligated by T4 DNA ligase, but the kinetics of ligation of such a structure have not been reported.

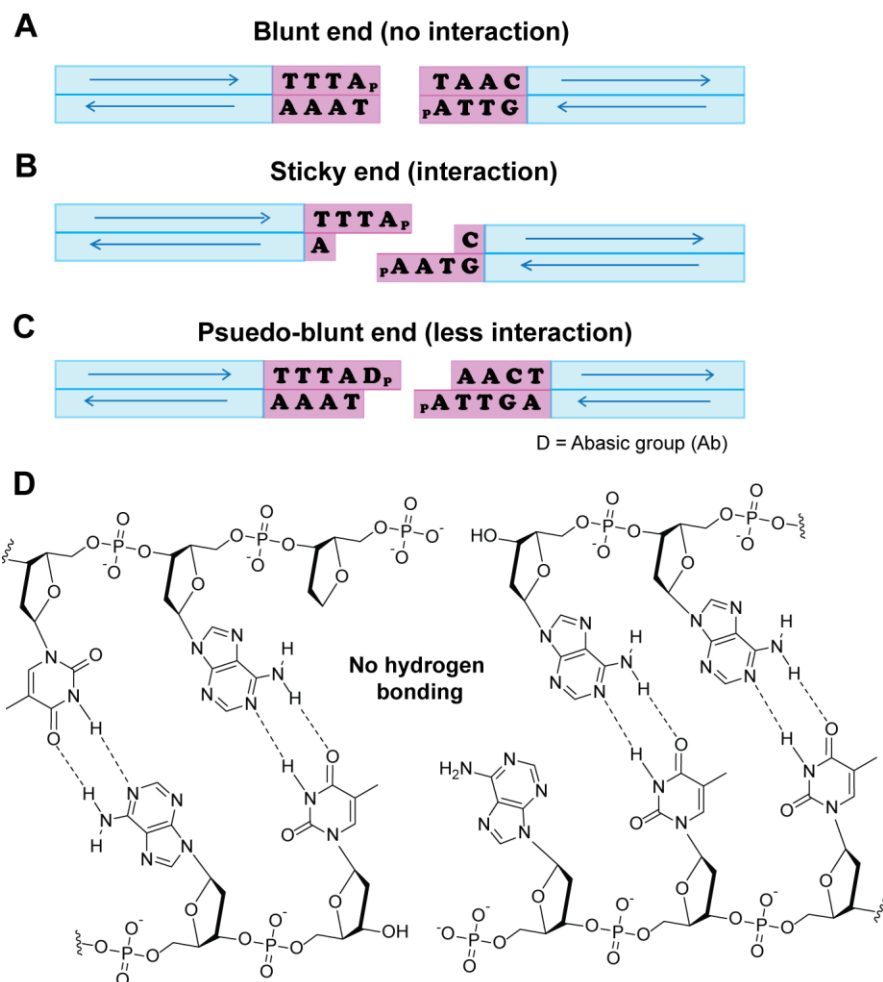


Figure 4.2 Schematic illustration of a) A) blunt end, B) sticky-end, and C) pseudo-blunt end. D) Chemical representation of the two fragments resulting in a pseudo-blunt end.

4.3 ATP-Dependent T4 DNA Ligase

To understand the role of ATP in both templated and pseudo-blunt end ligation, it is helpful to first review the structure and mechanism of T4 DNA ligase. All DNA ligases are divalent metal cation-dependent enzymes that catalyze the formation of a phosphodiester bond between a 5'-

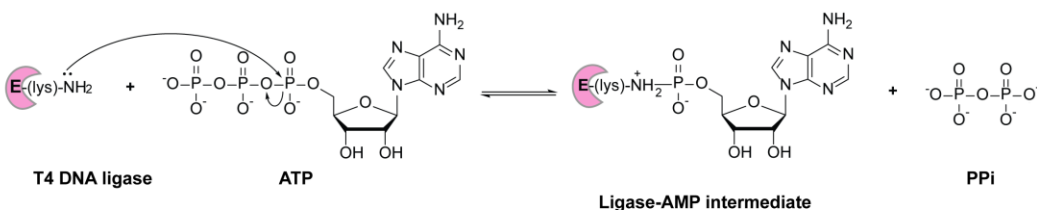
phosphoryl and 3'-hydroxy group.¹⁹²⁻¹⁹⁴ They are ubiquitously found in all organisms and play an important role in DNA replication, DNA recombination, and DNA repair.¹⁹²⁻¹⁹⁵ In DNA replication, DNA ligase are required to join different Okazaki fragments to make a continuous lagging strand.^{192, 194} In DNA recombination, after exchange of DNA strands has occurred, DNA ligase seals the breaks present in the DNA.¹⁹² Regarding DNA repair, DNA in the body is susceptible to damage by endogenous and exogenous factors. As a result, single-stranded or double-stranded DNA breaks can occur or be generated as a response to DNA repair.¹⁹⁶ Chatterjee and Walker reported that in an hour, around 2300 single-stranded breaks occur in the mammalian cell.¹⁹⁶ DNA ligases are employed to repair nicked sites in the body as part of the DNA repair pathway.^{192, 196} DNA ligases are categorized into two groups based on their required cofactor: adenosine triphosphate (ATP) or nicotinamide adenine dinucleotide (NAD⁺).¹⁹²⁻¹⁹⁴ T4 DNA ligase was the first discovered ATP-dependent ligase, which is now widely utilized in molecular biology (such as cloning, sequencing, and gene synthesis) and was discovered in 1987 by Weiss and Richardson.^{184, 192-193, 197} Shi *et al.* recently reported the first crystal structure of T4 DNA ligase bound with DNA.¹⁹²

With T4 DNA ligase, the DNA templated or sticky-end ligation reaction occurs in two main steps: (1) the DNA strands must form a nicked duplex DNA and stay together long enough for the enzyme to bind for nick sealing and (2) the ligation process is catalyzed by T4 DNA ligase. The latter occurs via a Ping-Pong mechanism in three steps as shown in Figure 4.3: A) adenylation (also known as adenylation or AMPylation) of enzyme by reaction with ATP; B) transfer of the adenylyl group to a 5'-phosphorylated polynucleotide to form an adenylylated-DNA (AppDNA); C) phosphodiester bond formation with release of AMP.^{193, 198-199} In the first step, the ATP cofactor is locked into the active site of the T4 DNA ligase where it is within hydrogen bonding distance

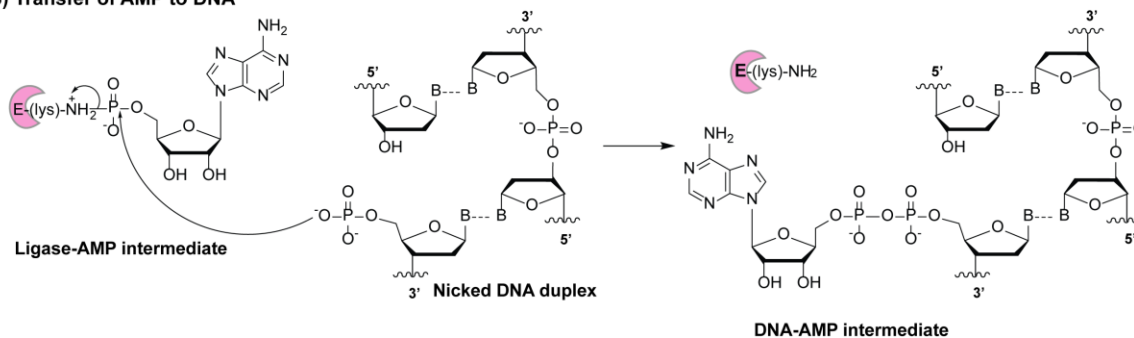
to three lysine residues: Lys159, Lys365, Lys367 (Figure 4.3A).^{192, 194} Lys159 is the catalytic residue that attacks the α -phosphorus atom (via an S_N2 reaction) of the ATP cofactor to form the ligase-AMP intermediate.¹⁹¹⁻¹⁹⁴ The other two lysine residues are believed to stabilize the intermediate formed during the adenylyl transfer reactions.¹⁹² A pyrophosphate (PPi) residue is produced as a by-product in this step.¹⁹²⁻¹⁹³ Following that, a (ligase-AMP)-DNA complex is formed, which Rossi *et al.* referred to as the 'T-complex' as it is transient.¹⁹¹ They reported that the adenylylated enzyme scans the duplex DNA through several T-complexes to find the 5'-phosphorylated end.¹⁹¹ Once located, the AMP group from the ligase-AMP intermediate is transferred to the 5'-phosphate of the nick site of the duplex DNA substrate resulting in a bridge structure bearing an inverted (5')-(5') pyrophosphate bond (Figure 4.3B).¹⁹¹ The resulting complex is an activated form of the DNA with a 5'-adenyl pyrophosphoryl cap, also known as AppDNA or 5'-adenylated DNA.^{191, 193} A stable complex (S-complex) is formed between the deadenylylated enzyme and the DNA-AMP intermediate as they are still bound together until the nick sealing occurs. This step is believed to be the rate-limiting step for DNA ligase turn-over reaction.¹⁹⁴ Finally, in the last step, a nucleophilic attack occurs between 3'-hydroxy of the DNA substrate and the AppDNA to form a covalent bond sealing the gap at the nick site (Figure 4.3C).^{191, 193} This step involves the liberation of the AMP group and the recycling of the enzyme.^{191, 193} To catalyze more ligation reactions, the enzyme active site is reloaded with AMP using another ATP molecule.^{191, 193, 199} Likewise, for blunt end DNA, the same DNA ligation procedure is applicable.^{188, 190} However in this case, there is a slight difference in step B as the 5'-phosphate group and the 3'-hydroxy group are on two different DNA duplexes. The S-complex is formed similarly with the deadenylylated enzyme and the AMP-DNA (short fragment).¹⁹¹ As this complex is stable, it exists long enough for the recruitment of a second DNA fragment bearing the 3'-

hydroxy group.¹⁹¹ Ligation reactions for sticky-ended duplexes are easier as they are stabilized and kept in place by hydrogen bonding in contrast to blunt ended duplexes where there is limited interaction between the duplexes.¹⁹¹

A) Adenylation of T4 DNA ligase



B) Transfer of AMP to DNA



C) Phosphodiester bond formation

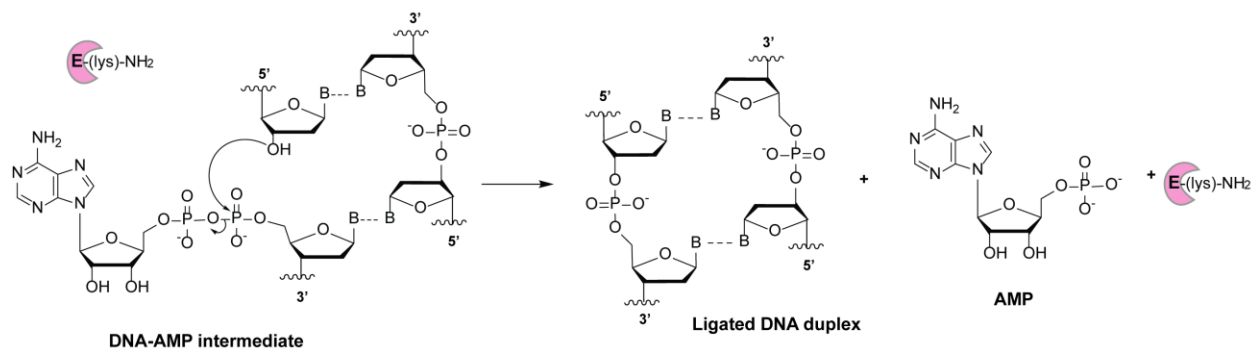


Figure 4.3 Mechanism of ligation catalyzed by T4 DNA ligase.

As seen in the mechanism, the energy source, ATP, plays an important role in the DNA ligation reaction of single DNA breaks. Shi *et al.* reported the structure of AMP inside the T4 DNA ligase active site (Figure 4.4). The structure of T4 DNA ligase consists of a total of 487 amino acids residues divided into three structural domains: an α -helical N-terminal DNA-binding domain

(DBD, residues 1-129), a nucleotidyltransferase domain (NTase, residues 133-367) and an oligonucleotide-binding domain (OBD, residues 370-487). The remaining residues are involved in short linkers that connect the three domains together.¹⁹² Though the active site of the enzyme consists of the NTase and the OBD, all the three domains are involved in the binding with the DNA substrate (Figure 4.4).¹⁹² They are positioned in such a way that allows them to wrap tightly around the minor groove of the DNA substrate.¹⁹² Extensive backbone contact is observed between the DNA backbone, and the residues of the domains. This is confirmed by the protein surface electrostatic potential (Figure 4.4C) where red symbolizes negative charge, blue positive charge and white is neutral. The DNA is positioned in the blue part (positive) as it stabilizes the negatively charged backbone of the DNA. In a zoomed-in version of the nick site inside the core of the enzyme, several non-covalent interactions are observed to be involved in stabilizing the nicked DNA (Figure 4.4D).¹⁹²

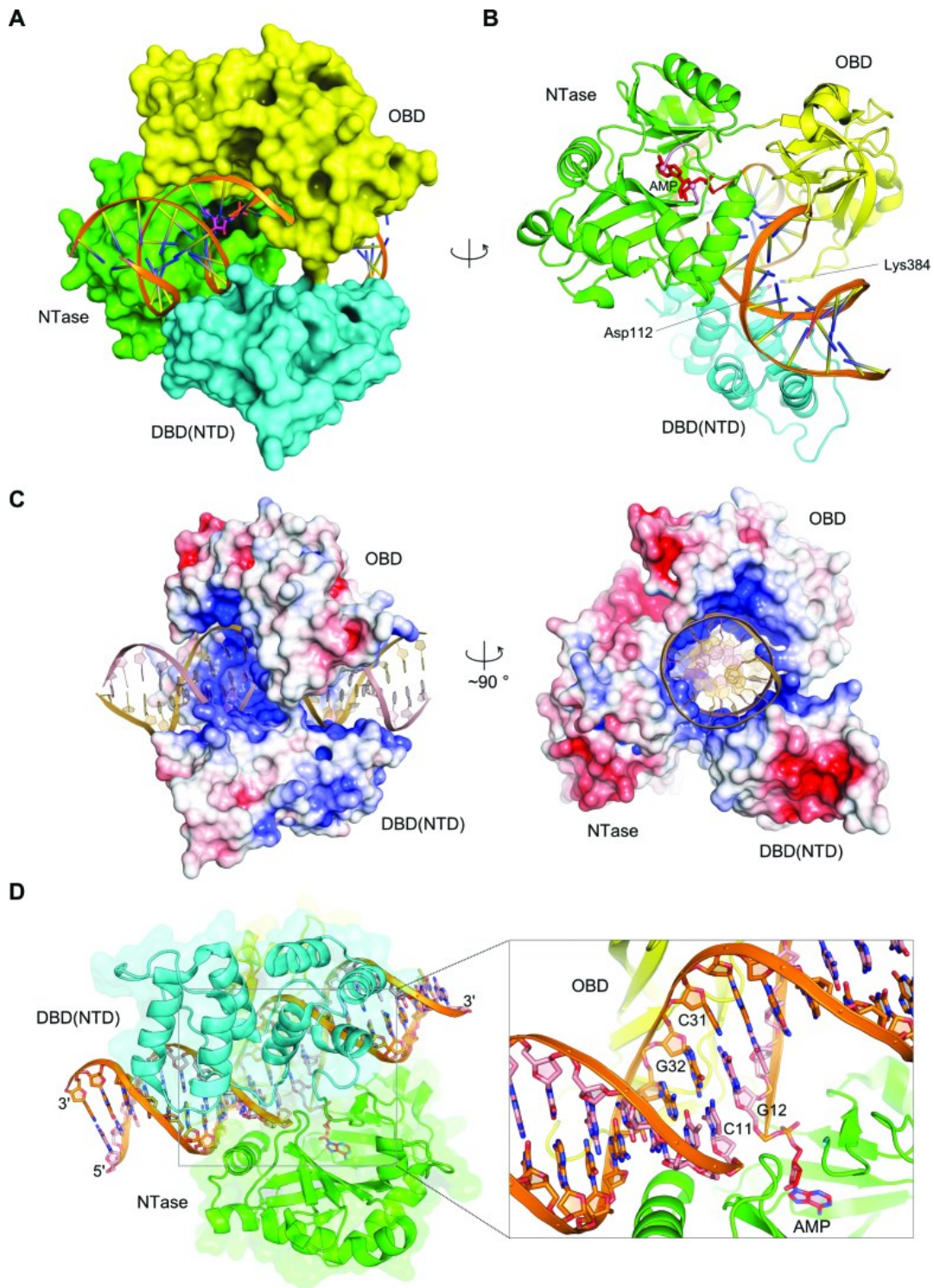


Figure 4.4 Structure of T4 DNA ligase-DNA complex: molecular surface(A), cartoon illustration(B), protein surface based on electrostatic potential(C) and representation of enzyme-

DNA interactions around the nick region(D). Image reproduced with permission from reference 192. Copyright © 2018 Oxford University Press.

The AMP group is also observed in Figure 4.4D. The nucleotidyltransferase (NTase) domain as the name suggests is where the AMP (nucleotide) transfer occurs from the ATP to a lysine (Lys159) residue of the ligase followed then to the 5'-phosphoryl group on the DNA. The residues in the NTase domain surrounding the AMP group stabilize the negatively charged intermediate during the adenylyl transfer reaction as well as ensure the proper alignment for the nucleophilic attack of the nick sealing to occur (Figure 4.5). Therefore, altering the ATP structure might affect the ligation reaction. In the same report, Shi *et al.* pointed at the importance of the 2'-hydroxy group on the ATP, which is involved in hydrogen bonding with a glutamic acid (residue 217) on the ligase (Figure 4.5).

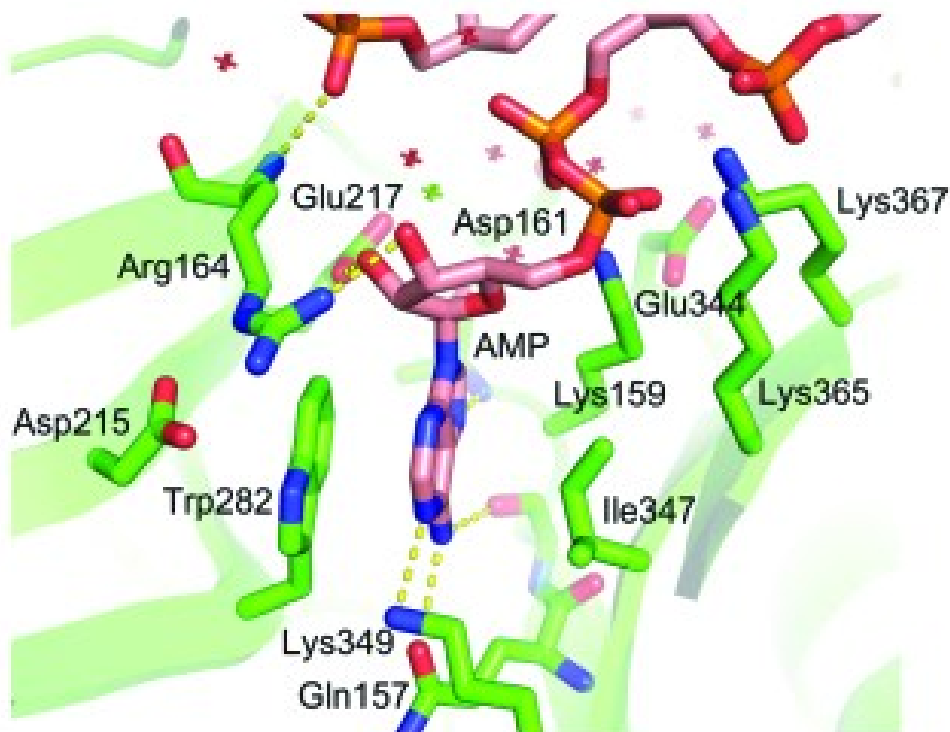


Figure 4.5 AMP interactions with the residues in the NTase domain. Red and green crosses represent water molecules and a magnesium ion present around the nick site, respectively. Image reproduced with permission from reference 192. Copyright © 2018 Oxford University Press.

4.4 Reports Investigating Various ATP Derivatives as a Cofactor for T4 DNA Ligase

A few reports have investigated the effect of different derivatives of ATP on the templated DNA ligation reaction using T4 DNA ligase. Montecucco *et al.* studied the kinetics of ligation catalyzed by T4 DNA ligase in the presence of ATP, dATP (deoxy-ATP) and their α -thio derivatives (oxygen atom on the α -phosphate group replaced by a sulphur atom).²⁰⁰ They observed that the ligation was completely shut down when dATP and thio-dATP were used (Figure 4.6).²⁰⁰ They observed that the first step of ligation with dATP successfully led to the generation of ligase-dAMP intermediate, but at the second step of ligation an inhibitory effect was seen. The authors reasoned that this is potentially due to the formation of a more stable ligase-dAMP complex that prevents the adenylyl transfer to the DNA.^{191, 200} A few years later, another report assessing the ability of T4 DNA ligase to use dATP as cofactor was published.²⁰¹ In this work, the author showed that a ligation reaction in the presence of dATP was possible, however at a very slow rate.²⁰¹ The ligation reaction was performed over a time duration of ~42 hours (Figure 4.6B). This result was not in agreement with previous reports, and the authors indicated that the previous reports failed to see any ligation reaction with dATP because the reaction time was too short (for example the above mentioned example performed the ligation for 45 minutes,²⁰⁰ Figure 4.6A). Kinoshita and Nishigaki also showed that 2-aminopurine riboside triphosphate can also be used instead of ATP as cofactor (Figure 4.6).²⁰¹

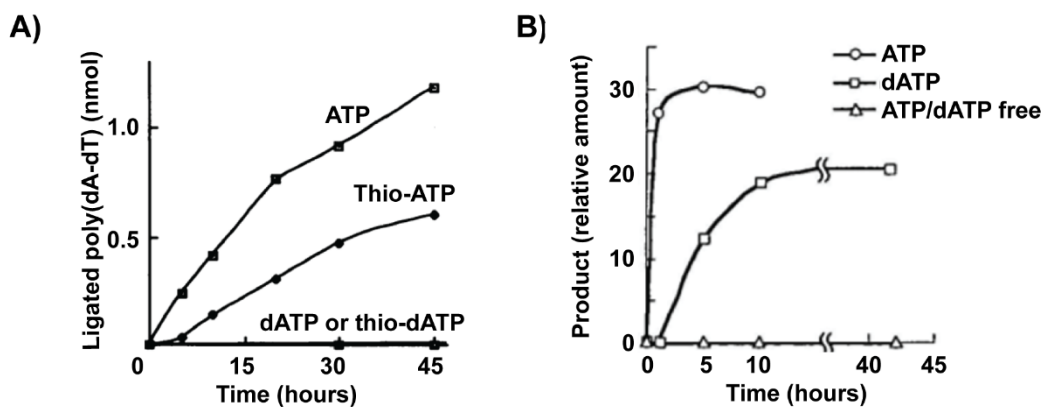
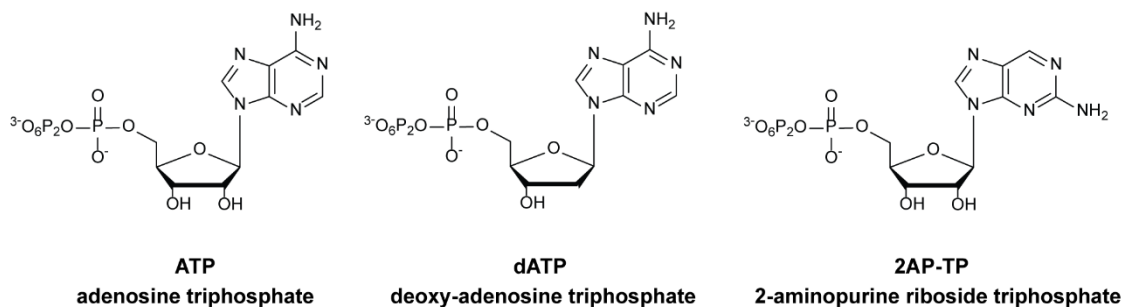


Figure 4.6 Structure of adenosine triphosphate (ATP), deoxy-adenosine triphosphate (dATP) and 2-aminopurine riboside triphosphate (2AP-TP). A) Kinetics of poly(dA-dT) circularization using T4 DNA ligase in the presence of ATP, thio-ATP, dATP and thio-dATP. The ligation reaction was performed at 30 °C using 300 CEU T4 DNA ligase enzyme for 45 min. Image reproduced with permission from reference 200. Copyright © 1990, Portland Press. B) Kinetics of ligation reaction of T4 DNA ligase in the presence of ATP and dATP and in the absence of both ATP/dATP. The ligation reaction was performed at 16 °C using 300 CEU enzyme. The image was regenerated with the permission of reference 201. Copyright © 1997, Oxford University Press.

Pawlowska *et al.* assessed the use of various ATP derivatives on the ligation reaction using T4 DNA ligase.¹⁹⁴ The authors goal was not to compare the efficiencies of ligation using ATP and the various modified ATP cofactors, rather they wanted to understand the stereo-preference of the enzyme. As shown in Figure 4.7, the ATP analogs used had modifications at either the 2' position

of the ribose sugar, the α -phosphate or between the β - and γ - phosphate (Figure 4.7). ATP, dATP as well as an ATP analog (β,γ -hypo-ATP), which contained a non-hydrolyzable β,γ -hypophosphate P-P bond was explored (Figure 4.7A-C). Analogs (D) ATP α S, (E) dATP α S, (F) β,γ -hypo-ATP α S were the thiol version of analogs (A), (B) and (C) whereby an oxygen atom had been replaced by a sulphur atom on the phosphate group at the α position (Figure 4.7). As a result of the sulphur substitution, a new stereogenic centre was created at the α -phosphate atom. Therefore, both the R_P and the S_P diastereomers were used in this study to determine if T4 DNA ligase exhibited stereoselective properties. As expected, product was observed for ATP (Figure 4.7, lane 2) and dATP (Figure 4.7, lane 8). Interestingly, β,γ -hypo-ATP (Figure 4.7, lane 7) and only the S_P epimer of ATP α S (Figure 4.7, lane 4) gave products. The R_P epimer of ATP α S (Figure 4.7, lane 3) as well as both diastereomers of dATP α S (Figure 4.7, lane 9-11) and β,γ -hypo-ATP α S (Figure 4.7, lane 5 and 6) did not yield any reaction. As the structure of T4 DNA ligase was not yet available, the authors used the structure of T7 DNA ligase that shares 22% of the protein sequence to understand the interactions of the enzyme with the different ATP analogs at the active site. They saw differences in interactions with the amino acid residues when the different modified cofactors were used. ATP α S was found to form additional hydrogen bonds with Lys232 and Lys10 since the negative charge of the phosphorothioate residue is located predominantly on the sulphur atom. As a result, ATP α S-S_P as a cofactor for T4 DNA ligase led to a ligation reaction while the R_P counterpart did not. On the other hand, for the β,γ -hypo-ATP α S that did not give any products. The author reasoned that absence of one oxygen atom between the β and the γ phosphorus atom and the presence of a sulphur atom on the α -phosphate group caused major disruption between the modified cofactor and the enzyme at the active site. Moreover, the hypophosphate anion is not a good leaving group as compared to pyrophosphate anion due to a higher pK_a of 1-2 for

hypophosphoric acid. As pertains to our study, this work revealed that the enzyme T4 DNA ligase can tolerate various modified ATP cofactors during a templated DNA-ligation reaction.¹⁹⁴

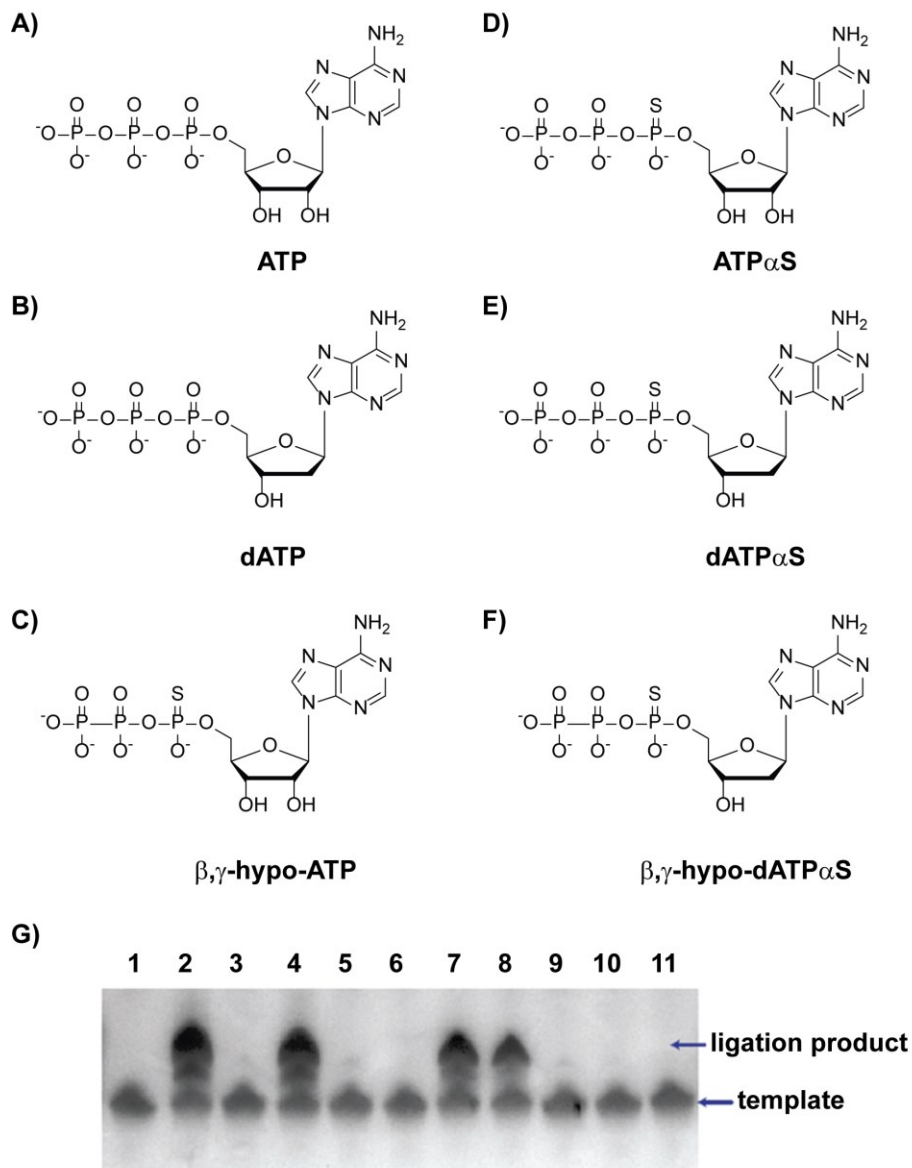


Figure 4.7 ATP analogs used as cofactor for T4 DNA ligase enzyme. (G) Polyacrylamide gel image of the ligation reaction after being stained by Stains-All dye. The ligation reactions of a nicked duplex DNA comprising of 30mer target, 20mer 5'-phosphate probe and 15mer 3'-hydroxy probe were performed using T4 DNA ligase (1500 CEU) at room temperature for 2 hours in the presence of 0.5 mM cofactor: Lane 1 – no cofactor, lane 2 – ATP (A), lane 3 - ATP α S-R_P (D),

lane 4 - ATP α S-S_P (D), lane 5 - β,γ -hypo-ATP α S-fast (F), lane 6 - β,γ -hypo-ATP α S-slow (F), lane 7 - β,γ -hypo-ATP (C), lane 8 - dATP (B), lane 9 – dATP α S mixed (E), lane 10 - dATP α S-S_P (E), lane 11 – dATP α S-R_P (E). Cofactor β,γ -hypo-ATP α S (F) was labelled fast or slow based on their chromatic mobility in reverse phase HPLC. Image reproduced with permission from reference 194. Copyright © 2016 Elsevier Inc. All rights reserved.

A more recent study that explored the effect of ATP modifications on the fidelity of DNA templated ligations was reported by the Hili group.¹⁸⁹ The context for this study was exploring how ATP derivatization could improve their LOOPER system for evolving highly functional nucleic acid aptamers that contain unnatural modifications in addition to the canonical nucleobases. LOOPER stands for ligase-catalyzed oligonucleotide polymerezation, and it involves the ligation of multiple nicked sites generated by the hybridization of a series of pentanucleotides (codon set = NNNNT) on a template.¹⁸⁹ To increase the fidelity of polymerization, i.e. the selective incorporation of the proper 5mer codon, the authors explored various parameters. For example, they varied the temperature of polymerization, which did not yield better fidelity.¹⁸⁹ Therefore, knowing how important and involved the ATP cofactor is in the ligation mechanism, they hypothesized that modifying the ATP cofactor might disrupt the kinetics of ligation resulting in better selectivity. For that to happen, the modification of the ATP must not be lost during the ligation mechanism (i.e. modification on the pyrophosphate will be lost during the adenylation step of the enzyme). That is, it should be passed on throughout the ligation mechanism to reach the 5'-phosphoryl group leading to a nick sealing with perturbed fidelity as the modified cofactor is sitting on the 5'-phosphate ends. Therefore, four specific sites on the ATP cofactor were selected for modification: the Hoogsteen face of the adenine nucleobase, the Watson-Crick face of the

adenine nucleobase, the 2' and 3' positions of the ribose sugar and the α -phosphate group of the triphosphate region (Figure 4.9A).¹⁸⁹ They explored ATP and 16 modified derivatives, and found that two ATP derivatives (ATP-2 and ATP-3, Figure 4.9B) provided sufficient rate of ligation and superior fidelity.

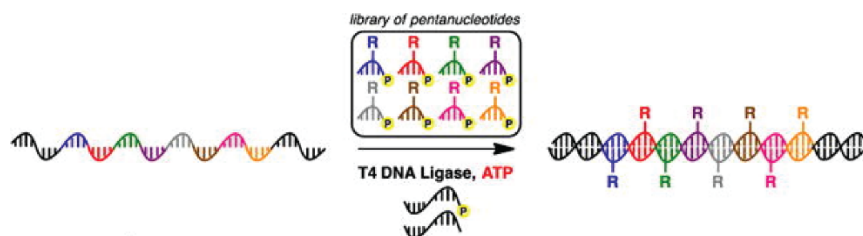


Figure 4.8 Schematic representation of LOOPER. In the presence of a template consisting of multiple codon reading frames and a library of pentanucleotides containing different R groups, a DNA duplex is formed with several nicked sites, which are ligated in the presence of T4 DNA ligase and ATP cofactor. Scheme reproduced with the permission of reference 189. Copyright © 2017 Royal Society of Chemistry.

4.5 Our Experimental Approach

The ATP derivatives used in this project were provided to us by the Hili group. Our goal was to assess the effect of the different modified ATP cofactors in LIDA. Specifically, we selected derivatives ATP-2 and ATP-3 because ligations using these cofactors were as fast as ATP but they provided higher sequence fidelity,¹⁸⁹ which suggested that they might be more selective in our pseudo-blunt end ligation. We also investigated ATP-1 (dATP) to determine how it impacted our background-triggered process (pseudo-blunt end ligation) vs LIDA initiated with a template. The LIDA procedure is described in Chapter 2 and Chapter 3 as well as briefly described in Chapter 4.6.4. The main difference experimentally in this study is the ligation buffer was prepared instead

of used from the supplier such that 1 mM or 0.025 mM of ATP or ATP derivative could be incorporated.

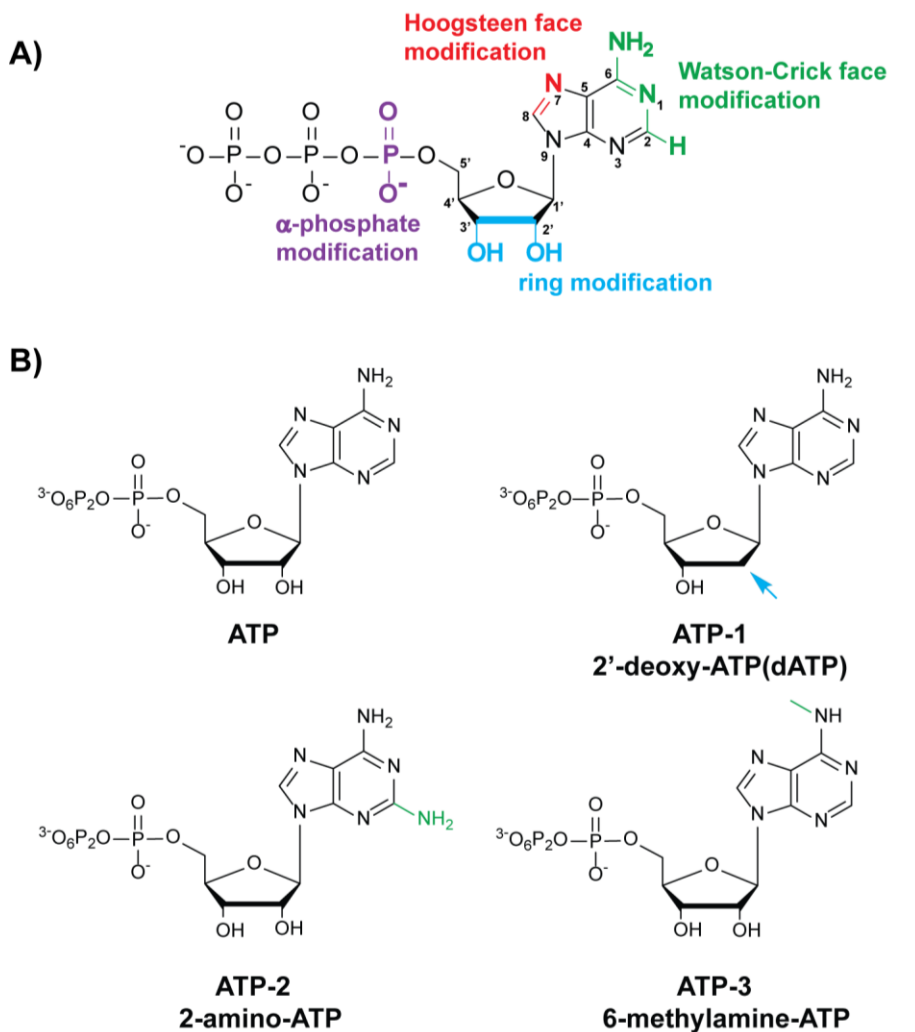


Figure 4.9 A) Modification regions of the ATP cofactor. B) Structure and naming system of modified ATP cofactors.

4.5.1 Preparation and Characterization of ATP Cofactor

Although the Hili lab explored many derivations, only two gave high ligation efficiency and fidelity in LOOPER.¹⁸⁹ The ATP derivatives were received in lyophilized form containing 0.4 μ mole of each. ATP is susceptible to degradation if subjected to multiple freezing and thawing.

Therefore, each ATP cofactor to be used was dissolved in nuclease-free water. After vortexing and centrifugation of the tubes, they were aliquoted, so each tube was removed once and used for only one reaction. The aliquots were stored in a -80 °C freezer.

4.5.2 LIDA using T4 DNA Ligase in the Presence of ATP Derivatives

Firstly, to make sure that the LIDA ligation reaction was not compromised by using our prepared buffer, we performed the cross-catalysis in the presence and absence of template **DNA-I** using the NEB buffer (containing 1 mM ATP and 10 mM DTT) as well as the prepared one with ATP (1 mM) added separately. Interestingly, a faster ligation reaction was observed when our buffer + ATP was used for both target-initiated and background-triggered LIDA (Figure 4.10, green). One reason might be the ATP concentration in the NEB buffer was higher than when it was added separately as lower ATP concentrations increases the rate of LIDA (*vide infra*).

Previous works have shown that the concentration of ATP can impact the ligation reaction.^{177, 187} As discussed in Chapter 3, lower concentration of ATP is required to facilitate RNA-templated ligation of DNA fragments using T4 DNA ligase (Chapter 3.2 and reference ¹⁷⁷). With regard to DNA-templated ligation of DNA, studies have shown that high ATP concentration has an inhibitory effect on the rate of the nick sealing step.^{189, 191, 198} Same has been observed for blunt end ligation, which intrinsically has a slower rate of ligation. When the concentration of ATP is high, the enzyme-ATP binding step predominates as compared to the ligation step.¹⁹⁸ That is, after the transfer of the AMP group from the adenylated ligase to the 5'-phosphate nicked double-stranded DNA (dsDNA), the enzyme is prematurely reloaded with another AMP group resulting in the dissociation of the enzyme before the ligation can occur.¹⁹¹ This leads to an increase in adenylated nick DNA in the system. On the other hand, at low concentration of ATP, the efficiency of blunt end ligation is greatly enhanced.¹⁹¹ In this case, the enzyme binds relatively slowly to ATP

than it binds to the nicked dsDNA allowing sufficient time to catalyze the ligation before getting reloaded.^{191, 198} Rossi *et al.* reported that a low concentration of 2.5 μM of ATP leads to a faster rate of blunt end ligation. Therefore, we decided to test both low and high concentration of the cofactors (0.025 mM and 1 mM) to see how the blunt end ligation was affected. When LIDA was performed in the presence of 0.025 mM ATP, a faster rate of ligation was observed only for the background-triggered reaction that had no initial template (Figure 4.10, purple trace). This was expected based on the literature as lower concentration of ATP is known to enhance blunt end ligation.¹⁹¹

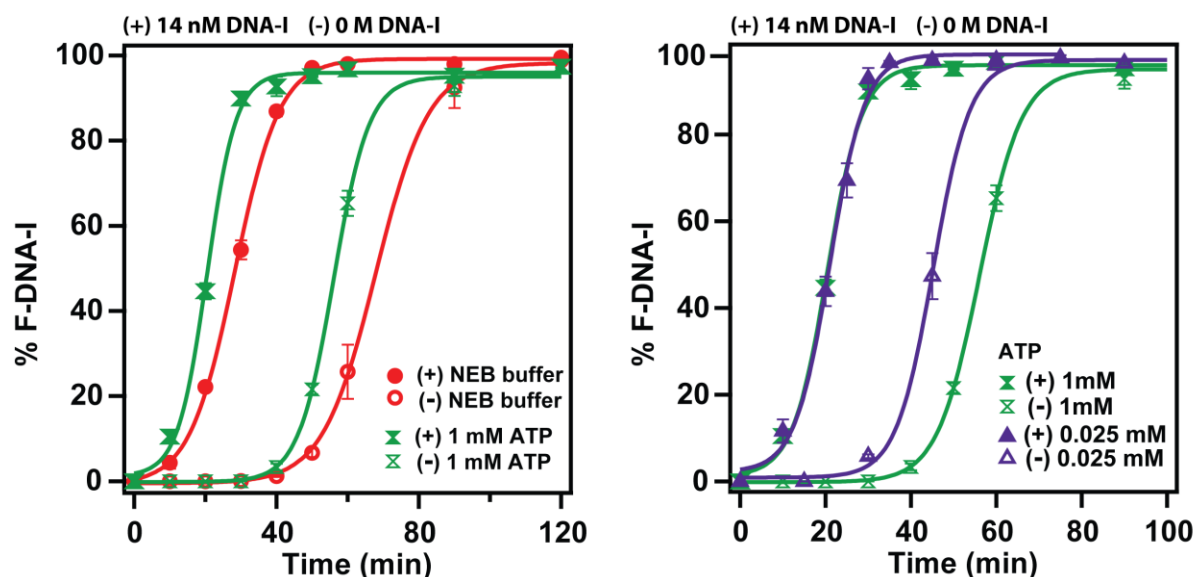


Figure 4.10 Kinetics F-DNA-I formation at 30 °C for cross catalysis initiated 14 nM (+) and 0 M (-) target DNA-I using NEB buffer or prepared buffer + ATP. *Experimental conditions:* 1.4 μM F-DNA-Ia; 2.8 μM DNA-Ib; 2.8 μM DNA-IIa; 2.8 μM DNA-IIb; 2000 CEU T4 DNA ligase, 50 mM TRIS-HCl, 10 mM MgCl₂, 1 mM or 0.025 mM ATP.

4.5.3 LIDA using T4 DNA Ligase in the Presence of the Modified ATP Cofactors

The first modification we utilized was dATP, the deoxy version of ATP, that has been widely explored in T4 DNA ligase mechanism.^{191, 200-201} In the presence of cofactor ATP-1 (dATP), a low yield (~8 %) was observed after 18 hours for the LIDA reaction initiated by target, while the LIDA reaction initiated without any target did not give any products, suggesting the pseudo-blunt end reaction was not successful. This slow rate of reaction was previously reported for the ligation of nicked DNA duplexes.¹⁸⁹ Since the reaction was so slow, this modified ATP was not considered for further experimentation.

As mentioned earlier, we then chose two ATP derivatives that gave the highest polymerization yield in LOOPER to be tested in our system: ATP-2 (2-amino-ATP) and ATP-3 (6-methylamine-ATP) at 1 mM and 0.025 mM concentration. Product was formed in LIDA reactions for both ATP-2 and ATP-3 at 1 mM concentration. When comparing them to the ATP (Figure 4.11C), we observed a significantly slower kinetic profile. At 0.025 mM ATP-2, a faster ligation reaction was observed compared to 1 mM ATP-2 (Figure 4.11A) consistent with our observations for ATP. We also concluded that the rate of ligation for ATP-2 is more pronounced for the background-triggered LIDA (0.025 mM vs 1 mM) compared to the templated ligation (0.025 mM vs 1 mM). This was expected as blunt end ligation is known to exhibit faster kinetics at lower concentration of ATP.¹⁹¹ Interestingly, with 40 times less amount of ATP-2 (0.025 mM), similar kinetics to ATP (1 mM) were observed with a slower pseudo-blunt end (Figure 4.11D). Finally, for 0.025 mM ATP-3, ~2% ligation was seen (Figure 4.11B, red trace), that is in agreement with Yi and Hili LOOPER system (they saw no reaction for this ATP cofactor at 0.025 mM). For 1 mM of ATP-3, a lower maximum yield (~80%) was seen (Figure 4.11B, blue trace), and we reason that premature AMP reloading might be preventing ligation to occur.

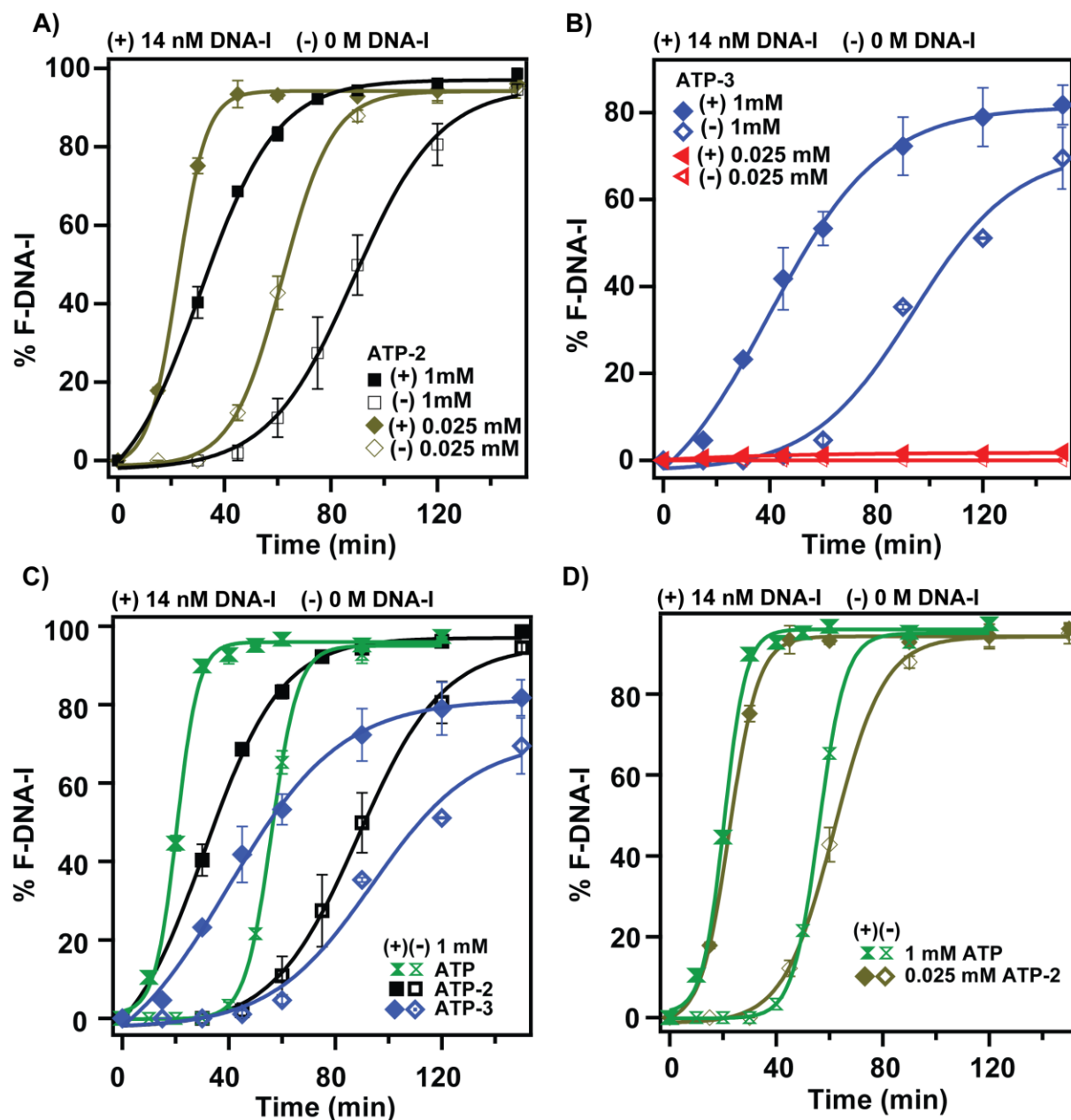


Figure 4.11 Kinetics F-DNA-I formation at 30 °C for cross catalysis initiated 14 nM (+) and 0 M (-) target **DNA-I** using prepared buffer and 1 mM or 0.025 mM of ATP, ATP-1, ATP-2 and ATP-3. *Experimental conditions:* 1.4 μ M **F-DNA-Ia**; 2.8 μ M **DNA-Ib**; 2.8 μ M **DNA-IIa**; 2.8 μ M **DNA-IIb**; 2000 CEU T4 DNA ligase, 50 mM TRIS-HCl, 10 mM MgCl₂, 1 mM or 0.025 mM ATP/ATP-1/ATP-2/ATP-3.

4.5.4 Efficiency of ATP-2 and ATP-3 in LIDA

Our hypothesis was that the ATP derivatives would selectively reduce the pseudo-blunt end ligation (background-triggered LIDA) and not affect the templated reaction. To use LIDA as a bio-diagnostic tool, the background-triggered process has to be suppressed in comparison to the template-initiated amplification. Therefore, we decided to analyze the difference in point-of-inflections (POI) (i.e. time to reach approximately 50% ligation conversion) between the sigmoidal fits to the kinetic traces that corresponded to the target-initiated and background-triggered (by pseudo-blunt end ligation) LIDA. By taking the difference of the POI(background-triggered) and POI(template-initiated) divided by POI(background-triggered) yields a discrimination factor that will give an indication of the separation between the two curves. This discrimination factor determined is compared to that measured in the presence of unmodified ATP. If the value is higher, it indicates that the LIDA process is better at discriminating the presence of initial target. These discrimination factors are listed in Table 4.1. Generally, at low concentration, we observed faster kinetics. However, based on the discrimination factor, 1 mM of cofactor gave better separation than 0.025 mM between the target-initiated and background-triggered reaction profiles. As mentioned earlier, 1 mM ATP gave similar results as 0.025 mM ATP-2 (Figure 4.11D). This was confirmed by the very close discrimination factor of 0.636 ± 0.002 for the former and 0.647 ± 0.008 for the latter. Lastly, a greater separation was observed at 1 mM ATP-2 with a discrimination factor of 0.653 ± 0.003 compared to ATP at 1 mM (discrimination factor = 0.636 ± 0.002) suggesting that ATP-2 should be utilized in subsequent detection strategies using LIDA.

Table 4.1 Discrimination factor of ATP and modified ATPs.

Cofactor	Cofactor conc. (mM)	Discrimination factor
ATP	0.025	0.525 ± 0.016
ATP	1	0.636 ± 0.002
ATP-1	0.025 and 1	NA*
ATP-2	0.025	0.647 ± 0.008
ATP-2	1	0.653 ± 0.003
ATP-3	0.025	NA*
ATP-3	1	0.579 ± 0.017

NA*: not applicable since very low yield was observed over a long time.

4.5.5 Effect of ATP and Modified ATP on Pseudo-Blunt End Ligation

To characterize the pseudo-blunt end reaction that triggers LIDA in the absence of initial target, an undergraduate student, Sarah Hales investigated both possible pseudo-blunt end reactions separately. She found that the pseudo-blunt end ligation of 5'-phosphate abasic nucleotide and 3'-hydroxy adenosine was observed in the presence of high enzyme concentrations like those used in LIDA (Table 4.2, *Pseudo-blunt end system I*). In contrast, no pseudo-blunt end ligation was observed between the 5'-phosphate adenosine and 3'-hydroxy thymidine (Table 4.2, *Pseudo-blunt end system II*).²⁰² Therefore, if we study *Pseudo-blunt end system I* using the ATP derivatives, we will have a better understanding of how these derivatives impact the background-triggered process of LIDA. In Figure 4.12, we saw that the ATP derivatives (ATP-2 and ATP-3) exhibited a slower background-triggered LIDA than the target-initiated LIDA in comparison to ATP. We hypothesize that the ligation of the destabilizing probes in the *Pseudo-blunt end system*

I is slower than the reaction in the presence of ATP. To test this hypothesis, we removed the 5'-phosphate group from one of the probes that constitutes the target sequence (**DNA-I**) to inhibit ligation of **DNA-Ia** and **DNA-Ib'** thereby shutting down cross-catalysis (Table 4.2). Also, we labelled the 3'-hydroxy adenosine probe (**F-DNA-IIb**) so as to monitor the ligation of that cycle using polyacrylamide gel electrophoresis (Table 4.2). Therefore, the yield that we obtain would reflect the ligation of the destabilizing probes only (blue DNA fragments).

Table 4.2 Probe DNA sequences involved in the pseudo-blunt end ligation. Color coded according to probes in Figure 4.1.

<u>Regular LIDA</u>		
<i>Regular Probes</i>	5'-TTG TTA AAT	pATT GAT AAG-3'
<i>Destabilizing probes</i>	3'-AAC AAT TTA (Ab)p	AA CTA TTC T _F -5'
<u>Pseudo-blunt end system I</u>		
<i>Regular Probes</i>	5'-TTG TTA AAT	ATT GAT AAG-3'
<i>Destabilizing probes</i>	3'-AAC AAT TTA (Ab)p	AA CTA TTC T _F -5'
<u>Pseudo-blunt end system II</u>		
<i>Regular Probes</i>	5'-T _F TG TTA AAT	pATT GAT AAG-3'
<i>Destabilizing probes</i>	3'-AAC AAT TTA (Ab)	AA CTA TTC T-5'

At 1 mM ATP, a yield of ~40% was observed over 6 hours (Figure 4.12, green) and 0.025 mM gave a higher yield of ~60%, which is consistent to what we observed for LIDA in the absence of target DNA (a faster background-triggered LIDA when 0.025 mM was used, Figure 4.10). For the derivatives, our observations confirmed our hypothesis. The rate at which the destabilized probes were ligated in the presence of modified ATP-2 and ATP-3 was much slower compared to the regular ATP at both concentrations (Figure 4.12). We propose that the presence of the modification on the ATP decreased the rate of nick sealing for both the pseudo blunt end and templated ligation reactions relative to the rate of enzyme adenylation. However, the effect was

more significant for the former leading to reloading of the enzyme prior to pseudo blunt end ligation but not prior to templated ligation. We analyzed the structure of AMP at the nick site shown in Figure 4.5 and concluded that both modifications on the ATP derivatives led to different interactions with the enzyme compared to the ATP. For ATP-2 (2-amino-ATP), the addition of an extra amine group at the position 2 of the base seems to be oriented in such a way that it will interact with residue Trp282 of the ligase. As for ATP-3, a hydrogen atom that is involved in hydrogen bonding is substituted by a methyl group, disturbing the stabilization. Therefore, both are disturbing the normal interaction involved with ATP, which we suggest decreases the rate of nick sealing. Finally, we also tested *Pseudo-blunt end system II* (Table 4.2) in which we added the 5'-phosphate from the probe that constitutes half the target sequence (**DNA-I**) while removing the phosphate from the 5'-abasic probe (**DNA-IIa**). As Sarah Hales observed, we also did not see any ligation from *Pseudo-blunt end system II* (data not shown).

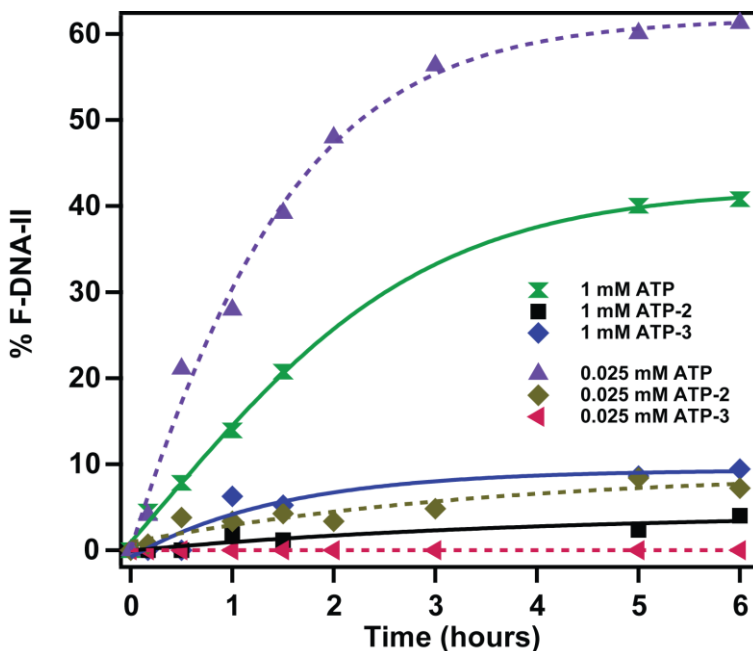


Figure 4.12 Kinetics of F-DNA-II formation at 16 °C using prepared buffer and 1 mM or 0.025 mM of ATP, ATP-1, ATP-2 and ATP-3. *Experimental conditions:* 1.4 μ M F-DNA-Ia; 2.8 μ M

DNA-Ib'; 2.8 μ M **DNA-IIa**; 2.8 μ M **DNA-IIb**; 2000 CEU T4 DNA ligase, 50 mM TRIS-HCl, 10 mM MgCl₂, 1 mM or 0.025 mM ATP/ATP-1/ATP-2/ATP-3. This experiment was performed only once.

4.6 Conclusion

We tested three derivations of ATP in our LIDA system. Overall, all three ATP cofactors were tolerated by T4 DNA ligase but resulted in slower kinetics of LIDA. The deoxy version of ATP, ATP-1 did not yield any ligation reaction until a long time (18 hours for 1 mM). On the other hand, ATP-3 yielded products at 1 mM and not 0.025 mM, which is consistent with the report of Yi and Hili in their ligase-catalyzed polymerization system.¹⁸⁹ However, at 1 mM ATP-3, a lower discrimination factor of 0.579 was observed compared to ATP (0.635), suggesting that this cofactor made the background process faster. At 1 mM, ATP-2 resulted in slower kinetics of LIDA but a better separation was observed between target-initiated and background-triggered (pseudo-blunt end triggered) processes, which indicates that this modified ATP has potential in increasing the sensitivity of LIDA. Further optimization of the system is needed, for example simultaneously optimizing the concentrations of ATP cofactors and temperatures of LIDA. Currently, we tested 0.025 mM and 1 mM, concentrations that lie very far apart. It would be interesting to see how the rate of LIDA and the discrimination factor change at intermittent as well as at higher concentrations of ATP-2. Additionally, the pseudo-blunt end experiment needs to be repeated as it was performed only once. We can also test the other 12 derivatives that were provided to us by the Hili group. Although these derivatives did not yield much ligation in the LOOPER system, it could unfold differently for LIDA. Ultimately, we showed that there is potential of using 2-amino-ATP to selectively reduce the background-triggered process of LIDA.

4.7 Experimental

4.7.1 General

For reagents, procedures and instrumentations used, refer to Chapter 2. 15 % PAGE gel making, running and imaging is also described in Chapter 2. The naming system and DNA sequences used in this project is listed in Table 4.3.

Table 4.3 DNA sequences used in this project.

Sequence name	DNA sequence
DNA-I	5'-TTGTTAAATATTGATAAG-3'
F-DNA-I	5'-TTGTTAAATATTGATAAG-3'
F-DNA-II	5'-T _F CTTATCAA(Ab)ATTTAACAA-3'
F-DNA-Ia	5'-T _F TGTTAAAT-3'
DNA-Ia	5'-TTGTTAAAT-3'
DNA-Ib	5'-pATTGATAAG-3'
DNA-Ib'	5'-ATTGATAAG-3'
DNA-IIa	5'-p(Ab)ATTTAACAA-3'
DNA-IIa'	5'-(Ab)ATTTAACAA-3'
DNA-IIb	5'-CTTATCAA-3'
F-DNA-IIb	5'-T _F CTTATCAA-3'

T_F: fluorescein-modified thymidine, p: phosphate, Ab: abasic lesion

4.7.2 Quantification and Analysis

Figure 4.11 represents the average and standard deviations of two sets of data while Figure 4.12 was performed only once. The % yield (% **F-DNA-I** or % **F-DNA-II**) for each LIDA and

pseudo-blunt end reaction was quantified from polyacrylamide gel images using the equation below. Also, is the equation used to calculate discrimination factor.

$$\% \text{ Yield} = \frac{\text{Intensity (Product Band)}}{\text{Intensity (Product Band + Reactant Band)}} \times 100\%$$

$$\text{Discrimination Factor} = \frac{\text{POI(Template initiated)} - \text{POI(Background - triggered)}}{\text{POI(Background - triggered)}}$$

4.7.3 Preparation of Ligation Buffer

Tris-HCl (9.09g) and MgCl₂ (3.06g) were weighed and dissolved in 100 mL of autoclaved MilliQ water. After all the solid was dissolved, the pH was adjusted to pH 7.5 using 6N HCl. The solution was then topped-up to 250 mL with autoclaved water. Following that, this solution was autoclaved.

4.7.4 LIDA- Cross Catalysis

For the DNA cross-catalysis ligation experiments, the reaction was set up as described in Chapter 2. Briefly, the target and the four probes were prepared in a total volume of 10 μL in an eppendorf tube. A master mix (MM) was prepared separately containing prepared buffer (TRIS-HCl and MgCl₂, 2.5 μL), 0.25 mM or 10 mM ATP derivative (1.5 μL) and T4 DNA ligase (6.5 CEU, 1 μL). From this MM, 5 μL was aliquoted to the reaction mixture. Total volume was 15 μL and final concentrations were 14 nM target **DNA-I**; 1.4 μM limiting fluorescent probe **F-DNA-I** and 2.8 μM for the other probes (**DNA-Ib**, **DNA-IIa** and **DNA-IIb**), 50 mM TRIS-HCl, 10 mM MgCl₂, 0.025 mM or 1 mM ATP derivative. A control reaction in the absence of the target was also set up simultaneously. The target was replaced by water in this case. Both templated and non-

templated reactions were incubated at 30 °C, and aliquots were taken at several time points to monitor the kinetics of ligation. Some of the reactions were set as half reactions in a total of 7.5 µL rather than 15 µL. Everything was done the same except that it was halved to reduce the required amount of enzyme and ATP derivative.

4.7.4 Pseudo-Blunt End Experiment

The pseudo-blunt end experiment was set up similar as the non-templated ligation reaction described in section 4.6.3 except for the 5'-phosphate and fluorescein-labelled probes used. In *Pseudo-blunt end system II*, **DNA-Ib'** (without 5'-phosphate) was used instead of **DNA-Ib** (with 5'-phosphate). As for *Pseudo-blunt end system I*, **DNA-IIa'** (without 5'-phosphate) was used instead of **DNA-IIa** (with 5'-phosphate) and **F-DNA-Ia** instead of **DNA-Ia**. As for **F-DNA-Iib**, we substituted it with the regular non-labelled probe **DNA-Iib**. The sequence for each system can be found above in Table 4.2 and 4.3. The final reaction volume was 7.5 µL with a final concentration of 50 mM TRIS-HCl, 10 mM MgCl₂, 0.025 mM or 1 mM ATP cofactors. The reaction was performed at 16 °C.

4.7.5 HPLC Procedure and HPLC Chromatogram

The purity of ATP derivatives used were analyzed by reverse phase high performance liquid chromatography, RP-HPLC. This technique was carried out using Agilent HPLC 1100 equipped with a C-18 column. The solvent system used was A: 0.03M triethylammonium acetate (TEAA) buffer and B: acetonitrile with 5% 0.03 M TEAA. The sample was run through the column at an elution gradient from 2% to 5% eluent B over 30 minutes with a flow rate of 2 mL/min at room temperature. The detector was set at 260 nm wavelength where ATP and related structures absorb. The chromatograms of ATP, ATP-1, ATP-2 and ATP-3 are shown below. All of them had one strong sharp peak suggesting that the compound was mostly pure and had not hydrolyzed

significantly. Small peaks observed were assigned to the ADP and the AMP versions of the ATP derivative.

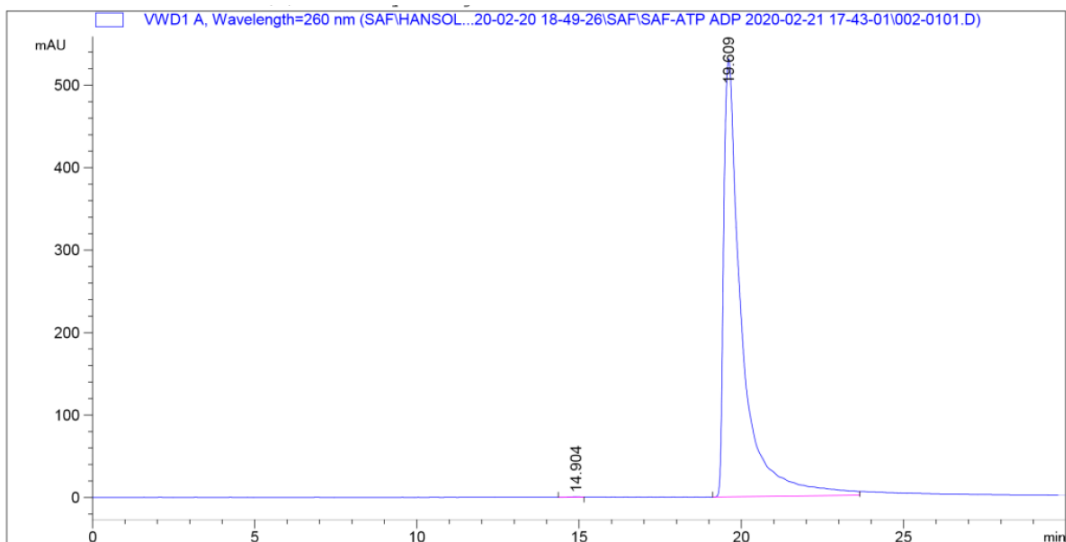


Figure 4.13 HPLC chromatogram of ATP

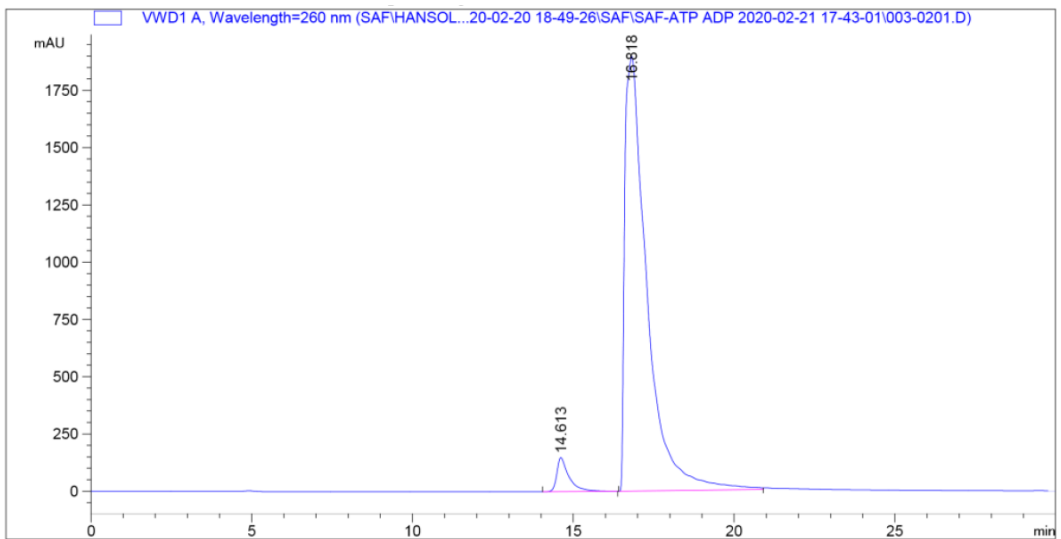


Figure 4.14 HPLC chromatogram of ADP

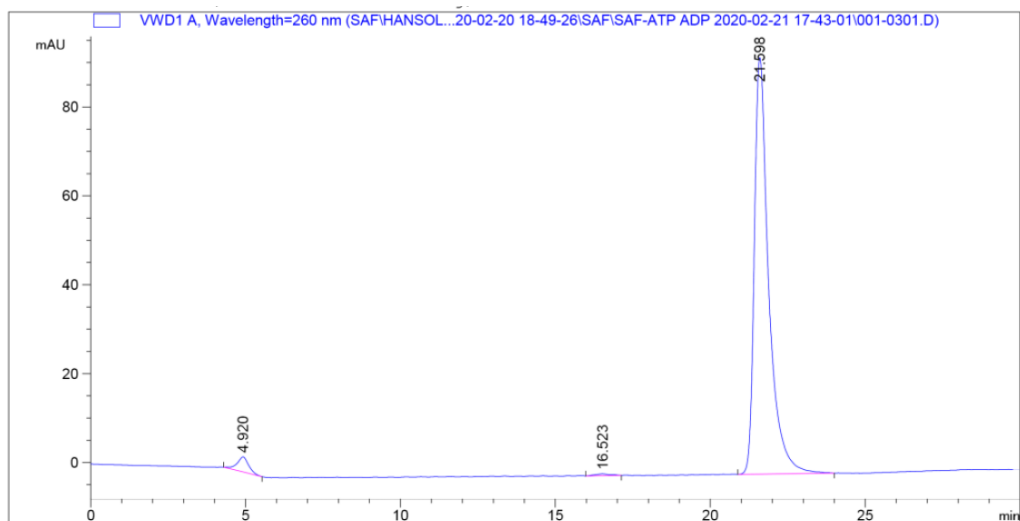


Figure 4.15 HPLC chromatogram of ATP-1

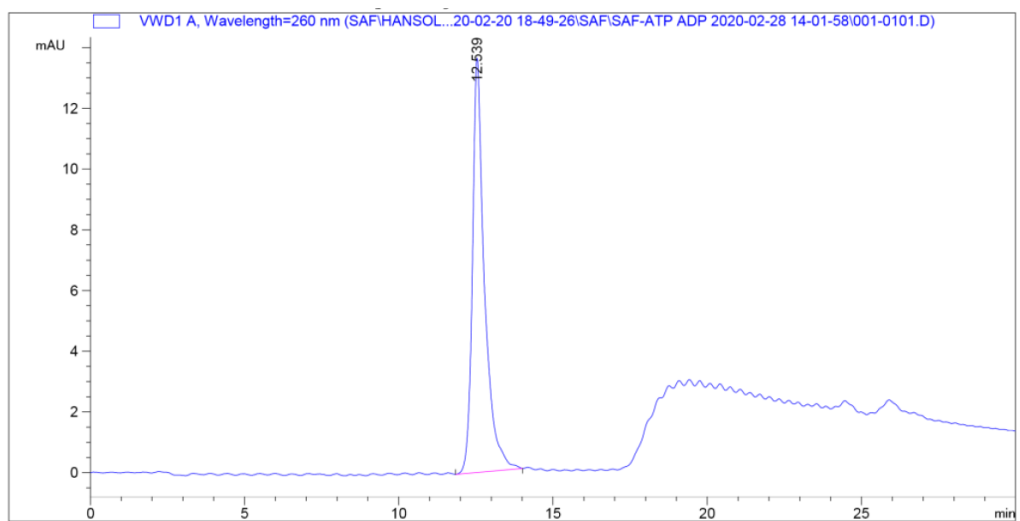


Figure 4.16 HPLC chromatogram of ATP-2

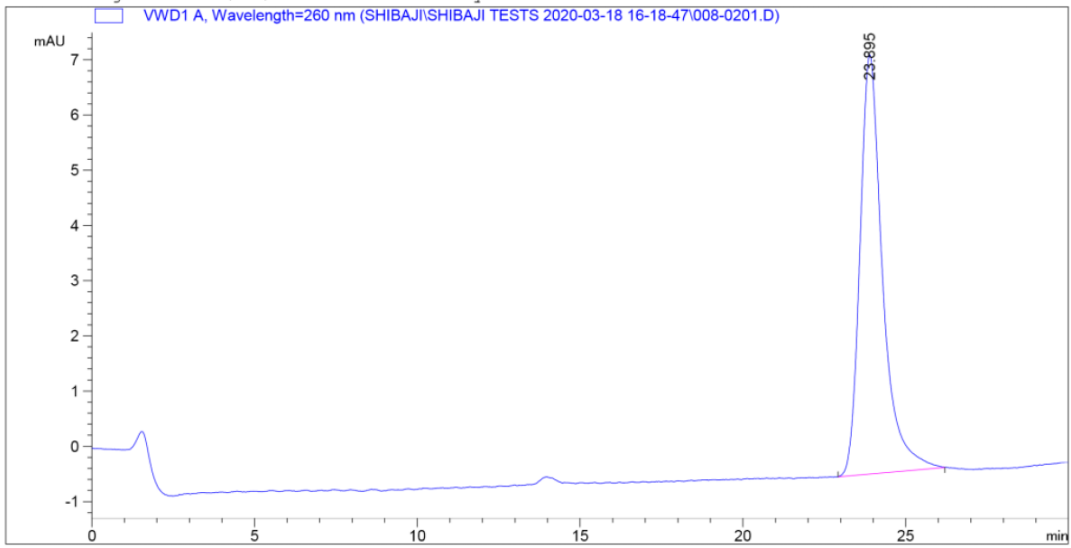


Figure 4.17 HPLC chromatogram of ATP-3

Chapter 5

Conclusions and Future Plans

5.1 General Conclusions

The aim of this thesis was to develop an equipment-free isothermal nucleic acid amplification test that can be performed over a wide range of room temperatures. To achieve this goal, we used lesion-induced DNA amplification as an amplification platform. LIDA was developed by our group and is an amplification technique that works at one temperature. To achieve turnover, a destabilizing group notably an abasic group (Ab) is used in this system. After ligation, the abasic lesion disturbs the product duplex, which causes it to dissociate for further hybridization and ligation. This process is temperature dependent and the ideal temperature, also referred as the optimum temperature (T_o), is dependent on the nucleic acid sequence and destabilizing group.

In Chapter 2, we demonstrated that the addition of a second destabilizing lesion had a significant impact on the stability of the nicked and product duplex causing the optimum temperature to shift from that of the abasic only system. Firstly, we showed that adding an A:G mismatch, 5 bases away from the nicked site, led to a faster kinetic of ligation at 30 °C, which is the T_o for the abasic only system. Then, upon investigating the ideal amplification temperature for the A:G + Ab system, we found that it works best at 26 °C, which is 4 °C lower than the Ab only system. Logically, we followed up with all the other mismatches that revealed a T_o range of 22 to 26 °C depending on the mismatch. Adding another abasic group instead of a mismatch to LIDA led to more destabilization with a T_o of 18 °C. Furthermore, the introduction of a second destabilizing group did not compromise the sensitivity of LIDA. Summing up, we achieved amplification using LIDA over a wide range of temperatures from 18 to 26 °C by introducing a second destabilizing element. Instead of using a heat incubator, we showed that we can perform LIDA using the system A:C + Ab (T_o is 22 °C) at room temperature on the bench in the laboratory.

Finally, we demonstrated when the abasic containing probe was combined with a mixture of the adjacent perfect and mismatched probe, there was selectivity towards the most complementary one even at temperatures where the matched probe had led to faster self-replication than the perfect probe in separate experiments. This result helps us understand the presence of competition in prebiotic self-replicating systems.

To further expand our range of biomarkers that we can detect using LIDA, in Chapter 3, we showed that LIDA can be used to amplify an RNA target by the addition of a reverse transcription step. Similar sensitivities as compared to LIDA with DNA target were achieved. Adding a mismatch to the system allowed us to detect RNA at room temperature. This system showed high specificity as no amplification was observed when using a mismatch and a random RNA as target. To mimic the complexity of a real biological sample, we tested the efficiency of our system in the presence of human lungs total RNA and *E. coli* total RNA. We observed that our system was not hindered by the presence of a large amount of random RNA when 105 fmol target was used. However, at lower concentration of RNA, slower kinetics was seen. To achieve room temperature detection along with amplification, we coupled our RNA triggered LIDA assay to our previously developed DNA modified aggregated gold nanoparticle detection platform. At a certain time-point, in the presence of an RNA target, a color change of purple to red was observed compared to the absence of RNA where no color change was observed. If the time is not chosen carefully, we could see color change in the control reaction that had no target RNA. The reason is the pseudo-blunt end process that arises from the four probes in the system.

To reduce the pseudo-blunt end ligation, in Chapter 4, we tested three modified ATP (T4 DNA ligase cofactor) from a library of 15 ATP derivatives that had various modifications at

different sites. ATP acts as a cofactor for T4 DNA ligase and is involved in all the steps in the mechanism of this enzyme. Therefore, having a modified ATP would generate a modified adenylated DNA, which would perturb the nick sealing step. Thus, we hypothesized that the pseudo-blunt end ligation would be mostly affected using different ATP derivatives as compared to the templated reaction. We tested the effect of three ATP derivatives on LIDA. LIDA using deoxy-ATP gave a slow reaction over a long time. For the other two (ATP-2 and ATP-3), amplification with a slower rate was observed at 1 mM. However, a better separation between the templated and the pseudo-blunt end was observed for ATP-2. To further understand how the pseudo-blunt end was affected by the modified ATP, we studied the two ligations that happen in the pseudo-blunt end separately by removing the 5'-phosphate on one side to prevent ligation. Firstly, the ligation occurs only between the probes containing the abasic group that constitutes the complementary sequence of the template. Exploring this ligation in the presence of the modified ATP revealed a significantly slow rate of ligation compared to the modified ATP. Despite these interesting results, further investigation is required to understand the effect of the ATP derivatives on pseudo-blunt end ligation.

5.2 Future Plans

5.2.1 Reducing the Background-triggered Amplification of LIDA

One limitation of our isothermal amplification technique developed by our group is the background reaction that stems from the ligation of the probes used in the system. Currently, without serial ligation we can detect 140 pM of target with LIDA because at lower concentrations, we cannot distinguish between the templated and the non-templated initiated LIDA reactions. Therefore, being able to reduce or shut down LIDA in the absence of a template would allow us to detect a lower amount of target making LIDA more sensitive. As mentioned in Chapter 4, further

optimization is required for the different ATP derivatives, for example varying the concentration of the ATP and the LIDA temperature. Assessing each cycle of LIDA separately, will give an insight on the rate of ligation for the different modified ATP cofactors. We saw that modified ATP (2-amino ATP), gave promising results in reducing the background-triggered LIDA at 1 mM. Therefore, we need to test the limit of detection of LIDA using this ATP derivative. We expect the sensitivity to go down by one or two orders of magnitude (i.e. we 140 fM = 2.1 amol). Reaching this limit of detection or lower will bring us closer to what is reported in the literature for isothermal techniques that work at room temperature (papers mentioned in Chapter 1).

Table 5.1 Room temperature isothermal nucleic acid techniques.

Ref.	Technique	Target	LOD	Real sample	Temp./°C	Duration/hr
57	RCA	Salmonella DNA	100 cells	Extracted Salmonella Genomic DNA	37, 94, 30 , 65	3
58	RCA	let-7a (s)	51 pM	HeLa cells	16, 30 , 37, 75	9hr
86	RCA	HPV DNA (s)	-	Cervical cell line W12	95, 30 , 65	16
87	RCA	miRNA-21 (s)	22 aM	A549 and HeLa cancer cells	95, 16,65, 30	>12
62	RPA	HIV Proviral DNA	10 copies*	ACH-2 cell line	25 - 43	2.5
163	CHA	HIV DNA (s)	2.6 pM	Spiked in serum	95, 25	3.5
109	TMSD	DNA (s)	5 fM	Spiked in serum	95, 26	4
53	TMSD	16s rRNA(s)	1 pM	<i>E. coli</i> bacteria	25-26	>5
117	HCR	DNA (s)	100 pM	-	95, 25	2
118	HCR	DNA (s)	0.4 nM	-	95, 25	3.5
115	HCR	HIV DNA (s)	1.18 nM	Spiked in serum	95, Room T.	7

120	HCR	DNA (s)	0.1 pM	-	95, 25	2
-----	-----	---------	--------	---	---------------	---

*Not the LOD but how much they detected in the paper.

(s): synthetic

Temperatures used in their entire assay. **Bold** is the amplification temperature.

5.2.2 Detection of Real Target with Sample Preparation

There are three steps for detection of a disease: DNA isolation, amplification and detection.

¹³ We have successfully shown that we can amplify and detect a target nucleic acid isothermally at room temperature. The only step that we have not explored yet is the DNA isolation. Our next goal should be to incorporate this step.

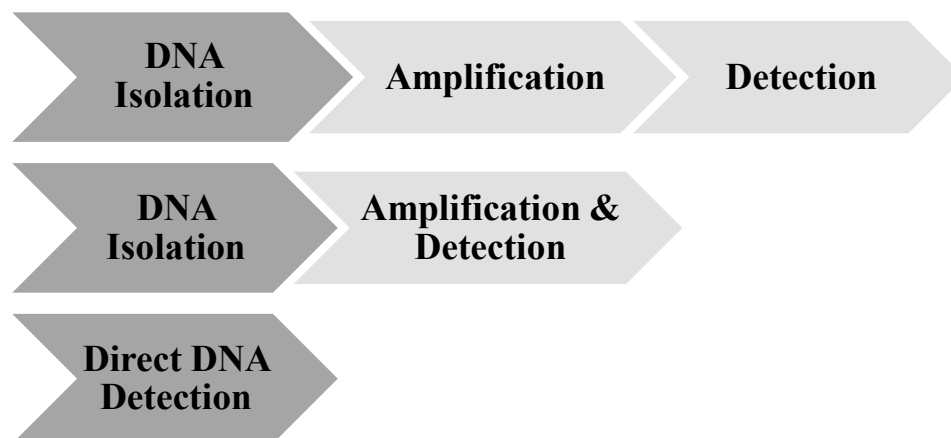


Figure 5.1 Nucleic acid test scheme. Image reproduced with permission from reference 37. Copyright © 2012, Royal Society of Chemistry.

In Chapter 3, we saw that amplification and detection of RNA using RT-LIDA in the presence of a total RNA sample was successful. Therefore, we decided to test miR-21, which is up-regulated in patients with breast cancer, making it a suitable biomarker. We have designed the probes for this system. Preliminary data showed that LIDA gave products using this miRNA-21 as target. However, more optimization is needed for this new system to find the perfect temperature. Then, we can detect the target of interest from real samples by growing the MCF-7

cell lines or collecting samples from patients. In doing so, we will incorporate sample preparation, which is a key step that we have not addressed until now.

References

1. World Health Organization, <https://www.who.int/emergencies/diseases/novel-coronavirus-2019/events-as-they-happen>.
2. Dietz, L.; Horve, P.; Coil, D.; Fretz, M.; Wymelenberg, K., *2019 Novel Coronavirus (COVID-19) Outbreak: A Review of the Current Literature and Built Environment (BE) Considerations to Reduce Transmission*. 2020.
3. Liu, Y.; Gayle, A. A.; Wilder-Smith, A.; Rocklöv, J., The reproductive number of COVID-19 is higher compared to SARS coronavirus. *Journal of Travel Medicine* **2020**, *27* (2).
4. Le Mauricien, <https://www.lemauricien.com/article/a-lesson-from-covid-19-invest-in-healthcare-not-the-military/>.
5. World Health Organization, <https://covid19.who.int/>.
6. Government of Canada, <https://www.canada.ca/en/public-health/services/diseases/2019-novel-coronavirus-infection.html>.
7. The novel coronavirus and its possible treatment by vaccines, therapeutics and drug delivery systems: Current status and future perspectives <https://pharmascope.org/ijrps/article/view/2144>.
8. <https://www.politico.eu/article/coronavirus-vaccine-how-long-will-it-take-to-develop/>.
9. Li, L.; Qin, L.; Xu, Z.; Yin, Y.; Wang, X.; Kong, B.; Bai, J.; Lu, Y.; Fang, Z.; Song, Q.; Cao, K.; Liu, D.; Wang, G.; Xu, Q.; Fang, X.; Zhang, S.; Xia, J.; Xia, J., Artificial Intelligence Distinguishes COVID-19 from Community Acquired Pneumonia on Chest CT. *Radiology*, 200905.
10. Xia, W.; Shao, J.; Guo, Y.; Peng, X.; Li, Z.; Hu, D., Clinical and CT features in pediatric patients with COVID-19 infection: Different points from adults. *Pediatric Pulmonology* **2020**, *55* (5), 1169-1174.
11. The Times, <https://www.thetimes.co.uk/article/britain-has-millions-of-coronavirus-antibody-tests-but-they-don-t-work-j7kb55g89>.
12. Tang, Y.-W.; Schmitz, J. E.; Persing, D. H.; Stratton, C. W., The Laboratory Diagnosis of COVID-19 Infection: Current Issues and Challenges. *Journal of Clinical Microbiology* **2020**, JCM.00512-20.
13. Tahamtan, A.; Ardebili, A., Real-time RT-PCR in COVID-19 detection: issues affecting the results. *Expert Review of Molecular Diagnostics* **2020**, *20* (5), 453-454.
14. Feng, H.; Liu, Y.; Lv, M.; Zhong, J., A case report of COVID-19 with false negative RT-PCR test: necessity of chest CT. *Japanese Journal of Radiology* **2020**, *38* (5), 409-410.
15. Hopman, J.; Allegranzi, B.; Mehtar, S., Managing COVID-19 in Low- and Middle-Income Countries. *JAMA* **2020**, *323* (16), 1549-1550.
16. Arumugam, A.; Faron, M. L.; Yu, P.; Markham, C.; Wong, S., A Rapid COVID-19 RT-PCR Detection Assay for Low Resource Settings. *bioRxiv* **2020**, 2020.04.29.069591.
17. Cara S Kosack, A.-L. P., Paul R Klatserc, A guide to aid the selection of diagnostic tests. *Bulletin of the World Health Organization* **2017**, (95), 639-645.
18. Warsinke, A., Point-of-care testing of proteins. *Analytical and Bioanalytical Chemistry* **2009**, *393* (5), 1393-1405.
19. Luppa, P. B.; Müller, C.; Schlichtiger, A.; Schlebusch, H., Point-of-care testing (POCT): Current techniques and future perspectives. *Trends in Analytical Chemistry* **2011**, *30* (6), 887-898.
20. Fomsgaard, A. S.; Rosenstjerne, M. W., An alternative workflow for molecular detection of SARS-CoV-2 - escape from the NA extraction kit-shortage. *medRxiv* **2020**, 2020.03.27.20044495.
21. Beltrán-Pavez, C.; Márquez, C. L.; Muñoz, G.; Valiente-Echeverría, F.; Gaggero, A.; Soto-Rifo, R.; Barriga, G. P., SARS-CoV-2 detection from nasopharyngeal swab samples without RNA extraction. *bioRxiv* **2020**, 2020.03.28.013508.

22. Diseases of poverty and the 10/90 gap
<https://www.who.int/intellectualproperty/submissions/InternationalPolicyNetwork.pdf>.
23. World Health Organization, <https://www.who.int/gho/hiv/en/>.
24. Manoto, S. L.; Lugongolo, M.; Govender, U.; Mthunzi-Kufa, P., Point of Care Diagnostics for HIV in Resource Limited Settings: An Overview. *Medicina* **2018**, *54* (1), 3.
25. LaBarre, P.; Boyle, D.; Hawkins, K.; Weigl, B., Instrument-free nucleic acid amplification assays for global health settings. *International Society for Optical Engineering* **2011**, 8029.
26. von Lode, P., Point-of-care immunotesting: Approaching the analytical performance of central laboratory methods. *Clinical Biochemistry* **2005**, *38* (7), 591-606.
27. Kabir, M. A.; Zilouchian, H.; Caputi, M.; Asghar, W., Advances in HIV diagnosis and monitoring. *Critical Reviews in Biotechnology* **2020**, 1-16.
28. Mabey, D.; Peeling, R. W.; Ustianowski, A.; Perkins, M. D., Diagnostics for the developing world. *Nature Reviews Microbiology* **2004**, *2* (3), 231-40.
29. Drain, P. K.; Hyle, E. P.; Noubary, F.; Freedberg, K. A.; Wilson, D.; Bishai, W. R.; Rodriguez, W.; Bassett, I. V., Diagnostic point-of-care tests in resource-limited settings. *The Lancet Infectious Diseases* **2014**, *14* (3), 239-249.
30. World Bank, <https://datahelpdesk.worldbank.org/knowledgebase/articles/906519-world-bank-country-and-lending-groups>.
31. Kimani, F. W.; Mwangi, S. M.; Kwasa, B. J.; Kusow, A. M.; Ngugi, B. K.; Chen, J.; Liu, X.; Cademartiri, R.; Thuo, M. M., Rethinking the Design of Low-Cost Point-of-Care Diagnostic Devices. *Micromachines* **2017**, *8* (11), 317.
32. Wamai, R. G., The Kenya Health System - Analysis of the situation and enduring challenges. *Japan Medical Association Journal* **2009**, *52*, 134-140.
33. Wu, G.; Zaman, M. H., Low-cost tools for diagnosing and monitoring HIV infection in low-resource settings. *Bulletin of World Health Organization* **2012**, *90* (12), 914-20.
34. Song, Y.; Huang, Y.-Y.; Liu, X.; Zhang, X.; Ferrari, M.; Qin, L., Point-of-care technologies for molecular diagnostics using a drop of blood. *Trends in biotechnology* **2014**, *32* (3), 132-139.
35. Liu, D., Molecular Medical Microbiology (Chapter 101). *Academic Press*, **2015**, 1781-1788.
36. Alexander, T. S., Serology or Molecular Infectious Disease Testing-Which, When, and Why? *Infectious Diseases in Clinical Practice* **2006**, *14* (6), 373-376.
37. Craw, P.; Balachandran, W., Isothermal nucleic acid amplification technologies for point-of-care diagnostics: a critical review. *Lab on a Chip* **2012**, *12* (14), 2469-86.
38. Niemz, A.; Ferguson, T. M.; Boyle, D. S., Point-of-care nucleic acid testing for infectious diseases. *Trends in Biotechnology* **2011**, *29* (5), 240-50.
39. Hu, Z.; Song, C.; Xu, C.; Jin, G.; Chen, Y.; Xu, X.; Ma, H.; Chen, W.; Lin, Y.; Zheng, Y.; Wang, J.; Hu, Z.; Yi, Y.; Shen, H., Clinical characteristics of 24 asymptomatic infections with COVID-19 screened among close contacts in Nanjing, China. *Science China Life Sciences* **2020**, *63* (5), 706-711.
40. Louie, M.; Louie, L.; Simor, A. E., The role of DNA amplification technology in the diagnosis of infectious diseases. *Canadian Medical Association Journal* **2000**, *163* (3), 301-309.
41. LaBarre, P.; Gerlach, J.; Wilmoth, J.; Beddoe, A.; Singleton, J.; Weigl, B. In *Non-instrumented nucleic acid amplification (NINA): Instrument-free molecular malaria diagnostics for low-resource settings*, 2010 Annual International Conference of the IEEE Engineering in Medicine and Biology, 31 Aug.-4 Sept. 2010; 2010; pp 1097-1099.
42. Snodgrass, R.; Gardner, A.; Semeere, A.; Koppaathy, V. L.; Duru, J.; Maurer, T.; Martin, J.; Cesarman, E.; Erickson, D., A portable device for nucleic acid quantification powered by sunlight, a flame or electricity. *Nature Biomedical Engineering* **2018**, *2* (9), 657-665.
43. Crannell, Z. A.; Rohrman, B.; Richards-Kortum, R., Equipment-free incubation of recombinase polymerase amplification reactions using body heat. *PLoS One* **2014**, *9* (11), e112146-e112146.

44. Zhao, Y.; Chen, F.; Li, Q.; Wang, L.; Fan, C., Isothermal Amplification of Nucleic Acids. *Chemical Reviews* **2015**, *115* (22), 12491-12545.
45. Niemz, A.; Ferguson, T.; Boyle, D., Point-of-Care Nucleic Acid Testing for Infectious Diseases. *Trends in Biotechnology* **2011**, *29*, 240-50.
46. Fakruddin, M.; Mannan, K. S. B.; Chowdhury, A.; Mazumdar, R. M.; Hossain, M. N.; Islam, S.; Chowdhury, M. A., Nucleic acid amplification: Alternative methods of polymerase chain reaction. *Journal of Pharmacy & Bioallied Sciences* **2013**, *5* (4), 245-252.
47. Zhou, L.; Chandrasekaran, A. R.; Punnoose, J. A.; Bonenfant, G.; Charles, S.; Levchenko, O.; Badu, P.; Cavaliere, C.; Pager, C. T.; Halvorsen, K., Programmable low-cost DNA-based platform for viral RNA detection. *bioRxiv* **2020**, 2020.01.12.902452.
48. Huang, S.; Do, J.; Mahalanabis, M.; Fan, A.; Zhao, L.; Jepeal, L.; Singh, S. K.; Klapperich, C. M., Low cost extraction and isothermal amplification of DNA for infectious diarrhea diagnosis. *PLoS One* **2013**, *8* (3), e60059-e60059.
49. Ma, F.; Liu, M.; Tang, B.; Zhang, C.-y., Sensitive Quantification of MicroRNAs by Isothermal Helicase-Dependent Amplification. *Analytical Chemistry* **2017**, *89* (11), 6182-6187.
50. Jeong, Y.-J.; Park, K.; Kim, D.-E., Isothermal DNA amplification in vitro: the helicase-dependent amplification system. *Cellular and Molecular Life Sciences* **2009**, *66* (20), 3325.
51. Curtis, K. A.; Rudolph, D. L.; Morrison, D.; Guelig, D.; Diesburg, S.; McAdams, D.; Burton, R. A.; LaBarre, P.; Owen, M., Single-use, electricity-free amplification device for detection of HIV-1. *Journal of Virological Methods* **2016**, *237*, 132-137.
52. Lam, P.; Keri, R. A.; Steinmetz, N. F., A Bioengineered Positive Control for Rapid Detection of the Ebola Virus by Reverse Transcription Loop-Mediated Isothermal Amplification (RT-LAMP). *ACS Biomaterials Science & Engineering* **2017**, *3* (3), 452-459.
53. Ravan, H., Isothermal RNA detection through the formation of DNA concatemers containing HRP-mimicking DNAzymes on the surface of gold nanoparticles. *Biosensors and Bioelectronics* **2016**, *80*, 67-73.
54. Song, J.; Mauk, M. G.; Hackett, B. A.; Cherry, S.; Bau, H. H.; Liu, C., Instrument-Free Point-of-Care Molecular Detection of Zika Virus. *Analytical Chemistry* **2016**, *88* (14), 7289-94.
55. Sun, Y.; Tian, H.; Liu, C.; Sun, Y.; Li, Z., One-step detection of microRNA with high sensitivity and specificity via target-triggered loop-mediated isothermal amplification (TT-LAMP). *Chemical Communications* **2017**, *53* (80), 11040-11043.
56. Yan, L.; Zhou, J.; Zheng, Y.; Gamson, A. S.; Roembke, B. T.; Nakayama, S.; Sintim, H. O., Isothermal amplified detection of DNA and RNA. *Molecular BioSystems* **2014**, *10* (5), 970-1003.
57. Kordas, A.; Papadakis, G.; Milioni, D.; Champ, J.; Descroix, S.; Gizeli, E., Rapid Salmonella detection using an acoustic wave device combined with the RCA isothermal DNA amplification method. *Sensing and Bio-Sensing Research* **2016**, *11* (2), 121-127.
58. Xu, H.; Wu, D.; Zhang, Y.; Shi, H.; Ouyang, C.; Li, F.; Jia, L.; Yu, S.; Wu, Z.-S., RCA-enhanced multifunctional molecule beacon-based strand-displacement amplification for sensitive microRNA detection. *Sensors and Actuators B: Chemical* **2018**, *258*, 470-477.
59. Liu, X.; Zou, M.; Li, D.; Yuan, R.; Xiang, Y., Hairpin/DNA ring ternary probes for highly sensitive detection and selective discrimination of microRNA among family members. *Analytica Chimica Acta* **2019**, *1076*, 138-143.
60. Ali, M. M.; Li, F.; Zhang, Z.; Zhang, K.; Kang, D.-K.; Ankrum, J. A.; Le, X. C.; Zhao, W., Rolling circle amplification: a versatile tool for chemical biology, materials science and medicine. *Chemical Society Reviews* **2014**, *43* (10), 3324-3341.
61. Xu, C.; Wang, X.; Li, H.; Han, C.; Wang, J.; Wang, Y.; Liu, S.; Huang, J., Branched RCA coupled with a NESA-based fluorescence assay for ultrasensitive detection of miRNA. *New Journal of Chemistry* **2017**, *41* (13), 5355-5361.

62. Lillis, L.; Lehman, D.; Singhal, M. C.; Cantera, J.; Singleton, J.; Labarre, P.; Toyama, A.; Piepenburg, O.; Parker, M.; Wood, R.; Overbaugh, J.; Boyle, D. S., Non-instrumented incubation of a recombinase polymerase amplification assay for the rapid and sensitive detection of proviral HIV-1 DNA. *PLoS One* **2014**, *9* (9), e108189-e108189.
63. Wang, J.; Wang, J.; Li, R.; Shi, R.; Liu, L.; Yuan, W., Evaluation of an incubation instrument-free reverse transcription recombinase polymerase amplification assay for rapid and point-of-need detection of canine distemper virus. *Journal of Virological Methods* **2018**, *260*, 56-61.
64. Boyle, D. S.; McNerney, R.; Teng Low, H.; Leader, B. T.; Pérez-Osorio, A. C.; Meyer, J. C.; O'Sullivan, D. M.; Brooks, D. G.; Piepenburg, O.; Forrest, M. S., Rapid detection of Mycobacterium tuberculosis by recombinase polymerase amplification. *PLoS One* **2014**, *9* (8), e103091-e103091.
65. Daher, R. K.; Stewart, G.; Boissinot, M.; Bergeron, M. G., Recombinase Polymerase Amplification for Diagnostic Applications. *Clinical Chemistry* **2016**, *62* (7), 947-958.
66. Zhang, D. Y.; Brandwein, M.; Hsuih, T.; Li, H. B., Ramification Amplification: A Novel Isothermal DNA Amplification Method. *Molecular Diagnosis* **2001**, *6* (2), 141-150.
67. Reid, M. S.; Le, X. C.; Zhang, H., Exponential Isothermal Amplification of Nucleic Acids and Assays for Proteins, Cells, Small Molecules, and Enzyme Activities: An EXPAR Example. *Angewandte Chemie International Edition* **2018**, *57* (37), 11856-11866.
68. Tenaglia, E.; Imaizumi, Y.; Miyahara, Y.; Guiducci, C., Isothermal multiple displacement amplification of DNA templates in minimally buffered conditions using phi29 polymerase. *Chemical Communications* **2018**, *54* (17), 2158-2161.
69. Walker, G. T.; Linn, C. P.; Nadeau, J. G., DNA Detection by Strand Displacement Amplification and Fluorescence Polarization With Signal Enhancement Using a DNA Binding Protein. *Nucleic Acids Research* **1996**, *24* (2), 348-353.
70. Toley, B. J.; Covelli, I.; Belousov, Y.; Ramachandran, S.; Kline, E.; Scarr, N.; Vermeulen, N.; Mahoney, W.; Lutz, B. R.; Yager, P., Isothermal strand displacement amplification (iSDA): a rapid and sensitive method of nucleic acid amplification for point-of-care diagnosis. *Analyst* **2015**, *140* (22), 7540-7549.
71. Alladin-Mustan, B. S.; Mitran, C. J.; Gibbs-Davis, J. M., Achieving room temperature DNA amplification by dialling in destabilization. *Chemical Communications* **2015**, *51* (44), 9101-9104.
72. Kausar, A.; McKay, R. D.; Lam, J.; Bhogal, R. S.; Tang, A. Y.; Gibbs-Davis, J. M., Tuning DNA Stability To Achieve Turnover in Template for an Enzymatic Ligation Reaction. *Angewandte Chemie International Edition* **2011**, *50* (38), 8922-8926.
73. Kausar, A.; Mitran, C. J.; Li, Y.; Gibbs-Davis, J. M., Rapid, isothermal DNA self-replication induced by a destabilizing lesion. *Angewandte Chemie International Edition* **2013**, *52* (40), 10577-81.
74. Food and Drug Administration, <https://www.fda.gov/media/136314/download>.
75. Azar, M. M.; Landry, M. L., Detection of Influenza A and B Viruses and Respiratory Syncytial Virus by Use of Clinical Laboratory Improvement Amendments of 1988 (CLIA)-Waived Point-of-Care Assays: a Paradigm Shift to Molecular Tests. *Journal of Clinical Microbiology* **2018**, *56* (7), e00367-18.
76. Dong, G.; Dai, J.; Jin, L.; Shi, H.; Wang, F.; Zhou, C.; Zheng, B.; Guo, Y.; Xiao, D., A rapid room-temperature DNA amplification and detection strategy based on nicking endonuclease and catalyzed hairpin assembly. *Analytical Methods* **2019**, *11* (19), 2537-2541.
77. Zaghoul, H.; El-Shahat, M., Recombinase polymerase amplification as a promising tool in hepatitis C virus diagnosis. *World Journal of Hepatology* **2014**, *6* (12), 916-22.
78. Obande, G. A.; Banga Singh, K. K., Current and Future Perspectives on Isothermal Nucleic Acid Amplification Technologies for Diagnosing Infections. *Infection and Drug Resistance* **2020**, *13*, 455-483.
79. Oxford Dictionary, <https://www.oxfordlearnersdictionaries.com/>.
80. Low Income Countries Population, <http://worldpopulationreview.com/countries/low-income-countries/>.

81. Glunt, K. D.; Blanford, J. I.; Paaijmans, K. P., Chemicals, climate, and control: increasing the effectiveness of malaria vector control tools by considering relevant temperatures. *PLoS Pathogens* **2013**, *9* (10), e1003602-e1003602.
82. Zhuang, J.; Lai, W.; Chen, G.; Tang, D., A rolling circle amplification-based DNA machine for miRNA screening coupling catalytic hairpin assembly with DNAzyme formation. *Chemical Communications* **2014**, *50* (22), 2935-8.
83. Notomi, T.; Okayama, H.; Masubuchi, H.; Yonekawa, T.; Watanabe, K.; Amino, N.; Hase, T., Loop-mediated isothermal amplification of DNA. *Nucleic Acids Research* **2000**, *28* (12), E63-E63.
84. Johne, R.; Müller, H.; Rector, A.; van Ranst, M.; Stevens, H., Rolling-circle amplification of viral DNA genomes using phi29 polymerase. *Trends in Microbiology* **2009**, *17* (5), 205-211.
85. Blanco, L.; Bernad, A.; Lázaro, J. M.; Martín, G.; Garmendia, C.; Salas, M., Highly efficient DNA synthesis by the phage phi 29 DNA polymerase. Symmetrical mode of DNA replication. *Journal of Biological Chemistry* **1989**, *264* (15), 8935-8940.
86. Rector, A.; Tachezy, R.; Van Ranst, M., A sequence-independent strategy for detection and cloning of circular DNA virus genomes by using multiply primed rolling-circle amplification. *Journal of Virology* **2004**, *78* (10), 4993-4998.
87. Chen, A.; Ma, S.; Zhuo, Y.; Chai, Y.; Yuan, R., In Situ Electrochemical Generation of Electrochemiluminescent Silver Nanoclusters on Target-Cycling Synchronized Rolling Circle Amplification Platform for MicroRNA Detection. *Analytical Chemistry* **2016**, *88* (6), 3203-3210.
88. Liu, H.; Li, L.; Duan, L.; Wang, X.; Xie, Y.; Tong, L.; Wang, Q.; Tang, B., High Specific and Ultrasensitive Isothermal Detection of MicroRNA by Padlock Probe-Based Exponential Rolling Circle Amplification. *Analytical Chemistry* **2013**, *85* (16), 7941-7947.
89. Cheng, Y.; Zhang, X.; Li, Z.; Jiao, X.; Wang, Y.; Zhang, Y., Highly Sensitive Determination of microRNA Using Target-Primed and Branched Rolling-Circle Amplification. *Angewandte Chemie International Edition* **2009**, *48* (18), 3268-3272.
90. de la Torre, T. Z. G.; Mezger, A.; Herthnek, D.; Johansson, C.; Svedlindh, P.; Nilsson, M.; Strømme, M., Detection of rolling circle amplified DNA molecules using probe-tagged magnetic nanobeads in a portable AC susceptometer. *Biosensors and Bioelectronics* **2011**, *29* (1), 195-199.
91. Murakami, T.; Sumaoka, J.; Komiyama, M., Sensitive isothermal detection of nucleic-acid sequence by primer generation-rolling circle amplification. *Nucleic Acids Research* **2008**, *37* (3), e19-e19.
92. Davari, M.; van Diepeningen, A. D.; Babai-Ahari, A.; Arzanlou, M.; Najafzadeh, M. J.; van der Lee, T. A. J.; de Hoog, G. S., Rapid identification of *Fusarium graminearum* species complex using Rolling Circle Amplification (RCA). *Journal of Microbiological Methods* **2012**, *89* (1), 63-70.
93. Piepenburg, O.; Williams, C. H.; Stemple, D. L.; Armes, N. A., DNA detection using recombination proteins. *PLoS Biology* **2006**, *4* (7), e204-e204.
94. Kersting, S.; Rausch, V.; Bier, F. F.; von Nickisch-Roseneck, M., Rapid detection of *Plasmodium falciparum* with isothermal recombinase polymerase amplification and lateral flow analysis. *Malaria Journal* **2014**, *13* (1), 99.
95. Wu, Y. D.; Xu, M. J.; Wang, Q. Q.; Zhou, C. X.; Wang, M.; Zhu, X. Q.; Zhou, D. H., Recombinase polymerase amplification (RPA) combined with lateral flow (LF) strip for detection of *Toxoplasma gondii* in the environment. *Veterinary Parasitology* **2017**, *243*, 199-203.
96. Lobato, I. M.; O'Sullivan, C. K., Recombinase polymerase amplification: Basics, applications and recent advances. *Trends in Analytical Chemistry* **2018**, *98*, 19-35.
97. Yang, Y.; Qin, X.; Zhang, W.; Li, Y.; Zhang, Z., Rapid and specific detection of porcine parvovirus by isothermal recombinase polymerase amplification assays. *Molecular and Cellular Probes* **2016**, *30* (5), 300-305.

98. Dean, F. B.; Hosono, S.; Fang, L.; Wu, X.; Faruqi, A. F.; Bray-Ward, P.; Sun, Z.; Zong, Q.; Du, Y.; Du, J.; Driscoll, M.; Song, W.; Kingsmore, S. F.; Egholm, M.; Lasken, R. S., Comprehensive human genome amplification using multiple displacement amplification. *PNAS* **2002**, *99* (8), 5261-5266.
99. Lasken, Roger S., Genomic DNA amplification by the multiple displacement amplification (MDA) method. *Biochemical Society Transactions* **2009**, *37* (2), 450-453.
100. Walker, F. M.; Hsieh, K., Advances in Directly Amplifying Nucleic Acids from Complex Samples. *Biosensors* **2019**, *9* (4), 117.
101. Spits, C.; Le Caignec, C.; De Rycke, M.; Van Haute, L.; Van Steirteghem, A.; Liebaers, I.; Sermon, K., Whole-genome multiple displacement amplification from single cells. *Nature Protocols* **2006**, *1* (4), 1965-1970.
102. Wang, Y.; Nair, S.; Nosten, F.; Anderson, T. J. C., Multiple displacement amplification for malaria parasite DNA. *The Journal of Parasitology* **2009**, *95* (1), 253-255.
103. George, S.; Xu, Y.; Sanderson, N.; Hubbard, A. T. M.; Griffiths, D. T.; Morgan, M.; Pankhurst, L.; Hoosdally, S. J.; Foster, D.; Thulborn, S.; Robinson, E.; Grace Smith, E.; Rathod, P.; Sarah Walker, A.; Peto, T. E. A.; Crook, D. W.; Dingle, K. E., MinION Nanopore Sequencing of Multiple Displacement Amplified Mycobacteria DNA Direct from Sputum. *bioRxiv* **2018**, 490417.
104. Liu, L.; Zhang, S.; Wu, D.; Song, J.; Li, A.; Zhang, H.; Wu, W.; Tan, Q.; Li, C.; Zhang, Q.; Zhou, H.; Liang, M.; Ke, C.; Li, D., Identification and genetic characterization of Zika virus isolated from an imported case in China. *Infection, Genetics and Evolution* **2017**, *48*, 40-46.
105. Chen, J.; Tang, L.; Chu, X.; Jiang, J., Enzyme-free, signal-amplified nucleic acid circuits for biosensing and bioimaging analysis. *Analyst* **2017**, *142* (17), 3048-3061.
106. Yurke, B.; Turberfield, A. J.; Mills, A. P., Jr.; Simmel, F. C.; Neumann, J. L., A DNA-fuelled molecular machine made of DNA. *Nature* **2000**, *406* (6796), 605-8.
107. Guo, Y.; Wei, B.; Xiao, S.; Yao, D.; Li, H.; Xu, H.; Song, T.; Li, X.; Liang, H., Recent advances in molecular machines based on toehold-mediated strand displacement reaction. *Quantitative Biology* **2017**, *5* (1), 25-41.
108. Dirks, R. M.; Pierce, N. A., Triggered amplification by hybridization chain reaction. *Proceedings of the National Academy of Sciences of the United States of America* **2004**, *101* (43), 15275.
109. Ravan, H.; Amandadi, M.; Hassanshahian, M.; Pourseyedi, S., Dual catalytic DNA circuit-induced gold nanoparticle aggregation: An enzyme-free and colorimetric strategy for amplified detection of nucleic acids. *International Journal of Biological Macromolecules* **2020**, *154*, 896-903.
110. Park, Y.; Lee, C. Y.; Kang, S.; Kim, H.; Park, K. S.; Park, H. G., Universal, colorimetric microRNA detection strategy based on target-catalyzed toehold-mediated strand displacement reaction. *Nanotechnology* **2018**, *29* (8), 085501.
111. Gliddon, H. D.; Howes, P. D.; Kaforou, M.; Levin, M.; Stevens, M. M., A nucleic acid strand displacement system for the multiplexed detection of tuberculosis-specific mRNA using quantum dots. *Nanoscale* **2016**, *8* (19), 10087-10095.
112. Park, C. R.; Park, S. J.; Lee, W. G.; Hwang, B. H., Biosensors Using Hybridization Chain Reaction - Design and Signal Amplification Strategies of Hybridization Chain Reaction. *Biotechnology and Bioprocess Engineering* **2018**, *23* (4), 355-370.
113. Bi, S.; Yue, S.; Zhang, S., Hybridization chain reaction: a versatile molecular tool for biosensing, bioimaging, and biomedicine. *Chemical Society Reviews* **2017**, *46* (14), 4281-4298.
114. Guo, Q.; Chen, Y.; Song, Z.; Guo, L.; Fu, F.; Chen, G., Label-free and enzyme-free sensitive fluorescent detection of human immunodeficiency virus deoxyribonucleic acid based on hybridization chain reaction. *Analytica Chimica Acta* **2014**, *852*, 244-249.
115. Zhang, S.; Wang, K.; Li, K.-B.; Shi, W.; Jia, W.-P.; Chen, X.; Sun, T.; Han, D.-M., A DNA-stabilized silver nanoclusters/graphene oxide-based platform for the sensitive detection of DNA through hybridization chain reaction. *Biosensors and Bioelectronics* **2017**, *91*, 374-379.

116. Zhao, T.; Zhang, H.-S.; Tang, H.; Jiang, J.-H., Nanopore biosensor for sensitive and label-free nucleic acid detection based on hybridization chain reaction amplification. *Talanta* **2017**, *175*, 121-126.
117. Liu, P.; Yang, X.; Sun, S.; Wang, Q.; Wang, K.; Huang, J.; Liu, J.; He, L., Enzyme-Free Colorimetric Detection of DNA by Using Gold Nanoparticles and Hybridization Chain Reaction Amplification. *Analytical Chemistry* **2013**, *85* (16), 7689-7695.
118. Song, C.; Yang, X.; Wang, K.; Wang, Q.; Huang, J.; Liu, J.; Liu, W.; Liu, P., Label-free and non-enzymatic detection of DNA based on hybridization chain reaction amplification and dsDNA-templated copper nanoparticles. *Analytica Chimica Acta* **2014**, *827*, 74-9.
119. Xu, Y.; Zheng, Z., Direct RNA detection without nucleic acid purification and PCR: Combining sandwich hybridization with signal amplification based on branched hybridization chain reaction. *Biosensors and Bioelectronics* **2016**, *79*, 593-599.
120. Bi, S.; Chen, M.; Jia, X.; Dong, Y.; Wang, Z., Hyperbranched Hybridization Chain Reaction for Triggered Signal Amplification and Concatenated Logic Circuits. *Angewandte Chemie International Edition* **2015**, *54* (28), 8144-8148.
121. Balcioglu, M.; Rana, M.; Hizir, M. S.; Robertson, N. M.; Haque, K.; Yigit, M. V., Rapid Visual Screening and Programmable Subtype Classification of Ebola Virus Biomarkers. *Advanced Healthcare Materials* **2017**, *6* (2), 1600739.
122. Xu, Y.; Zheng, Z., Hybridization Chain Reaction for Direct mRNA Detection Without Nucleic Acid Purification. In *RNA Detection: Methods and Protocols*, Gaspar, I., Ed. Springer New York: New York, NY, 2018; pp 187-196.
123. Zheng, J.; Ji, X.; Du, M.; Tian, S.; He, Z., Rational construction of a DNA nanomachine for HIV nucleic acid ultrasensitive sensing. *Nanoscale* **2018**, *10* (36), 17206-17211.
124. Chen, Y.-X.; Huang, K.-J.; Niu, K.-X., Recent advances in signal amplification strategy based on oligonucleotide and nanomaterials for microRNA detection-a review. *Biosensors and Bioelectronics* **2018**, *99*, 612-624.
125. Chandran, H.; Rangnekar, A.; Shetty, G.; Schultes, E. A.; Reif, J. H.; LaBean, T. H., An autonomously self-assembling dendritic DNA nanostructure for target DNA detection. *Biotechnology Journal* **2013**, *8* (2), 221-227.
126. Lafleur, L. K.; Bishop, J. D.; Heiniger, E. K.; Gallagher, R. P.; Wheeler, M. D.; Kauffman, P.; Zhang, X.; Kline, E. C.; Buser, J. R.; Kumar, S.; Byrnes, S. A.; Vermeulen, N. M. J.; Scarr, N. K.; Belousov, Y.; Mahoney, W.; Toley, B. J.; Ladd, P. D.; Lutz, B. R.; Yager, P., A rapid, instrument-free, sample-to-result nucleic acid amplification test. *Lab on a Chip* **2016**, *16* (19), 3777-3787.
127. Lam, M. K.; Gadzikwa, T.; Nguyen, T.; Kausar, A.; Alladin-Mustan, B. S.; Sikder, M. D.; Gibbs-Davis, J. M., Tuning Toehold Length and Temperature to Achieve Rapid, Colorimetric Detection of DNA from the Disassembly of DNA-Gold Nanoparticle Aggregates. *Langmuir* **2016**, *32* (6), 1585-1590.
128. Chan, E. H.; Brewer, T. F.; Madoff, L. C.; Pollack, M. P.; Sonricker, A. L.; Keller, M.; Freifeld, C. C.; Blench, M.; Mawudeku, A.; Brownstein, J. S., Global capacity for emerging infectious disease detection. *PNAS* **2010**, *107* (50), 21701-21706.
129. Clerc, O.; Greub, G., Routine use of point-of-care tests: usefulness and application in clinical microbiology. *Clinical Microbiology and Infection* **2010**, *16* (8), 1054-1061.
130. Patel, J. C.; Lucchi, N. W.; Srivastava, P.; Lin, J. T.; Sug-Aram, R.; Aruncharus, S.; Bharti, P. K.; Shukla, M. M.; Congpuong, K.; Satimai, W.; Singh, N.; Udhayakumar, V.; Meshnick, S. R., Field evaluation of a real-time fluorescence loop-mediated isothermal amplification assay, RealAmp, for the diagnosis of malaria in Thailand and India. *Journal of Infectious Diseases* **2014**, *210* (8), 1180-7.
131. Hopkins, H.; Gonzalez, I. J.; Polley, S. D.; Angutoko, P.; Ategeka, J.; Asimwe, C.; Agaba, B.; Kyabayinze, D. J.; Sutherland, C. J.; Perkins, M. D.; Bell, D., Highly sensitive detection of malaria parasitemia in a malaria-endemic setting: performance of a new loop-mediated isothermal amplification kit in a remote clinic in Uganda. *Journal of Infectious Disease* **2013**, *208* (4), 645-52.

132. Michaelis, J.; Roloff, A.; Seitz, O., Amplification by Nucleic Acid-Templated Reactions. *Organic & Biomolecular Chemistry* **2014**, *12*.
133. Gill, P.; Ghaemi, A., Nucleic acid isothermal amplification technologies: a review. *Nucleosides Nucleotides Nucleic Acids* **2008**, *27* (3), 224-43.
134. Cordray, M.; Richards-Kortum, R., Review: Emerging Nucleic Acid Based Tests for Point-of-Care Detection of Malaria. *The American Journal of Tropical Medicine and Hygiene* **2012**, *87* (2), 223-30.
135. Li, J.; Macdonald, J., Advances in isothermal amplification: novel strategies inspired by biological processes. *Biosensors and Bioelectronics* **2015**, *64*, 196-211.
136. Nyan, D. C.; Ulitzky, L. E.; Cehan, N.; Williamson, P.; Winkelman, V.; Rios, M.; Taylor, D. R., Rapid detection of hepatitis B virus in blood plasma by a specific and sensitive loop-mediated isothermal amplification assay. *Clinical Infectious Diseases* **2014**, *59* (1), 16-23.
137. Motre, A.; Kong, R.; Li, Y., Improving isothermal DNA amplification speed for the rapid detection of Mycobacterium tuberculosis. *Journal of Microbiological Methods* **2011**, *84* (2), 343-5.
138. Peeling, R. W.; Mabey, D., Point-of-care tests for diagnosing infections in the developing world. *Clinical Microbiology and Infection* **2010**, *16* (8), 1062-9.
139. Kersting, S.; Rausch, V.; Bier, F. F.; von Nickisch-Roseneck, M., Rapid detection of Plasmodium falciparum with isothermal recombinase polymerase amplification and lateral flow analysis. *Malaria Journal* **2014**, *13*, 99.
140. Jung, C.; Ellington, A. D., Diagnostic Applications of Nucleic Acid Circuits. *Accounts of Chemical Research* **2014**, *47* (6), 1825-1835.
141. Gaffney, B. L.; Jones, R. A., Thermodynamic comparison of the base pairs formed by the carcinogenic lesion O6-methylguanine with reference both to Watson-Crick pairs and to mismatched pairs. *Biochemistry* **1989**, *28* (14), 5881-5889.
142. Allawi, H. T.; SantaLucia, J., Nearest Neighbor Thermodynamic Parameters for Internal G-A Mismatches in DNA. *Biochemistry* **1998**, *37* (8), 2170-2179.
143. Allawi, H. T.; SantaLucia, J., Jr., Nearest-neighbor thermodynamics of internal A.C mismatches in DNA: sequence dependence and pH effects. *Biochemistry* **1998**, *37* (26), 9435-44.
144. Taylor, B. J.; Howell, A.; Martin, K. A.; Manage, D. P.; Gordy, W.; Campbell, S. D.; Lam, S.; Jin, A.; Polley, S. D.; Samuel, R. A.; Atrazhev, A.; Stickel, A. J.; Birungi, J.; Mbonye, A. K.; Pilarski, L. M.; Acker, J. P.; Yanow, S. K., A lab-on-chip for malaria diagnosis and surveillance. *Malaria Journal* **2014**, *13* (1), 179.
145. Ramachandran, S.; Fu, E.; Lutz, B.; Yager, P., Long-term dry storage of an enzyme-based reagent system for ELISA in point-of-care devices. *Analyst* **2014**, *139* (6), 1456-62.
146. Manage, D. P.; Lauzon, J.; Atrazhev, A.; Chavali, R.; Samuel, R. A.; Chan, B.; Morrissey, Y. C.; Gordy, W.; Edwards, A. L.; Larison, K.; Yanow, S. K.; Acker, J. P.; Zahariadis, G.; Pilarski, L. M., An enclosed in-gel PCR amplification cassette with multi-target, multi-sample detection for platform molecular diagnostics. *Lab on a Chip* **2013**, *13* (13), 2576-84.
147. Silverman, A. P.; Kool, E. T., Detecting RNA and DNA with Templated Chemical Reactions. *Chemical Reviews* **2006**, *106* (9), 3775-3789.
148. Patzke, V.; von Kiedrowski, G., Self replicating systems. *Arkivoc* **2007**, *5*, 293-310.
149. Grossmann, T. N.; Strohbach, A.; Seitz, O., Achieving turnover in DNA-templated reactions. *ChemBiochem* **2008**, *9* (14), 2185-92.
150. Lincoln, T. A.; Joyce, G. F., Self-sustained replication of an RNA enzyme. *Science* **2009**, *323* (5918), 1229-32.
151. Sievers, D.; von Kiedrowski, G., Self-Replication of Hexadeoxynucleotide Analogues: Autocatalysis versus Cross-Catalysis. *Chemistry – A European Journal* **1998**, *4* (4), 629-641.
152. Sievers, D.; von Kiedrowski, G., Self-replication of complementary nucleotide-based oligomers. *Nature* **1994**, *369* (6477), 221-224.

153. Zhang, D. Y.; Turberfield, A. J.; Yurke, B.; Winfree, E., Engineering entropy-driven reactions and networks catalyzed by DNA. *Science* **2007**, *318* (5853), 1121-5.
154. Xi, X.; Li, T.; Huang, Y.; Sun, J.; Zhu, Y.; Yang, Y.; Lu, Z., RNA Biomarkers: Frontier of Precision Medicine for Cancer. *Non-Coding RNA* **2017**, *3* (1), 9.
155. Quinn, J. F.; Patel, T.; Wong, D.; Das, S.; Freedman, J. E.; Laurent, L. C.; Carter, B. S.; Hochberg, F.; Keuren-Jensen, K. V.; Huentelman, M.; Spetzler, R.; Kalani, M. Y. S.; Arango, J.; Adelson, P. D.; Weiner, H. L.; Gandhi, R.; Goilav, B.; Putterman, C.; Saugstad, J. A., Extracellular RNAs: development as biomarkers of human disease. *Journal of Extracellular Vesicles* **2015**, *4*, 10.3402/jev.v4.27495.
156. Cella, L. N.; Blackstock, D.; Yates, M. A.; Mulchandani, A.; Chen, W., Detection of RNA viruses: current technologies and future perspectives. *Critical Reviews in Eukaryotic Gene Expression* **2013**, *23* (2), 125-37.
157. Koo, B.; Jin, C. E.; Lee, T. Y.; Lee, J. H.; Park, M. K.; Sung, H.; Park, S. Y.; Lee, H. J.; Kim, S. M.; Kim, J. Y.; Kim, S. H.; Shin, Y., An isothermal, label-free, and rapid one-step RNA amplification/detection assay for diagnosis of respiratory viral infections. *Biosensors and Bioelectronics* **2017**, *90*, 187-194.
158. Priye, A.; Bird, S. W.; Light, Y. K.; Ball, C. S.; Negrete, O. A.; Meagher, R. J., A smartphone-based diagnostic platform for rapid detection of Zika, chikungunya, and dengue viruses. *Scientific Reports* **2017**, *7*, 44778.
159. Dvorak, Z.; Pascussi, J. M.; Modriansky, M., Approaches to messenger RNA detection - comparison of methods. *Biomedical papers of the Medical Faculty of the University Palacky Olomouc Czech Republic* **2003**, *147* (2), 131-5.
160. Rijpens, N.; Jannes, G.; Herman, L., Messenger RNA-based RT-PCR detection of viable Salmonella. *International Dairy Journal* **2002**, *12* (2), 233-238.
161. Islam, M. N.; Gopalan, V.; Haque, M. H.; Masud, M. K.; Hossain, M. S. A.; Yamauchi, Y.; Nguyen, N. T.; Lam, A. K.; Shiddiky, M. J. A., A PCR-free electrochemical method for messenger RNA detection in cancer tissue samples. *Biosensors and Bioelectronics* **2017**, *98*, 227-233.
162. Fan, J.; Zhang, X.; Cheng, Y.; Xiao, C.; Wang, W.; Liu, X.; Tong, C.; Liu, B., Increasing the sensitivity and selectivity of a GONS quenched probe for an mRNA assay assisted with duplex specific nuclease. *RSC Advances* **2017**, *7* (57), 35629-35637.
163. Dong, H.; Lei, J.; Ding, L.; Wen, Y.; Ju, H.; Zhang, X., MicroRNA: Function, Detection, and Bioanalysis. *Chemical Reviews* **2013**, *113* (8), 6207-6233.
164. Wang, W.; Kong, T.; Zhang, D.; Zhang, J.; Cheng, G., Label-Free MicroRNA Detection Based on Fluorescence Quenching of Gold Nanoparticles with a Competitive Hybridization. *Analytical Chemistry* **2015**, *87* (21), 10822-9.
165. Tian, Y.; Zhang, L.; Wang, H.; Ji, W.; Zhang, Z.; Zhang, Y.; Yang, Z.; Cao, Z.; Zhang, S.; Chang, J., Intelligent Detection Platform for Simultaneous Detection of Multiple MiRNAs Based on Smartphone. *ACS Sensors* **2019**, *4* (7), 1873-1880.
166. Marmot, M., Social determinants of health inequalities. *The Lancet* **2005**, *365* (9464), 1099-104.
167. Zhang, K.; Wang, K.; Zhu, X.; Xie, M., A one-pot strategy for the sensitive detection of miRNA by catalyst-oligomer-mediated enzymatic amplification-based fluorescence biosensor. *Sensors and Actuators B: Chemical* **2016**, *223*, 586-590.
168. Hwu, S.; Blickenstorfer, Y.; Tiefenauer, R. F.; Gonnelli, C.; Schmidheini, L.; Luchtefeld, I.; Hoogenberg, B. J.; Gisiger, A. B.; Voros, J., Dark-Field Microwells toward High-Throughput Direct miRNA Sensing with Gold Nanoparticles. *ACS Sensors* **2019**, *4* (7), 1950-1956.
169. Shen, Y.; Tian, F.; Chen, Z.; Li, R.; Ge, Q.; Lu, Z., Amplification-based method for microRNA detection. *Biosensors and Bioelectronics* **2015**, *71*, 322-331.
170. Li, X.; Ni, M.; Zhang, C.; Ma, W.; Zhang, Y., A convenient system for highly specific and sensitive detection of miRNA expression. *RNA* **2014**, *20* (2), 252-9.

171. Chugh, P.; Dittmer, D. P., Potential pitfalls in microRNA profiling. *Wiley Interdisciplinary Reviews: RNA* **2012**, *3* (5), 601-16.
172. Zhou, D.-M.; Du, W.-F.; Xi, Q.; Ge, J.; Jiang, J.-H., Isothermal Nucleic Acid Amplification Strategy by Cyclic Enzymatic Repairing for Highly Sensitive MicroRNA Detection. *Analytical Chemistry* **2014**, *86* (14), 6763-6767.
173. Fang, S.; Lee, H. J.; Wark, A. W.; Corn, R. M., Attomole Microarray Detection of MicroRNAs by Nanoparticle-Amplified SPR Imaging Measurements of Surface Polyadenylation Reactions. *Journal of the American Chemical Society* **2006**, *128* (43), 14044-14046.
174. Ko, G.; Cromeans, T. L.; Sobsey, M. D., Detection of infectious adenovirus in cell culture by mRNA reverse transcription-PCR. *Applied and Environmental Microbiology* **2003**, *69* (12), 7377-84.
175. Yin, B.-C.; Liu, Y.-Q.; Ye, B.-C., One-Step, Multiplexed Fluorescence Detection of microRNAs Based on Duplex-Specific Nuclease Signal Amplification. *Journal of the American Chemical Society* **2012**, *134* (11), 5064-5067.
176. Du, W.; Lv, M.; Li, J.; Yu, R.; Jiang, J., A ligation-based loop-mediated isothermal amplification (ligation-LAMP) strategy for highly selective microRNA detection. *Chemical Communications* **2016**, *52* (86), 12721-12724.
177. Nilsson, M.; Antson, D.-O.; Barbany, G.; Landegren, U., RNA-templated DNA ligation for transcript analysis. *Nucleic Acids Research* **2001**, *29* (2), 578-581.
178. Zhang, W.; Zhang, P.; Zhang, F.; Cheng, W.; Xu, Y.; Zhang, Y.; Chen, L.; Wang, H.; Zhou, Q.; Zhang, X., Real-time and rapid quantification of microRNAs in cells and tissues using target-recycled enzyme-free amplification strategy. *Talanta* **2020**, *217*, 121016.
179. Li, S.; Xu, L.; Ma, W.; Wu, X.; Sun, M.; Kuang, H.; Wang, L.; Kotov, N. A.; Xu, C., Dual-Mode Ultrasensitive Quantification of MicroRNA in Living Cells by Chiroplasmonic Nanopyramids Self-Assembled from Gold and Upconversion Nanoparticles. *Journal of the American Chemical Society* **2016**, *138* (1), 306-312.
180. Degliangeli, F.; Kshirsagar, P.; Brunetti, V.; Pompa, P. P.; Fiammengo, R., Absolute and Direct MicroRNA Quantification Using DNA–Gold Nanoparticle Probes. *Journal of the American Chemical Society* **2014**, *136* (6), 2264-2267.
181. Zhao, X.; Xu, L.; Sun, M.; Ma, W.; Wu, X.; Kuang, H.; Wang, L.; Xu, C., Gold-Quantum Dot Core–Satellite Assemblies for Lighting Up MicroRNA In Vitro and In Vivo. *Small* **2016**, *12* (34), 4662-4668.
182. Liu, Y., Applications of Responsive Assembly and Disassembly of Colloids (Master's thesis). **2019**, 75.
183. Kausar, A., Tuning DNA stability to achieve isothermal DNA amplification (PhD thesis). *University of Alberta* **2014**, 232.
184. Lohman, G. J. S.; Tabor, S.; Nichols, N. M., DNA Ligases. *Current Protocols in Molecular Biology* **2011**, *94* (1), 3.14.1-3.14.7.
185. Doherty, A. J.; Ashford, S. R.; Subramanya, H. S.; Wigley, D. B., Bacteriophage T7 DNA ligase. Overexpression, purification, crystallization, and characterization. *The Journal of Biological Chemistry* **1996**, *271* (19), 11083-11089.
186. Cai, L.; Hu, C.; Shen, S.; Wang, W.; Huang, W., Characterization of bacteriophage T3 DNA ligase. *The Journal of Biochemistry* **2004**, *135* (3), 397-403.
187. Ferretti, L.; Sgaramella, V., Specific and reversible inhibition of the blunt end joining activity of the T4 DNA ligase. *Nucleic Acids Research* **1981**, *9* (15), 3695-3705.
188. Gaastra, W.; Hansen, K., Ligation of DNA with T4 DNA Ligase. In *Nucleic Acids*, Walker, J. M., Ed. Humana Press: Totowa, NJ, 1984; pp 225-230.
189. Lei, Y.; Hili, R., Structure-activity relationships of the ATP cofactor in ligase-catalysed oligonucleotide polymerisations. *Organic & Biomolecular Chemistry* **2017**, *15* (11), 2349-2352.

190. Wu, D. Y.; Wallace, R. B., Specificity of the nick-closing activity of bacteriophage T4 DNA ligase. *Gene* **1989**, *76* (2), 245-254.
191. Rossi, R.; Montecucco, A.; Ciarrocchi, G.; Biamonti, G., Functional characterization of the T4 DNA ligase: a new insight into the mechanism of action. *Nucleic Acids Research* **1997**, *25* (11), 2106-2113.
192. Shi, K.; Bohl, T. E.; Park, J.; Zasada, A.; Malik, S.; Banerjee, S.; Tran, V.; Li, N.; Yin, Z.; Kurniawan, F.; Orellana, K.; Aihara, H., T4 DNA ligase structure reveals a prototypical ATP-dependent ligase with a unique mode of sliding clamp interaction. *Nucleic Acids Research* **2018**, *46* (19), 10474-10488.
193. Lohman, G. J. S.; Chen, L.; Evans, T. C., Jr., Kinetic characterization of single strand break ligation in duplex DNA by T4 DNA ligase. *The Journal of Biological Chemistry* **2011**, *286* (51), 44187-44196.
194. Pawlowska, R.; Korczynski, D.; Nawrot, B.; Stec, W. J.; Chworos, A., The α -thio and/or β - γ -hypophosphate analogs of ATP as cofactors of T4 DNA ligase. *Bioorganic Chemistry* **2016**, *67*, 110-115.
195. Eun, H.-M., Ligases. In *Enzymology Primer for Recombinant DNA Technology (Chapter 2)*, Academic Press: 1996; pp 109-144.
196. Chatterjee, N.; Walker, G. C., Mechanisms of DNA damage, repair, and mutagenesis. *Environmental and Molecular Mutagenesis* **2017**, *58* (5), 235-263.
197. Weiss, B.; Richardson, C. C., Enzymatic breakage and joining of deoxyribonucleic acid, I. Repair of single-strand breaks in DNA by an enzyme system from Escherichia coli infected with T4 bacteriophage. *Proceedings of the National Academy of Sciences of the United States of America* **1967**, *57* (4), 1021-1028.
198. Cherepanov, A. V.; de Vries, S., Kinetics and thermodynamics of nick sealing by T4 DNA ligase. *European Journal of Biochemistry* **2003**, *270* (21), 4315-4325.
199. Bauer, R. J.; Jurkiw, T. J.; Evans, T. C.; Lohman, G. J. S., Rapid Time Scale Analysis of T4 DNA Ligase–DNA Binding. *Biochemistry* **2017**, *56* (8), 1117-1129.
200. Montecucco, A.; Lestingi, M.; Pedrali-Noy, G.; Spadari, S.; Ciarrocchi, G., Use of ATP, dATP and their alpha-thio derivatives to study DNA ligase adenylation. *The Biochemical Journal* **1990**, *271* (1), 265-268.
201. Kinoshita, Y.; Nishigaki, K., Unexpectedly General Replaceability of ATP in ATP-Requiring Enzymes. *The Journal of Biochemistry* **1997**, *122* (1), 205-211.
202. Park, H.; Kosikova, T.; Hales, S.; Philp, D.; Gibbs, J. M., Minimizing Product Inhibition in DNA Self-Replication: Insights for Prebiotic Replication from the Role of the Enzyme. **2020**, (in preparation).